PROJECT ADMINISTRATION DATA SHEET

[X] ORIGINAL   [ ] REVISION NO. _____

Project No./(Center No.) E-25-625   (R6331-OAO) _____   GTRC/~~GIIX~~   DATE 7 / 6 / 87

Project Director: A.F. Ferri _____   School/~~Lab~~ ME _____

Sponsor: National Science Foundation _____

Agreement No. : MSM-8707846 _____

Award Period: From __6/15/87__ To __11/30/89__ (Performance) __2/28/90__ Reports

Sponsor Amount: **New With This Change**   **Total to Date**

Contract Value: $ __59,982__ $ __59,982__

Funded: $ __59,982__ $ __59,982__

Cost Sharing No./(Center No.) E-25-342 (F6331-OAO) Cost Sharing: $ __29,839__

Title: Analysis and Design of Large Space Structures with Nonlinear Joints _____

ADMINISTRATIVE DATA

'OCA Contact __John B. Schonk__   x4-4820

1) Sponsor Technical Contact: 2) Sponsor Issuing Office:

Elbert L. Marsh _____   Andrea R. Kline _____

National Science Foundation _____   National Science Foundation _____

ENG/MSM _____   DGC/ENG _____

Washington, DC 20550 _____   Washington, DC 20550 _____

202/357-9542 _____   202/357-9602 _____

Military Security Classification: _____   ONR Resident Rep. is ACO: _____ Yes __X__ No
(or) Company/Industrial Proprietary: _____ Defense Priority Rating: _____

RESTRICTIONS

See Attached _____ NSF _____ Supplemental Information Sheet for Additional Requirements.

Travel: Foreign travel must have prior approval — Contact OCA in each case. Domestic travel requires sponsor

approval where total will exceed greater of $500 or 125% of approved proposal budget category.

Equipment: Title vests with __GIT__ _____

COMMENTS:

No funds may be expended after 11/30/89.
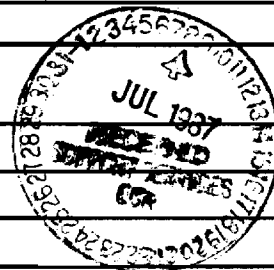
COPIES TO: SPONSOR'S I.D. NO. _____

Project Director   Procurement/GTRI Supply Services   GTRC
Research Administrative Network   Research Security Services   Library
Research Property Management   Project File
Accounting   Research Communications   Other _____

FORM OCA 65:1086

NOTICE OF PROJECT CLOSEOUT

Closeout Notice Date 02/28/90
Original Closeout Started ********

Project No. E-25-625_____   Center No. R6331-0A0_____

Project Director FERRI A A_____   School/Lab ME_____

Sponsor NATL SCIENCE FOUNDATION/GENERAL_____

Contract/Grant No. MSM-8707846_____   Contract Entity GTRC

Prime Contract No. _____

Title ANALYSIS & DESIGN OF LARGE SPACE STRUCTURES WITH NONLINEAR JOINTS_____

Effective Completion Date 891130 (Performance) 900228 (Reports)

Closeout Actions Required:	Y/N	Date Submitted
Final Invoice or Copy of Final Invoice	N	_____
Final Report of Inventions and/or Subcontracts	N	_____
Government Property Inventory & Related Certificate	N	_____
Classified Material Certificate	N	_____
Release and Assignment	N	_____
Other _____	N	_____

Subproject Under Main Project No. _____

Continues Project No. _____

Distribution Required:

Project Director	Y
Administrative Network Representative	Y
GTRI Accounting/Grants and Contracts	Y
Procurement/Supply Services	Y
Research Property Managment	Y
Research Security Services	N
Reports Coordinator (OCA)	Y
GTRC	Y
Project File	Y
OCA/CSD	N
Other _____	N
_____	N

Final Report

Analysis and Design of Large Space Structures With
Nonlinear Joints

by Aldo A. Ferri

January 1990

Summary

Large space structures (LSS) with energy-dissipating, nonlinear joints were investigated. The research involved the modeling and computational analysis of these systems and the design of LSS for improved damping performance. Active and passive joint designs were developed that enhanced the damping contribution from the connecting joints of LSS. A number of important results have emerged from this research:

- Models of built-up structures that allow normal forces (forces applied normal to the frictional interface) to vary with structural displacement are useful in helping to understand the vibratory and damping properties of these structures. The simulated behavior of these models agrees qualitatively with available experimental results.

- When normal forces in a structural joint vary with transverse displacement the overall damping properties are very similar to those of a linear, viscously damped structure. This is an important result because it implies that the modeling and analysis process for large structures with many nonlinear joints may be easier to perform than previously thought to be possible.

- The damping characteristics of built-up and joined structures may be substantially increased if the inter-member interfaces are designed to take full advantage of displacement-dependent normal forces.

- Controlling the normal forces to a frictional interface through use of an active feedback system can substantially increase the damping of large flexible space structures. In fact, it is possible to give the joint linear characteristics through the proper selection of the feedback control law.

These results as well as copies of the technical papers resulting from this work are contained in this report.

Table of Contents

1. Introduction

One of the major problems remaining in the development of large space structures (LSS) is the anticipated low level of passive damping. This low level of damping impacts the feasibility of placing large flexible space structures in orbit for a number of reasons. Perhaps the most important reason is that it is difficult to design attitude and shape controllers for lightly damped flexible structures. Since the open-loop system has low relative stability, it is quite possible that perturbations to the control scheme, such as observation spillover or plant uncertainty, can drive the closed-loop system unstable [1]. Many researchers have aimed to circumvent this problem by designing better (often more complicated and sophisticated) control systems. A review of the literature up until 1984 can be found in reference [2]. An alternate approach is to design structures to have a greater passive damping capacity. It has been shown that the addition of passive damping to a flexible structure can greatly facilitate the model reduction and control design of flexible structures [3,4]. Since connecting joints have long been considered to be an important contributor to the overall passive damping of traditional flexible truss-like structures [5,6], this research has concentrated on the modeling, analysis and design of connecting joints of large space structures.

The primary damping mechanism in truss structure joints is dry (Coulombic) friction. The analysis of structures with dry friction has received considerable attention. See, for example, Ferri [7] or the references cited therein. In most of these studies, it is assumed that the normal force to the sliding interface is constant. This may be termed the "classic" dry friction damped case. It is shown in this report that when the normal force is allowed to vary with displacement, the damping properties of the structure can be substantially modified. This result is very important to a number of aerospace applications: large space structures, aircraft structures, jet engines and helicopters. However, these results also concern a variety of ground-based applications, including turbomachinery and rail and road vehicles.

One of the results of this research is that it is often possible to obtain viscous-like damping properties solely through the use of dry friction. The viscous-like damping property suggests that many mechanical designs can be improved by configuring frictional interfaces in ways that allow the normal forces to vary with displacement. In some applications, classic dry friction is inadequate to suppress vibration. For example, turbine blade systems experiencing flutter cannot be globally stabilized with classic dry friction. See for example Ferri [8] and Griffin and Sinha [9]. The deficiency stems from the fact that the damping level of dry friction damped systems with constant normal forces varies inversely with the amplitude of response. Hence, for a sufficiently large disturbance, it is possible for the energy input to the system by aerodynamic forces to overcome the energy dissipation provided by dry friction. In the field of LSS dynamics and control, the instabilities resulting from uncertainties and inaccuracies in the system model also result in forces which are in-

1

phase with displacements and/or velocities. In these cases however, the external forces are provided by the force and torque actuators which are driven by a feedback control law. By designing connecting joints to have frictional forces which are dependent on relative joint displacements and velocities, it may be possible to greatly increase the stable operating range of an LSS attitude or shape controller.

It should be noted that viscous damping augmentation, especially in the form of viscoelastic materials such as those used in constrained layer damping, are subject to problems of "outgassing" in space environments [10]. This causes the material properties of the viscoelastic material to change with time, resulting in a degradation of the effectiveness of the damping treatment. An active or passive joint design which is based on energy dissipation from dry friction could provide a viscous-like damping, but still be well suited to a space environment.

The outline of the remainder of this final report follows. Section 2 contains a description of the modeling work for flexible structures jointed by nonlinear sleeve joints. Section 3 presents results of an analysis technique based on the frequency domain, steady-state harmonic balance method. Section 4 contains a description of the design work aimed at improving the energy-dissipative capabilities of large space structures. Finally, conclusions are contained in Section 5.

2. Modeling of Nonlinear Sleeve Joints

One of the three objectives of the research was to investigate modeling techniques for nonlinear joints used to join flexible truss members together. In previous work, a very detailed model for a sleeve joint was developed [11-13]. In that previous work, it was found that the complicated interaction of sleeve and the inserted portion of the adjacent beam could be largely modeled by a combination of piecewise linear springs and dampers in the rotational and transverse directions. As part of this research, these simplified joints were incorporated in a flexible system consisting of three linear, flexible Euler-Bernoulli beams interconnected with two sleeve joints. The development of the equations of motion were facilitated by the use of component-mode-analysis. Details are contained in Appendix A.

A major finding of this work is that the CMA method provides a relatively simple methodology for generating the equations of motion for these interconnected space systems. It was also found that the resulting system exhibited significant nonlinear response when subjected to impulsive and sinusoidal excitation. In particular, hardening spring behavior was evident in the frequency response curves; the "natural frequencies" were dependent on the amplitude of response; subharmonic and superharmonic response was evident in the steady-state response to harmonic excitation. These findings can have important consequences for the control of these types of space structures.

2

This work is currently being extended in a number of significant ways. The model is being extended to include beam foreshortening effects due to large amplitude transverse displacements of the beam system. This effect could prove to be crucial to the correct determination of the damping contribution from the joints. A second extension is the replacement of the simplified-joint models with more complicated and detailed sleeve-joint models.

3. Analysis of LSS with Nonlinear Joints

Extensive use of time integration was used in the simulation of the nonlinear models developed for this research. In addition, a harmonic balance algorithm was also investigated for its suitability to these types of problems. In previous work [14], it was found that a multi-harmonic, frequency domain approach could be used on systems with non-smooth nonlinearities (in particular, dry friction damped systems). However, the determination of the appropriate number of temporal harmonics to include in the analysis had to be chosen carefully. If chosen too low (too few harmonics) accuracy could suffer; if chosen too large (too many harmonics) the computation time might be excessive. The purpose of this research was to determine an a-posteriori error estimate for harmonic balance solutions to harmonically excited nonlinear systems, and to optimize the solution algorithm by incorporating an FFT routine. The details of this technique are included in Appendix B.

4. Design of Joints for LSS

A substantial effort was directed at designing nonlinear joints for large space structures to maximize energy dissipation through dry friction. Both active and passive strategies were considered. The details of this work can be found in Appendix C.

The chief results of this work were that it is possible to significantly effect the type and the amount of damping from dry friction in structural joints. It was seen that passive frictional interfaces could be designed so as to give the structure a "classic" frictional behavior (damping inversely proportional to amplitude), a viscous-like behavior (damping invariant with respect to amplitude), a hydraulic type damping (damping directly proportional to amplitude) or even a damping proportional to the square of amplitude. In fact, the type of damping that a system exhibits could depend on the magnitude and the distribution of the excitation forces. This may explain why experiments on dry friction damped, built-up structures have resulted in so many different types of vibratory behavior.

The results of the active joint reveal that substantial enhancement of "passive" damping of a structure can be obtained through a relatively light (low mass) and inexpensive means. It was found that one could even linearize the joint, making the overall

3

dynamics of the dry friction damped system behave in a linear manner. A more extensive investigation of the active joint is continuing. Among the topics that are important to consider are: experimental verification, optimal feedback control, and interaction of the active joints with global shape and pointing control strategies.

5. Conclusions and Recommendations for Future Work

The research has uncovered a number of interesting and important results:

- Models of built-up structures that allow normal forces (forces applied normal to the frictional interface) to vary with structural displacement are useful in helping to understand the vibratory and damping properties of these structures. The simulated behavior of these models agrees qualitatively with available experimental results.

- When normal forces in a structural joint vary with transverse displacement the overall damping properties are very similar to those of a linear, viscously damped structure. This is an important result because it implies that the modeling and analysis process for large structures with many nonlinear joints may be easier to perform than previously thought to be possible.

- The damping characteristics of built-up and joined structures may be substantially increased if the inter-member interfaces are designed to take full advantage of displacement-dependent normal forces.

- Controlling the normal forces to a frictional interface through use of an active feedback system can substantially increase the damping of large flexible space structures. In fact, it is possible to give the joint linear characteristics through the proper selection of the feedback control law.

On a more general note, it is interesting to find that while nonlinearities in the joints present very challenging impediments to the analysis and modeling of LSS, they provide a number of potential benefits to the design and performance of closed-loop LSS control systems.

Future work should include:

- inclusion of beam foreshortening to models of nonlinear sleeve joints in flexible space structures

- investigation of stick-slip behavior in dry friction damped systems with amplitude-dependent friction forces

- experimental verification of vibratory characteristics of systems with amplitude-dependent dry friction

- development of adaptive harmonic balance solution algorithm that makes use of the a-posteriori error estimate discussed above

- development of optimal control strategies for actively controlled joint

- investigation of interaction between active and/or passive joints and spacecraft attitude and shape controllers

- investigation of performance degradation in closed-loop control systems attributable to unmodeled spacecraft nonlinearities in joints

- experimental verification of active and/or passive joints incorporated into flexible structures

References

1. Balas, M.J., "Active Control of Flexible Systems," Journal of Optimization Theory and Applications, Vol. 25, No. 3, 1978, pp. 415-436.

2. Nurre, G.S., Ryan, R.S., Scofield, H.N. and Sims, J.L., "Dynamics and Control of Large Space Structures," Journal of Guidance and Control, Vol. 7, No. 5, 1984, pp. 514-526.

3. Alberts, T.E., Hastings, G.G., Book, W.J., and Dickerson, S.L., "Experiments in Optimal Control of a Flexible Arm with Passive Damping," Fifth VPI&SU/AIAA Symposium on Dynamics and Control of Large Structures, 12-14 June 1985, Blacksburg, VA.

4. Alberts, T.E., "Augmenting the Control of a Flexible Manipulator with Passive Mechanical Damping," Ph.D. Thesis, School of Mechanical Engineering, Georgia Institute of Technology, Atlanta, GA, September 1986.

5. Hertz, T.J. and Crawley, E.F., "The Effects of Scale on the Dynamics of Flexible Space Structures," Report No. SSL 18-83, Space Systems Laboratory, Department of Aeronautics and Astronautics, Massachusetts Institute of Technology, Cambridge, MA, September 1983.

6. Hertz, T.J., and Crawley, E.F., "Damping in Space Structure Joints," AIAA Dynamics Specialists Conference, 17-18 May 1984, Palm Springs, California.

7. Ferri, A.A., "The Dynamics of Dry Friction Damped Systems," Ph.D. Thesis, Department of Mechanical and Aerospace Engineering, Princeton University, Princeton, NJ, September 1985.

8. Ferri, A.A., and Dowell, E.H., "The Behavior of a Linear, Damped Modal System with a Nonlinear Spring-Mass-Dry Friction Damper System Attached, Part II," Journal of Sound Vibration, Vol. 101, No. 1, 1985, pp. 55-74.

9. Griffin, J.H. and Sinha, A., "Friction Damping of Flutter in Gas Turbine Engine Airfoils," AIAA J. Aircraft, Vol. 20, No. 4, pp. 372-376.

10. Trudell, R.W., Curley, R.C. and Rogers, L.C., "Passive Damping in Large Space Structures," AIAA Paper No. AIAA-80-0677, 13 pgs.

11. Ferri, A.A., "The Influence of Nonlinear Joints on the Dynamics of Large Space Structures," Final Report, Honeywell, Inc., Space and Strategic Avionics Division, Clearwater, FL, April 1987.

12. Ferri, A.A., "Investigation of Damping From Nonlinear Sleeve Joints of Large Space Structures," Proceedings of the ASME 11th Biennial Conference on Mechanical Vibrations and Noise, Boston, MA, September 27-30, 1987.

13. Ferri, A.A., "Modeling and Analysis of Nonlinear Sleeve Joints of Large Space Structures," AIAA Journal of Spacecraft and Rockets, Vol. 25, No. 5, 1988, pp. 354-360.

14. Ferri, A.A. and Dowell, E.H., "Frequency Domain Solutions to Multi-Degree-of-Freedom, Dry Friction Damped Systems," Journal of Sound and Vibration, Vol. 124, No. 2, 1988, pp. 207-224.

Appendix A

Modeling of Nonlinear Joints for Large
Flexible Space Structures

1. Ferri, A.A., "Modeling and Analysis of Nonlinear Sleeve Joints of Large Space Structures," AIAA Journal of Spacecraft and Rockets, Vol. 25, No. 5, 1988, pp. 354-360.

2. Ferri, A.A., "Analysis of Flexible Structures with Nonlinear Joints," Proceedings of the Seventh International Modal Analysis Conference, Las Vegas, NV, Jan. 30-Feb. 2, 1989.

Modeling and Analysis of Nonlinear Sleeve Joints of Large Space Structures

Aldo A. Ferri*

Georgia Institute of Technology, Atlanta, Georgia

A nonlinear sleeve joint model that accounts for the presence of clearances, impact damping, and dry (Coulombic) friction is developed. By studying the free and forced response of this model, it is seen that the overall damping appears to be predominantly viscous-like in nature. This is found to be true even for the cases studied in which dry friction is the sole source of energy dissipation. In addition, the nonlinear behavior of a rigid beam inserted into a sleeve joint is investigated and discussed.

I. Introduction

RECENT interest in the dynamics and control of large space structures (LSS) has spurred a need for a better understanding of truss structure joints. The main function of these joints is to connect one or more truss elements together to form space-frame structures. However, another important function that they serve is to provide passive damping to these flexible space structures.[1,2] It is well known that low levels of passive damping are a major concern of controls designers. The low relative stability of LSS may cause small perturbations to the control scheme, such as observation spillover or plant uncertainty, to result in poor performance or even instability in the closed-loop system.[3,4] Recently, it has been shown (quantitatively) that passive damping not only reduces the tendency for instability in flexible structures, but also lessens the model reduction error caused by mode truncation.[5,6] Thus, joints may be a simple but effective way to ease the stringent requirements on the controls design. From a mathematical perspective, however, the joints are nonlinear elements and hence are difficult to analyze. For this reason, it is difficult to determine analytically or computationally the overall damping contribution from the joints. Experimental determination of truss structural damping is also hampered by the joint nonlinearities.[7] The prestressing of the joints caused by gravity loading in a laboratory environment causes the measured properties to differ from their operational values encountered in a zero-*g*, zero-atmosphere space environment. Also, because of the large size and low natural frequencies of these systems, it is difficult to perform full-size testing, especially if one wishes to place the entire structure in a vacuum in order to simulate a space atmospheric environment.

This paper addresses the mathematical modeling and numerical analysis of a nonlinear sleeve joint. Although the modeling and control of linear flexible structures has received considerable interest, relatively little has been done on the modeling and control of structures with multiple nonlinear joints. Some work, however, is relevant to the present effort. Hertz and Crawley have studied the experimental and analytical determination of damping in nonlinear LSS.[1,2,8,9] In particular, Refs. 1 and 2 develop simple joint models and single harmonic analyses are performed to estimate loss factors. Hertz and Crawley's work serves as a starting point for the present research effort.

Many of the dissipative mechanisms in space structure joints are tied to nonlinear behavior. One of the major dissipative mechanisms in joints is dry (Coulombic) friction. The general problem of analyzing structures with dry friction has received considerable attention. See, for example, Ferri[10] or the references cited therein. It has been shown that dry friction can cause some significantly nonlinear behavior in an otherwise linear structure. Clearances in mechanical systems are another source of nonlinear behavior in large truss structures. These clearances are often present because of imperfections in nominally "snug" joints or because of wear that can take place on an initially snug design. At times, clearances are purposely designed into a joint in order to facilitate deployment or permit relative slip and impact to occur. In fact, this "impact damping" may be an important contributing factor to the overall damping level of the structure.[2] However, clearances introduce so-called "dead zone" nonlinearities and hysteresis into the system. The clearances further complicate the situation since they can cause the structures to behave differently in space than they do on the ground. This is caused by both the presence of oxidation in the ground environment and ground-level gravity fields that cause different operating points to become effective.[7,9]

The outline of the remainder of the paper is as follows. Section II contains the development of the equations of motion for a rigid beam partially inserted into a sleeve joint as shown in Fig. 1. Results obtained through time integration of this model are presented in Sec. III. Some concluding remarks are contained in Sec. IV.

II. Sleeve Joint Model Development

This section deals with the modeling of a generic sleeve joint. Although many types of truss structure joint designs are currently used, sleeve joints are relatively simple in concept but still retain many of the important characteristics of more complicated joint geometries. (See Refs. 1 and 2 for a description of other commonly used joint types.) A brief outline of the modeling steps follows. For a more detailed development, see Ferri.[11]

The generic sleeve joint consists of a cylindrical outer sleeve that fits around the end of a mating beam or truss member. As previously mentioned, Hertz and Crawley have developed simple models for such types of joints.[1,2] Their model considers only dry friction nonlinearities. Loss factors are calculated assuming simple harmonic motion and taking a one mode approximation for the beam motion. This model is used as the starting point for the present study.

The major characteristics that need to be modeled in order to develop an accurate general-purpose sleeve joint model are the following:

Dissipative effects
    Damping caused by dry friction.
    Damping caused by impact.
    Material damping caused by deformation of the joint.

Geometry and elastic effects

Overall beam/sleeve geometry including possible clearances between the beam and sleeve.

Hardening spring characteristics caused by large deformations of the beam and/or sleeve.

An attempt has been made to account for the possibility of any of the foregoing effects in the joint models. Although, as pointed out in Ref. 9, many of these effects are difficult to quantify, the qualitative effects of each joint characteristic can be studied through parameter variation.

For the purpose of modeling, it is assumed that the sleeve joint is composed of two parts: an outer sleeve that moves with the one beam and an inner cylinder that moves with the other beam. Figure 1 shows a closeup schematic of the sleeve joint model. Six degrees of freedom are identified to describe the planar motion of the sleeve joint system. Note that y_1, x_1, and θ_1 are the lateral displacement, longitudinal displacement, and rotation of the end of the left-hand beam (beam 1) and y_2, x_2, and θ_2 represent the corresponding quantities for the right-hand beam (beam 2). These six generalized coordinates fully describe the interaction of the outer sleeve and the inner cylinder. Three coordinate systems can be identified: the i,j coordinate system that remains fixed in inertial space, the i_1,j_1 system that is fixed on sleeve 1, and the i_2,j_2 system that is fixed on inner cylinder 2. Unit vectors in the longitudinal and transverse beam directions are respectively represented by i and j; θ is defined to be positive in the counterclockwise direction. Kinematic relationships are used to derive expressions for the distances between beam and sleeve contact points and for the relative velocities between the sleeve and the beam, both tangent to and normal to the contact plane.

One of the main reasons for choosing the six generalized coordinates just defined is the ease with which the relative motion of the sleeve and cylinder can be expressed. Another motivation for this choice of coordinates is that it provides a relatively easy way of incorporating the sleeve joint model into a flexible truss system using either the finite-element method or component mode synthesis techniques. The analysis presented next is developed for the simplified case in which the sleeve is fixed in inertial space, and only beam 2 is allowed to move. The equations and methodology can be extended to the case in which both the sleeve and inner cylinder can move.

Figure 2 shows the deflected position of the sleeve (shown with solid lines) together with the undeflected state (shown with dotted lines). It is seen that the distance from point E to side BC can be expressed as

$$\delta_E = j_1 \cdot r_{EB} \tag{1}$$

where r_{EB} is the vector from B to point E as shown in Fig. 2. After describing r_{EB} in terms of sleeve length and deflection parameters, Eq. (1) gives

$$\delta_E = (x_1 - x_2 - L_1)\sin\theta_1 + (y_2 - y_1)\cos\theta_1 + L_2\sin(\theta_1 - \theta_2)$$

$$- (d_2/2)\cos(\theta_1 - \theta_2) + (d_1/2) \tag{2}$$

Fixing the sleeve in inertial space is accomplished by setting $x_1 = y_1 = \theta_1 = 0$. This yields

$$\delta_E = y_2 - L_2\sin\theta_2 - (d_2/2)\cos\theta_2 + (d_1/2) \tag{3}$$

A similar analysis can be performed to obtain δ_F, defined to be the distance from point F to side AD. The distance from point I to side AB is similarly defined as δ_I. The remaining distances are defined along the direction transverse to the beam; δ_C and δ_D are defined as the distances from point C to side EH and from point D to side FG, respectively. In each case, the distances are defined to be positive when contact is not occurring at that respective point. Complete details and expressions may be found in Ref. 11.
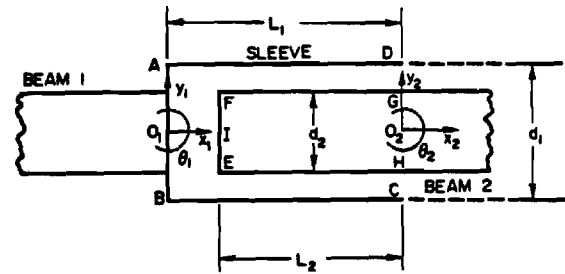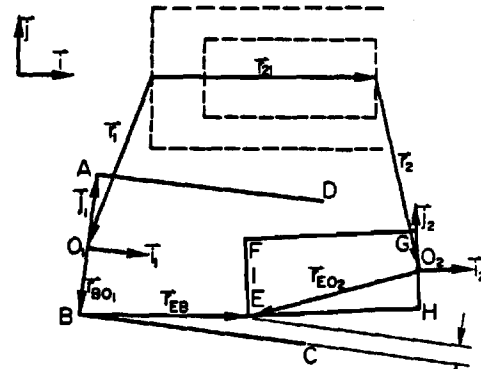

Fig. 1 Sleeve joint model.

Fig. 2 Deflected position of sleeve joint. δ_E

In order to model the contact forces, nonlinear, one-way springs are placed at the four contact points. (See Fig. 3.) The term "one-way" implies that the spring forces can be only compressive in nature; no tension is allowed. Mathematically, the spring force at contact point E is given by

$$F_{E_1} = F_{E_1}j; \qquad F_{E_1} = \begin{cases} K_1|\delta_E| + \epsilon_1|\delta_E|^3 & \delta_E \le 0 \\ 0 & \delta_E > 0 \end{cases} \tag{4}$$

where K_1 represents the linearized, small deformation elastic constant and ϵ_1 is typically a small, positive quantity that determines the spring "hardening" characteristic at contact points E and F. As seen in Fig. 3, parameters K_2 and ϵ_2 correspond to stiffness characteristics at contact points C and D. For a particular sleeve joint, K_1, K_2, ϵ_1, and ϵ_2 might be found from a finite-element model or perhaps by approximate methods from the theory of elasticity. Expressions similar to that shown in Eq. (4) can be obtained for the spring forces at contact points F, C, and D. Note that forces F_{E1} and F_{F1} act normal to sides BC and AD, respectively, and that forces F_{D1} and F_{C1} act normal to sides FG and EH, respectively.

In addition to the four transverse springs already discussed, a linear spring is placed at location I to model the retaining characteristic of the sleeve joint, if any. Only this spring at location I is allowed to transmit both tension and compression.

The total compressive force at locations E, F, D, and C will consist of the elastic force from the springs plus any viscous damping or rate-dependent forces. In order to model the rate-dependent forces caused by material deformation and impact, viscous damping elements are placed in parallel with the one-way nonlinear springs as shown in Fig. 3. Like the springs, the dampers are also permitted to transmit compressive forces only. Thus, the viscous damping forces are nonzero only when contact has occurred ($\delta < 0$) and when the relative velocity is such that further compression takes place; that is, $\dot\delta < 0$.

The viscous damping forces are proportional to the rate of deflection of the beam or sleeve. These deflection rates can be

found by differentiating the corresponding expressions for δ. For example, the expression for $\dot{\delta}_E$ is

$$\dot{\delta}_E = \dot{y}_2 - L_2\dot{\theta}_2 \cos\theta_2 + (d_2/2) \dot{\theta}_2 \sin\theta_2 \qquad (5)$$

The corresponding expression for the viscous damping force at point E is given by

$$F_{E_2} = F_{E_2} j; \qquad F_{E_2} = \begin{cases} C_1|\dot{\delta}_E| & \delta_E \leq 0, \quad \dot{\delta}_E \leq 0 \\ 0 & \text{otherwise} \end{cases} \qquad (6)$$

Similar expressions can be found for the other contact points. Whereas the dampers at points E, F, C, and D are one-way in nature, the damper at location I is two-way and is, in fact, a fully linear viscous damper.

The total compressive force at contact point E is found by summing the spring and damper forces:

$$F_E = F_{E_1} + F_{E_2} = F_E j \qquad (7)$$

When contact occurs, friction forces come into play, acting tangent to the contact plane. The friction forces can be modeled approximately by Coulomb's Law. In the most general case, two coefficients of friction can be defined: a static coefficient of friction μ_s that applies when sticking has occurred, and a dynamic or kinetic coefficient of friction μ_d that applies when slipping occurs. When sticking takes place, the friction force has whatever value it needs to maintain equilibrium at that contact point. If the force required is greater than $\mu_s N$, where N is the normal force to the contact plane, then slipping is said to occur. In the case of slipping, the friction force has magnitude $\mu_d N$ and a direction that opposes the relative movement of the contact plane.

As discussed in the preceding paragraph, the friction forces depend on the signs of the relative slip speeds. Note that the relative slip speed is the component of the relative velocity along the contact plane (or contact line for the planar system under consideration). For contact point E, the relative velocity in question is the difference in the absolute velocities of points E_1 and E_2, where E_1 is the point along side BC of the sleeve (body 1) that is in contact with the corner E_2 on the inner cylinder (body 2). That is,

$$V_{E_1/E_2} = V_{E_1} - V_{E_2} \qquad (8)$$

Since the sleeve is fixed in space, $V_{E_1} = 0$. The coordinates x_2, y_2, and θ_2 can be used to find V_{E_2}

$$V_{E_2} = \frac{d}{dt}(r_2 + r_{EO_2}) \qquad (9)$$

Vectors r_2 and r_{EO_2} are seen in Fig. 2 to be given by

$$r_2 = x_2 i + y_2 j; \qquad r_{EO_2} = -L_2 i_2 - (d_2/2) j_2$$

Substituting these expressions into Eq. (9) and accounting for the rotation of the unit vectors i_2 and j_2 gives

$$V_{E_2} = (\dot{x}_2 i + \dot{y}_2 j) + \dot{\theta}_2 k \times [-L_2 i_2 - (d_2/2) j_2] \qquad (10a)$$

$$V_{E_2} = [\dot{x}_2 + (d_2/2) \dot{\theta}_2 \cos\theta_2 + L_2\dot{\theta}_2 \sin\theta_2] i$$
$$+ [\dot{y}_2 + (d_2/2) \dot{\theta}_2 \sin\theta_2 - L_2\dot{\theta}_2 \cos\theta_2] j \qquad (10b)$$

The relative slip speed is the component of the difference in absolute velocities in the direction of the contact plane (side BC)

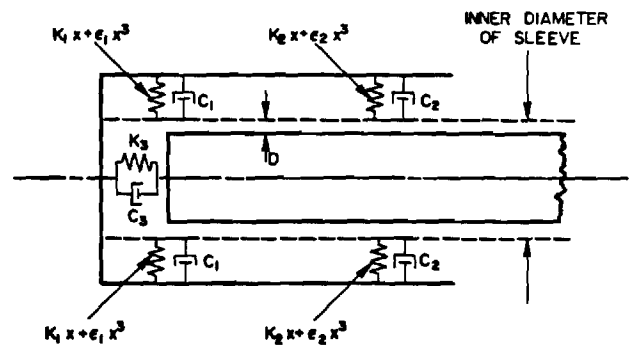$$V_{E12} = (V_{E_1} - V_{E_2}) \cdot i \qquad (11a)$$

Fig. 3 Sleeve joint model showing nonlinear, one-way springs and impact dampers (x = compression of the springs).

$$V_{E12} = -\dot{x}_2 - (d_2/2) \dot{\theta}_2 \cos\theta_2 - L_2\dot{\theta}_2 \sin\theta_2 \qquad (11b)$$

Again, similar expressions can be found for the other contact points.

The friction force at point E is determined using the relative slip speed and Coulomb's Law

$$f_E = \begin{cases} f_E i, & f_E \leq \mu_s F_E \quad V_{E12} = 0 \\ \mu_d F_E \, \text{sgn}(V_{E12}) i & V_{E12} \neq 0 \end{cases} \qquad (12)$$

where

$$\text{sgn} V = \begin{cases} 1 & V > 0 \\ 0 & V = 0 \\ -1 & V < 0 \end{cases} \qquad (13)$$

The friction forces at contact points F, C, and D can be found in a similar manner. Note that the contact line (and, hence, the friction forces) at locations C and D are parallel to the sides EH and FG, respectively.

Equations of Motion

The normal forces and friction forces constitute all of the forces exerted on the beam by the sleeve. In addition to the beam-sleeve interaction forces, an externally applied excitation force $F(t) = F(t)j$ acts on the beam as seen in the free-body diagram shown in Fig. 4. The equations of planar motion for this system are obtained from two force balances and one moment balance about the beam's center of gravity (c.g.)

$$m \ddot{x}_c = F_x \qquad (14)$$

$$m \ddot{y}_c = F_y + F(t) \qquad (15)$$

$$I_C \ddot{\theta} = F_F\left(\frac{L_2}{2} \cos\theta + \frac{d_2}{2} \sin\theta\right) + f_F\left(\frac{L_2}{2} \sin\theta - \frac{d_2}{2} \cos\theta\right)$$
$$+ F_E\left(-\frac{L_2}{2} \cos\theta + \frac{d_2}{2} \sin\theta\right) + f_E\left(\frac{L_2}{2} \sin\theta + \frac{d_2}{2} \cos\theta\right)$$
$$+ \frac{L_2}{2} F_I \sin\theta - (F_D - F_C)\frac{L_2}{2} - (f_D - f_C)\frac{d_2}{2}$$
$$+ F_D r_{D_2G} - F_C r_{C_2H} + L_4 \sin\theta \, F_x - L_4 \cos\theta \, F_y$$
$$+ \left(L_F \cos\theta + \frac{d_2}{2} \sin\theta\right) F(t) \qquad (16)$$

where m is the mass of the beam, I_c is the mass moment of inertia about the beam's c.g., F_x and F_y are beam-sleeve
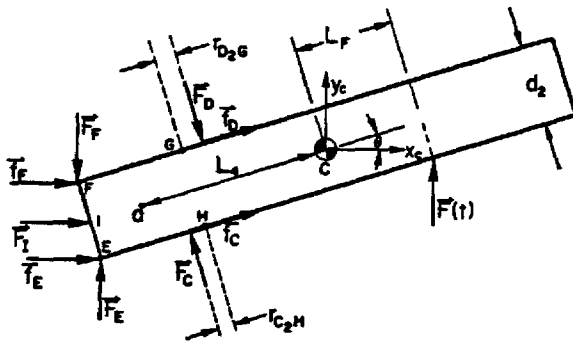
Fig. 4 Beam free-body diagram.

interaction forces in the x and y directions, respectively

$$F_x = F_I + f_E + f_F + (F_D - F_C) \sin\theta + (f_D + f_C) \cos\theta \quad (17)$$

$$F_y = F_E - F_F + (F_C - F_D) \cos\theta + (f_D + f_C) \sin\theta \quad (18)$$

and where r_{D_2G} and r_{C_2H} are given by

$$r_{D_2G} = [x_2^2 - x_2 d_2 \sin\theta + (d_2/2)^2 + y_2^2 - y_2(d_1 - d_2 \cos\theta)$$

$$+ (d_1/2)^2 - (d_1 d_2/2) \cos\theta]^{1/2} \quad (19)$$

$$r_{C_2H} = [x_2^2 + x_2 d_2 \sin\theta + (d_2/2)^2 + y_2^2 + y_2(d_1 - d_2 \cos\theta)$$

$$+ (d_1/2)^2 - (d_1 d_2/2) \cos\theta]^{1/2} \quad (20)$$

Equations (14-16) form the equations of motion for a rigid beam partially inserted into a sleeve joint. Defining the state vector as

$$x = [x_c, y_c, \theta, \dot{x}_c, \dot{y}_c, \dot{\theta}]^T$$

the equations of motion can be summarized in first-order vector form

$$\dot{x} = f[x, F(t)] \quad (21)$$

III. Results for the Sleeve Joint Model

One of the advantages of the rigid beam fixed-sleeve model developed in Sec. II is that it isolates the sleeve joint so that an accurate assessment of its effects can be made. For example, since the beam is rigid, the total damping of this system is entirely caused by the dry friction and material damping in the joint. Hence, the damping contribution of the joint to the system is easily determined. Another advantage of this model is that it allows one to perform many parametric studies at a relatively low computational cost.

A baseline configuration for the fully nonlinear joint model was chosen to have the parameter values given in Table 1. Length dimension nomenclature is defined in Fig. 5. The coefficient of friction μ is the baseline value for both the static and dynamic coefficients of friction; that is, $\mu_s = \mu_d = \mu$. Unless otherwise stated, parameters may be assumed to have their baseline value.

A sample time response is shown in Figs. 6 and 7. The quantity y_2 refers to the transverse displacement of the beam at a position that lies just outside the sleeve (see Fig. 1). The figures show the free response of y_2 and θ for the baseline set of parameter values and a particular set of initial conditions: $x_2 = 0$, $y_2 = 0.003$ m, $\theta = 0.09$ rad. The plotted quantities are normalized by various system parameters. The displacement y_2 is normalized with respect to the clearance $D = (d_1 - d_2)/2$. If $|y_2/D| > 1$, it implies that contact is taking place. The beam rotation θ is normalized with respect to $D/(L_2/2)$. This is the approximate beam rotation (in radians) when contact begins to occur. Thus, $|\theta \cdot L_2/(2D)| > 1$ also implies that contact has occurred.

The motion shown in Figs. 6 and 7 is largely composed of two frequencies: a highly damped, high-frequency motion (~ 24 rad/s) related to transverse displacement of the beam's

end, and a dominant low-frequency motion (~ 0.4 rad/s at high amplitudes) related to the gross rotation of the beam.

The significance of these two types of motions can be determined by examining the linearized equations of motion for a sleeve joint model with no clearances

$$m \ddot{x}_c + K_x x_c = 0 \quad (22)$$

$$m \ddot{y}_c + K_y y_c - L_4 K_y \theta = 0 \quad (23)$$

Table 1 Baseline parameter values for sleeve joint model

| Item	Symbol	Baseline value	Units
Mass	m	1.3493	kg
Mass moment of inertia	I_c	0.12167	kg·m^2
Lateral stiffness	K_1	100	N/m
Lateral stiffness	K_2	100	N/m
Longitudinal stiffness	K_3	100	N/m
Cubic stiffness	ϵ_1	0	N/m^3
Cubic stiffness	ϵ_2	0	N/m^3
Lateral damping	C_1	0	N·s/m
Lateral damping	C_2	0	N·s/m
Longitudinal damping	C_3	0	N·s/m
Coefficient of friction	μ	0.47	--
Sleeve length	L_1	0.0401	m
Inner cylinder length	L_2	0.04	m
Distance from c.g. to point 2	L_3	0.48	m
Distance from c.g. to point a	L_4	0.50	m
Distance from c.g. to forcing	L_F	0	m
Total beam length	L_{total}	1.04	m
Inner sleeve diameter	d_1	0.0252	m
Outer beam diameter	d_2	0.0250	m
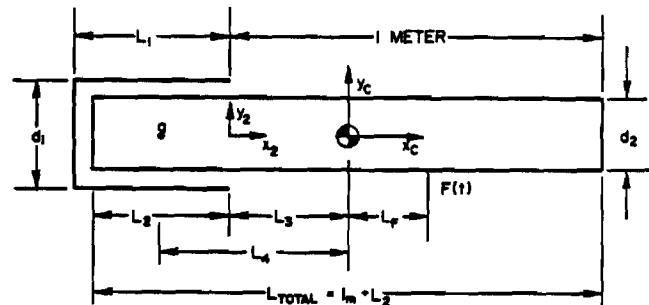
Fig. 5 Definition of length and displacement parameters.
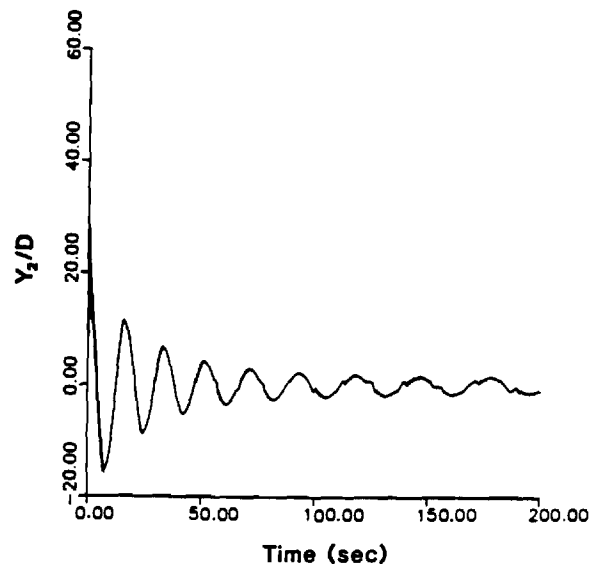
Fig. 6 y_2/D vs time. Baseline sleeve joint model. Initial conditions $x_2(0) = 0.0$, $y_2(0) = 0.003$ m, $\theta(0) = 0.09$ rad.
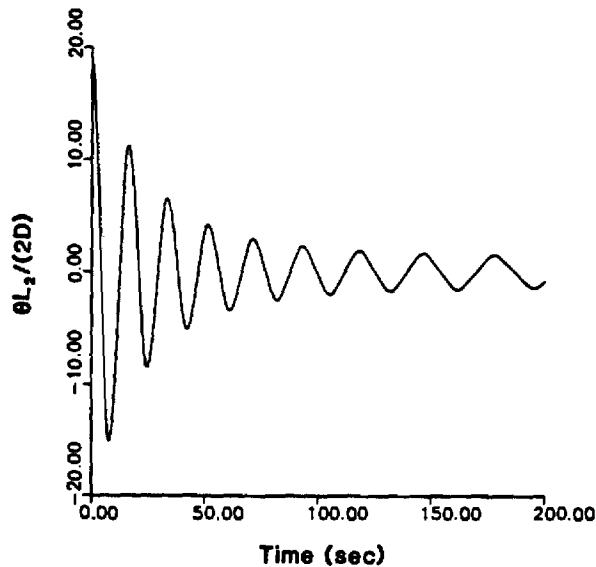
Time (sec)

Fig. 7 $\theta L_2/(2D)$ vs time. Baseline sleeve joint model. Initial conditions $x_2(0) = 0.0$, $y_2(0) = 0.003$ m, $\theta(0) = 0.09$ rad.

$$I_c \ddot{\theta} - K_y L_4 y_c + (K_\theta + K_y L_4^2)\theta = 0 \qquad (24)$$

K_x, K_y, and K_θ can be defined approximately as follows:

$$K_x = K_3$$

$$K_y = K_1 + K_2$$

$$K_\theta = (L_2^2/4)(K_1 + K_2)$$

Since Eq. (22) is uncoupled from Eqs. (23) and (24), we can easily identify the natural frequency for longitudinal motion to be

$$\omega_1 = \sqrt{K_x/m} = \sqrt{K_3/m} \qquad (25)$$

The natural frequencies associated with the remaining two equations are found to be (if we assume $K_1 = K_2$)

$$\omega_{2,3}^2 = K_1 \left[\frac{m L^2 + 2I_c \pm \sqrt{(mL^2 + 2I_c)^2 - 4m I_c L_2^2}}{2m I_c} \right] \qquad (26)$$

where $L^2 = 1/2 L_2^2 + 2L_4^2$. If we use baseline parameters, this gives

$$\omega_1 = \sqrt{K_3} (0.861), \quad \omega_2 = \sqrt{K_1} (0.0417), \quad \omega_3 = \sqrt{K_1} (2.366) \qquad (27)$$

It is seen that the natural frequencies of the system grow as $\sqrt{K}$. More important, the difference between ω_3 and ω_2 also grows with $\sqrt{K_1}$, causing the equations of motion to become numerically "stiff" as the joint gets physically stiffer.[12] Numerical solutions to stiff differential equations require large amounts of computer time in order to maintain accuracy. For this reason, most of the simulations presented here are done for the cases of relatively low joint stiffness, with results for higher stiffnesses based on extrapolation and relatively fewer numerical simulations.

When we examine the eigenvectors associated with Eqs. (23) and (24), it is seen that for the case $K_1 = K_2 = 100$ N/m ($K_y = 200$ N/m), the low-frequency motion corresponds to the case where y_2 and θ are "in phase" and the high-frequency motion corresponds to the case where y_2 and θ are "out of phase." Although the longitudinal degree of freedom does not interact strongly with the other two degrees of freedom, it is very important in accurately predicting the losses caused by

friction. Hence, the longitudinal degree of freedom is retained for the subsequent computations, but concentration will be directed to y_2 and θ since these quantities dominate the global motion of the beam.

There are two aspects of Figs. 6 and 7 that are worth noting. The first is that the envelopes of decay are largely exponential. Note that the entire damping of this system is the result of dry friction, since the baseline model has the impact damping parameters set equal to zero ($C_1 = C_2 = C_3 = 0$). In classical dry friction damped systems, the normal forces are independent of amplitude and, consequently, the envelopes of decay are linear.[13] In this case, however, the normal forces at the contact points vary depending on the beam motion; in particular, they are dependent on the compression of the one-way springs. As a result of this amplitude dependence, the envelopes of decay are exponential. This type of behavior has been found in other systems with amplitude-dependent friction as well.[1,14]

A second important observation from Figs. 6 and 7 is that the frequency appears to be strongly affected by the amplitude of response. As the amplitude grows smaller, the frequency of response becomes lower. This can be understood by examining a describing function approximation of the piecewise linear springs of the simplified sleeve joint model. As the amplitude decreases, the effective spring constant also decreases. In fact, for amplitudes of response smaller than the clearance displacement, the effective spring constant is zero.

The damping ratio for the low-frequency motion was estimated using the log decrement approach. The formula for the damping ratio, provided that $\zeta \ll 1$, is[13]

$$\zeta = (1/2\pi) \delta = (1/2\pi) \ln (\xi_1/\xi_2) \qquad (28)$$

where ξ_1 is the amplitude of one peak in a free response and ξ_2 is the amplitude of the next peak. It should be noted that the log decrement approach is derived for single-degree-of-freedom (single-DOF) linear systems; thus, it is only an approximate formula when applied to nonlinear, multi-DOF systems. From Fig. 6, we see that initially, when $y_2/D = 30$, the damping ratio is approximately $\zeta = 0.146$. After the amplitude decreases, $y_2/D = 12$, the damping ratio is reduced to $\zeta = 0.079$. Thus, it is seen that, qualitatively, low-amplitude motions are more lightly damped than high-amplitude motions. This characteristic was seen in many of the results of this research.

The effect of beam sleeve geometry on overall damping is shown in Fig. 8 for a stiffness of $K_1 = K_2 = K_3 = 10$ N/m. The quantity D/L_2 is essentially a relative clearance defined as the true clearance, $D = (d_1 - d_2)/2$, divided by the sleeve length L_2. It is seen that the damping ratio is inversely proportional to D/L_2; that is, small clearances are more beneficial for dry friction damping than large clearances. Note that the abscissa of the graph is the (unnormalized) amplitude of y_2. (This quantity is left unnormalized because the clearance D is being varied from curve to curve.) It is also seen that for a given D/L_2, the damping ratio increases with amplitude.

The effects of sleeve joint stiffness and coefficient of friction were also studied. Damping ratios were computed for joint stiffness values ranging from $K_1 = K_2 = K_3 = 0.1$ N/m to 10×10^6 N/m. It was found that, even over such a broad range of values, the system damping ratio was relatively insensitive to changes in joint stiffness. Of course, increasing the sleeve stiffness increases system natural frequencies so that the response decays to zero faster, but it undergoes the same number of oscillations before it settles out. A variation of the coefficient of friction between 0 and 1.0 revealed that μ affects the damping ratio in a linear manner.

The baseline system was forced with a sinusoidal point force to generate frequency-response information. The forcing is assumed to be applied to the center of mass of the beam; that is, $L_F = 0$. A normalization for the forcing amplitude was chosen to be $F_n = K_y D L_2/(2L_4)$ where $K_y = K_1 + K_2$. It may be

noted that this is the static force necessary to deflect the beam through an angle of $2D/L_2$ rad. Using baseline parameters, F_n is 8×10^{-4} N. The frequency-response curves for $F/F_n = 3$, 3/2, and 3/16 are shown in Fig. 9. The amplitude shown is the peak response per cycle. Observations of the time histories of the forced response revealed that the motion was often multi-harmonic in nature. At low frequencies, the motion typically had a third or fifth harmonic of the forcing frequency significantly present. An example of such superharmonic response is shown in Fig. 10 for a forcing frequency of $\omega = 0.1$ rad/s and forcing level $F/F_n = 3$. At or near resonance, the motion was mainly sinusoidal in nature. However, at higher frequencies, subharmonic response was typical. Figure 11 shows the response for $\omega = 1.0$ rad/s and $F/F_n = 3$. It is seen that the motion is dominated by a 1/5 subharmonic response; that is, the motion repeats after every five cycles of the forcing. Such types of motion were typical at the higher frequencies at each of the three force levels investigated. Often, very low-order subharmonics were observed (on the order of 1/20th) or even at times aperiodic beating motion, which indicated the presence of two or more noncommensurable frequencies of re-
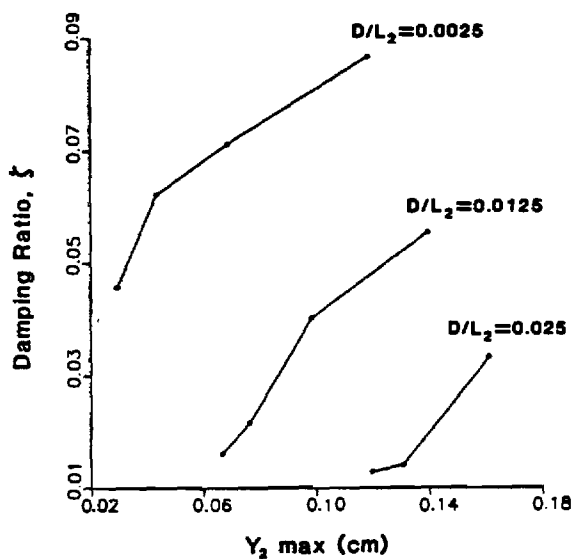

Fig. 10 Steady-state forced response for baseline sleeve joint model. $F/F_n = 3.0$, $\omega = 0.1$ rad/s.

Fig. 8 Damping ratio vs peak displacement y_2 in centimeters; various values of D/L_2.
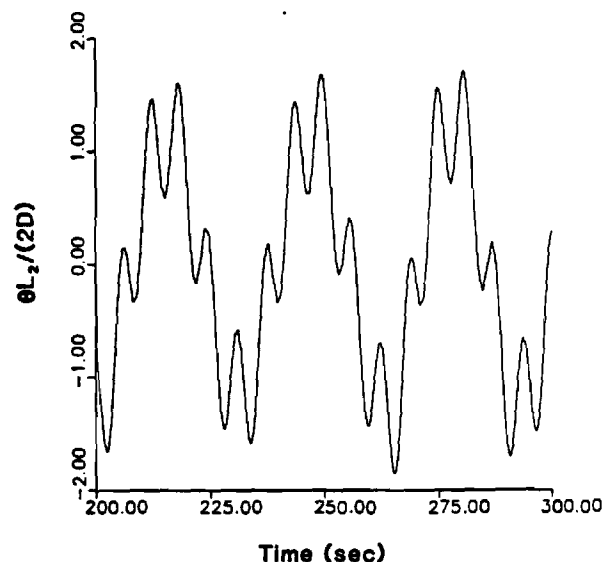
Fig. 11 Steady-state forced response for baseline sleeve joint model. $F/F_n = 3.0$, $\omega = 1.0$ rad/s.

sponse.[15] It should be added that such unusual behavior is not uncommon for nonlinear systems and, in particular, for systems with clearances. See, for example, the papers by Shaw and Holmes,[16,17] which examine the existence of chaos in mechanical systems with clearances.

IV. Concluding Remarks

A generic sleeve joint model has been developed that accounts for clearances, geometric stiffening, dry friction, and impact damping. This model was then tested using numerical integration to determine the damping contribution from the joint and the overall dynamic behavior of the beam-sleeve system. A parametric study was conducted to determine the qualitative influence of various joint characteristics on the damping contribution of the joint. It was found that the overall damping was qualitatively similar to viscous damping, even for the case of zero impact damping. It was also seen that the system damping ratio was dependent on the amplitude of response: high-amplitude motions had greater damping than low-amplitude motions. Forced response to harmonic excitation revealed noticeable hardening spring behavior. In addition, the time response to harmonic excitation displayed both subharmonic and superharmonic response.
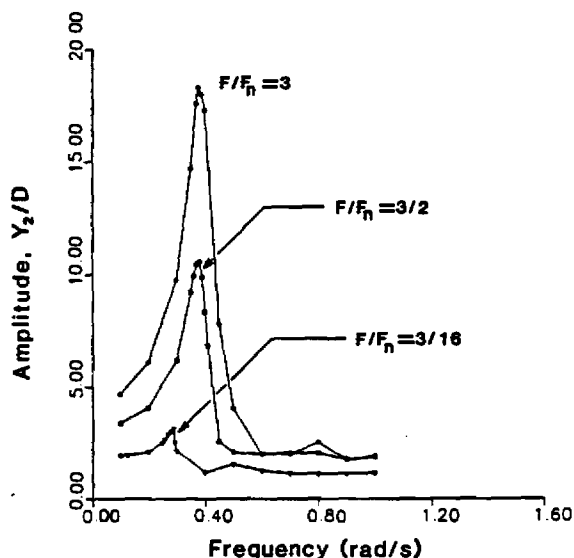

Fig. 9 Amplitude y_2/D vs frequency of excitation; various levels of excitation amplitude (baseline sleeve joint model).

References
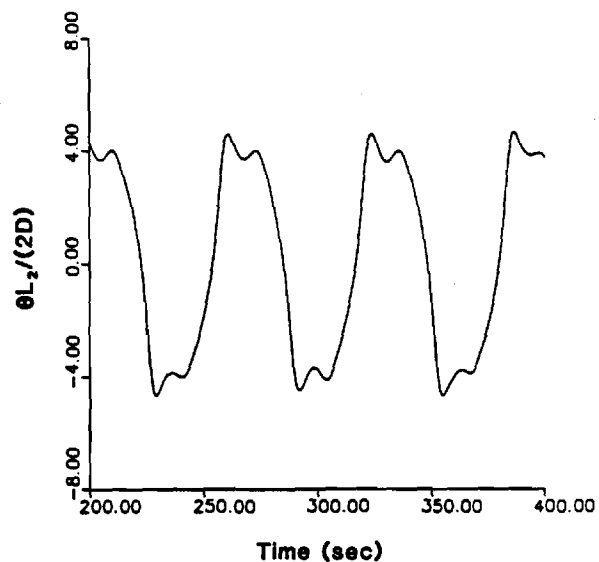
[1]Hertz, T. J. and Crawley, E. F., "Damping in Space Structure Joints," AIAA Paper 84-1039, May 1984.

[2]Hertz, T. J. and Crawley, E. F., "The Effects of Scale on the Dynamics of Flexible Space Structures," Space Systems Lab., Dept. of Aeronautics and Astronautics, MIT, Rept. SSL 18-83, Cambridge, MA, Sept. 1983.

[3]Balas, M. J., "Active Control of Flexible Systems," *Journal of Optimization Theory and Applications*, Vol. 25, July 1978, pp. 415–436.

[4]Nurre, G. S., Ryan, R. S., Scofield, H. N., and Sims, J. L., "Dynamics and Control of Large Space Structures," *Journal of Guidance, Control, and Dynamics*, Vol. 7, Sept.-Oct. 1984, pp. 514–526.

[5]Alberts, T. E., Hastings, G. G., Book, W. J., and Dickerson, S. L., "Experiments in Optimal Control of a Flexible Arm with Passive Damping," *Proceedings of the 5th VPI & SU/AIAA Symposium on Dynamics and Control of Large Structures*, AIAA New York, June 1985, pp. 423–435.

[6]Alberts, T. E., "Augmenting the Control of a Flexible Manipulator with Passive Mechanical Damping," Ph.D. Thesis, School of Mechanical Engineering, Georgia Inst. of Technology, Atlanta, GA, Sept. 1986.

[7]Hanks, B. R. and Pinson, L. D., "Large Space Structures Raise Testing Challenges," *Astronautics and Aeronautics*, Vol. 21, Oct. 1983, pp. 34–40.

[8]Crawley, E. F., Sarver, G. L., and Mohr, D. G., "Experimental Measurement of Passive Material and Structural Damping for Flexible Space Structures," *Acta Astronautica*, Vol. 10, May–June 1983, pp. 381–393.

[9]Crawley, E. F. and Aubert, A. C., "Identification of Nonlinear Structural Elements by Force-State Mapping," *AIAA Journal*, Vol. 24, Jan. 1986, pp. 155–162.

[10]Ferri, A. A., "The Dynamics of Dry Friction Damped Systems," Ph.D. Thesis, Dept. of Mechanical and Aerospace Engineering, Princeton Univ., Princeton, NJ, Sept. 1985.

[11]Ferri, A. A., "The Influence of Nonlinear Joints on the Dynamics of Large Flexible Space Structures," Honeywell, Inc., Space and Strategic Avionics Division, Clearwater, FL, Final Rept. April 1987.

[12]Gear, C. W., *Numerical Initial Value Problems in Ordinary Differential Equations*, Prentice-Hall, Englewood Cliffs, NJ, 1971.

[13]Meirovitch, L., *Elements of Vibration Analysis*, McGraw-Hill, New York, 1975.

[14]Bielawa, R. L., "An Analytic Study of the Energy Dissipation of Turbomachines Bladed-Disk Assemblies Due to Inter-Shroud Segment Rubbing," *Journal of Mechanical Design, Transaction of ASME*, Vol. 100, April 1978, pp. 222–228.

[15]Hayashi, C., *Nonlinear Oscillations in Physical Systems*, McGraw-Hill, New York, 1964.

[16]Shaw, S. W. and Holmes, P. J., "A Periodically Forced Piece-Wise Linear Oscillator," *Journal of Sound and Vibration*, Vol. 90, Sept. 1983, pp. 129–155.

[17]Shaw, S. W. and Holmes, P. J., "A Periodically Forced Impact Oscillator with Large Dissipation," *ASME Journal of Applied Mechanics*, Vol. 50, Dec. 1983, pp. 849–857.

ANALYSIS OF FLEXIBLE STRUCTURES WITH NONLINEAR JOINTS

Aldo A. Ferri
Assistant Professor
School of Mechanical Engineering
Georgia Institute of Technology
Atlanta, GA 30332-0405

ABSTRACT

A simplified model of a flexible space structure consisting of three visco-elastic beams and two nonlinear sleeve joints is investigated. Numerical results showing the relationship between system dynamic behavior and various joint properties are presented. It is found that system damping appears to be directly dependent on amplitude. It is also found that even a small amount of play in the sleeve joints causes nonlinear, hardening spring behavior to become evident in free and forced response.

NOMENCLATURE

Symbol	Definition
c_1	transverse damping coefficient for joints of three-beam system
c_2	rotational damping coefficient for joints of three-beam system
d_o	outer diameter of flexible beam
E	Young's modulus
e_1	transverse clearance in joints
e_2	rotational clearance in joints
F	amplitude of harmonic excitation
F_1	transverse shear force transmitted by the first joint of the three-beam system
F_2	transverse shear force transmitted by the second joint of the three-beam system
f_i	constraint relation, or governing equation
I	moment of inertia for flexible beam cross-section
k_1	transverse joint stiffness
k_2	rotational joint stiffness
L	length of the flexible beams
L^*	modified Lagrangian
M	total mass of one flexible beam, or total number of generalized coordinates
M_1	moment transmitted by the first joint
M_2	moment transmitted by the second joint
m	mass/unit length
p_i	transverse displacements for flexible beam ends
Q_i	generalized force
q_i	generalized coordinate
r_i	angular displacements for flexible beam ends
T	kinetic energy
V	potential energy
$w_i(x_i,t)$	transverse displacement of ith flexible beam
x_p	coordinate location for external force
x_i	spacial coordinate of the ith flexible beam
β_i	Lagrange multiplier
δq_i	virtual displacement of ith generalized coordinate
δW	virtual work
ζ_{ij}	j^{th} modal damping ratio of ith flexible beam
η_{ij}	j^{th} modal amplitude for i^{th} flexible beam
$\phi_{ij}(x_i)$	j^{th} mode shape of the ith flexible beam
ω	frequency of excitation
ω_{ij}	j^{th} natural frequency of ith flexible beam
$\cdot$	denotes a derivative with respect to time
$'$	$= d/dx_i$
$\underline{\quad}$	denotes a column vector
[ ]	denotes a matrix quantity

INTRODUCTION

A major problem remaining in the development of large flexible spacecraft and space platforms is that of accurately predicting the passive damping level. In addition to vibration suppression, passive damping determines the relative stability of the uncontrolled (open-loop) structure. A low level of passive damping can limit the robustness of closed-loop attitude and shape controllers. In particular, observer spillover associated with modelling errors becomes much more serious a problem in systems with low relative stability [1]. A related problem is that light damping tends to increase the model uncertainty tied to modal truncation [2,3].

It is generally believed that joints in large space structures (LSS) are a major source of energy dissipation [4-6]. A considerable amount of research has been directed towards designing joints which take maximum advantage of energy dissipative mechanisms such as dry friction and impact. Still, very little analytical work has been performed that predicts the damping and the dynamic behavior of structures with nonlinear joints. One of the complicating aspects of the problem is that the major energy dissipative mechanisms, impact and dry friction, are both nonlinear phenomena. Thus, the analysis of structures with numerous joints is a formidable task. Here, a generic model of a flexible system with two nonlinear joints is studied to

examine the qualitative trends and consequences of having nonlinearities at discrete locations in an otherwise linear structure.

In previous work [7,8], a mathematical model for a nonlinear sleeve joint was developed. The joint model included the effects of impact damping, dry friction and clearances in fit. In the present study, the simplified joint model described in Ref. [8] is incorporated into a flexible structure consisting of three visco-elastic beams and two sleeve joints as shown in Figure 1. In the following section, the equations of motion for the system are developed. The Results section contains a presentation and discussion of numerical results.

DEVELOPMENT OF EQUATIONS OF MOTION

The equations of motion for the three-beam system of Figure 1 are developed using the Component Mode Analysis (CMA) technique. CMA is a technique by which collections of subsystems can be analyzed. It is very convenient for systems that consist of linear sub-structures interconnected by discrete nonlinear elements. See, for example, the work of Dowell and co-workers [9-12].

A simplified way of applying CMA is to use Lagrange's equations with a modified Lagrangian, L^*:

$$L^* = T - V + \sum_{j=1}^{C} \beta_j f_j \qquad (1)$$

where the f_j's are constraint equations, the β_j's are Lagrange multipliers and C is the total number of constraints. The modified Lagrangian is used in the standard form of Lagrange's equations [13]

$$\frac{d}{dt}\left[\frac{\partial L^*}{\partial \dot{q}_i}\right] - \frac{\partial L^*}{\partial q_i} = Q_i \qquad i = 1,M \qquad (2)$$

The Q_i's are obtained from an expression for virtual work [13]

$$\delta W = \sum_{j=1}^{M} Q_j \, \delta q_j \qquad (3)$$

The analysis procedure can be separated into five tasks: 1) obtain an expression for kinetic energy, 2) obtain an expression for potential energy, 3) obtain an expression for virtual work, 4) determine constraint relations between redundant generalized coordinates and 5) substitute these expressions into Lagrange's equations (2). These five tasks are presented in order in the sequel.

Kinetic Energy

The kinetic energy of the system is the sum of the kinetic energies of the three beams. To simplify the development, it is assumed that the three beams are identical in physical dimension and material properties. It is also assumed that the joints are massless. The kinetic energy of the ith beam can be written

$$T_i = \frac{1}{2}\int_0^L m \left(\frac{\partial w_i}{\partial t}\right)^2 dx_i \qquad (4)$$

where L is length and m is the mass per unit length for each beam. x_i is the spacial variable and $w_i(x_i,t)$ is the transverse displacement function associated with the ith beam. For each beam, a finite modal expansion for the displacement function is used, retaining N of the natural modes

$$w_i(x_i,t) = \sum_{j=1}^{N} \eta_{ij}(t) \, \phi_{ij}(x_i) \qquad (5)$$

Taking into account the "pinned-pinned" conditions of the three-beam system, the ϕ_{1i}'s are chosen to be the natural modes associated with a uniform pinned-free beam of length L_1; the ϕ_{2i}'s are chosen to be the natural modes of a uniform free-free beam of length L_2; the ϕ_{3i}'s are chosen to be the natural modes of a uniform free-pinned beam of length L_3.

Substituting (5) into (4) and making use of the orthogonality of the mode shapes, expression (4) becomes

$$T_i = \frac{1}{2}\sum_{j=1}^{N} m_{ij} \dot{\eta}_{ij}^2 \qquad (6)$$

where

$$m_{ij} = m \int_0^L \phi_{ij}^2(x_i)dx_i \qquad (7)$$

The mode shapes are normalized such that $m_{ij} = M$, where $M = mL$ is the total mass of one beam. Using this fact, the total kinetic energy of the three-beam system can be written

$$T = \frac{1}{2} M \sum_{i=1}^{3} \sum_{j=1}^{N} \dot{\eta}_{ij}^2 \qquad (8)$$

Potential Energy

The potential energy of the combined system is the sum of the potential energies associated with flexure of the three elastic beams plus the potential energies associated with the elastic deformation of the joints. The potential energy of the ith beam is given by

$$V_i = \frac{1}{2}\int_0^L EI \left(\frac{\partial^2 w_i}{\partial x_i^2}\right)^2 dx_i \qquad (9)$$

where EI is the (constant) flexural rigidity of the beams. Substituting (5) into (9) and again using the orthogonality of the mode shapes, equation (9) gives

$$V_i = \frac{1}{2}\sum_{j=1}^{N} M\omega_{ij}^2 \, \eta_{ij}^2 \qquad (10)$$

where ω_{ij} is the jth natural frequency of the ith beam assuming the previously discussed boundary conditions. Note that $M\omega_{ij}^2$ is given in terms of the flexural rigidity and the modeshapes as

$$M\,\omega_{ij}^2 = \int_0^L EI\left(\frac{\partial^2\phi_{ij}}{\partial x_i^2}\right)^2 dx_i \tag{11}$$

The potential energies associated with the sleeve joints is best obtained by introducing "extra" or redundant generalized coordinates p_k and r_k defined in Figure 2. The p_k's are the transverse displacements at the ends of the beams which connect to the joints. The r_k's are the rotations at the beam ends. Based on the simplified model of the sleeve joint developed in Ref. [8], we assume that a nonlinear transverse spring is placed between p_1 and p_2 and between p_3 and p_4. Similarly, a nonlinear rotational spring is placed between coordinates r_1 and r_2 and between r_3 and r_4. The potential energy will be a scalar function of the quantities (p_2-p_1), (p_4-p_3), (r_2-r_1) and (r_4-r_3). Labeling the potential energies as V_{Li} = the potential energy associated with the lateral spring of the ith sleeve joint and V_{Ri} = the potential energy associated with the rotational spring of the ith joint, we can write an expression for the total potential energy of the 3-beam system

$$V = \sum_{i=1}^{3} V_i + V_{L1}(p_2-p_1) + V_{L2}(p_4-p_3)$$
$$+ V_{R1}(r_2-r_1) + V_{R2}(r_4-r_3) \tag{12}$$

Virtual Work

The virtual work of the total system is the sum of virtual work done by non-conservative forces. In this case, there are three sources of virtual work: viscous damping of the beams, damping of the joints, and external excitation forces. The virtual work associated with viscous damping of the ith beam can be written

$$\delta W_i = -\sum_{j=1}^{N} 2\varsigma_{ij}\omega_{ij}M\,\dot{\eta}_{ij}\,\delta\eta_{ij} \tag{13}$$

A discussion of the virtual work associated with joint damping will be deferred until later in this section. The virtual work of the external force, shown in Figure 1 to be a time varying point force applied to the first beam, is

$$\delta W_F = F(t)\cdot\delta w_1(x_1=x_F, t) \tag{14}$$

Substituting (5) into (14) gives

$$\delta W_F = \sum_{j=1}^{N} F(t)\,\phi_{1j}(x_1=x_F)\,\delta\eta_{1j} \tag{15}$$

Summing together δW_1, δW_2, δW_3 and δW_F and comparing the resulting expression with (3) yields the following generalized forces:

$$Q_{ij} = \begin{cases} -2\varsigma_{ij}\omega_{ij}M\dot{\eta}_{ij}+F(t)\phi_{1j}(x_F) & ; \quad i = 1 \\[2ex] -2\varsigma_{ij}\omega_{ij}M\dot{\eta}_{ij} & ; \quad i \neq 1 \end{cases} \tag{16}$$

where Q_{ij} is the generalized force associated with η_{ij}.

Constraints

Mathematical constraints are introduced to require that the p_i and r_i coordinates move and rotate with the ends of the beam. Assuming small angles, eight constraint relations can be obtained which relate the modal coordinates to the displacements and rotations of the beams' ends. The eight relations can be written in the matrix form

$$\underline{q} = [G]\,\underline{\eta} \tag{17}$$

where

$$\underline{q} = [p_1, r_1, p_2, r_2, p_3, r_3, p_4, r_4]^T \tag{18}$$

$$\underline{\eta} = [\eta_{11}, \eta_{12}, \ldots, \eta_{1N}, \ldots, \eta_{2N}, \eta_{31}, \ldots, \eta_{3N}]^T \tag{19}$$

[G] is the following 8x3N constant coefficient matrix

$$[G] = \begin{bmatrix} \underline{\phi}_1(L)^T & \underline{0}_N^T & \underline{0}_N^T \\ \underline{\phi}_1'(L)^T & \underline{0}_N^T & \underline{0}_N^T \\ \underline{0}_N^T & \underline{\phi}_2(0)^T & \underline{0}_N^T \\ \underline{0}_N^T & \underline{\phi}_2'(0)^T & \underline{0}_N^T \\ \underline{0}_N^T & \underline{\phi}_2(L)^T & \underline{0}_N^T \\ \underline{0}_N^T & \underline{\phi}_2'(L)^T & \underline{0}_N^T \\ \underline{0}_N^T & \underline{0}_N^T & \underline{\phi}_3(0)^T \\ \underline{0}_N^T & \underline{0}_N^T & \underline{\phi}_3'(0)^T \end{bmatrix} \tag{20}$$

where

$$\underline{\phi}_n(x) = [\phi_{n1}(x), \phi_{n2}(x), \ldots, \phi_{nN}(x)]^T \tag{21}$$

and where $\underline{0}_N$ is an Nx1 zero-vector.

Equations of Motion

At this point, all the items needed for Lagrange's equations (1) and (2) have been assembled. The result of substituting (8), (12), (16) and (17) into (1) and (2) yields 3N+8 governing equations. The 8 equations associated with the generalized coordinates p_i and r_i are simply algebraic relations:

$$-F_1=-\beta_1 \quad ; \quad -M_1=-\beta_2 \quad ; \quad F_1=-\beta_3 \quad ; \quad M_1=-\beta_4 \tag{22}$$

$$-F_2 = -\beta_5 \quad ; \quad -M_2 = -\beta_6 \quad ; \quad F_2 = -\beta_7 \quad ; \quad M_2 = -\beta_8 \qquad (23)$$

The F_i and M_i are forces and moments, respectively, exerted on the beams by the joints. Note that the Lagrange multipliers in this problem are simply the forces and moments of constraint. Combining relations (22) and (23) gives

$$\beta_1 = -\beta_3, \ \beta_2 = -\beta_4, \ \beta_5 = -\beta_7, \ \beta_6 = -\beta_8 \qquad (24)$$

The 3N governing equations associated with the generalized coordinates η_{ij} can be written in the concise matrix-vector form:

$$[M] \, \ddot{\underline{n}} + [C] \, \dot{\underline{n}} + [K] \, \underline{n} = \underline{\phi}_F \, F(t) + [B] \, \underline{\beta} \qquad (25)$$

where [M] is a 3N x 3N diagonal mass matrix with diagonal elements all equal to M and off diagonal elements all equal to zero. [C] is also diagonal and is of the form

$$[C] = \text{Diag}([C^1], \ [C^2], \ [C^3]) \qquad (26)$$

where each N x N $[C^n]$ matrix is given by

$$[C^n] = 2M \, \text{Diag}(\varsigma_{n1}\omega_{n1}, \ \varsigma_{n2}\omega_{n2}, \ldots, \ \varsigma_{nN}\omega_{nN}) \qquad (27)$$

Similarly, the [K] matrix is block diagonal, of the form

$$[K] = \text{Diag}([K^1], \ [K^2], \ [K^3]) \qquad (28)$$

with

$$[K^n] = M \, \text{Diag}(\omega_{n1}^2, \ \omega_{n2}^2, \ldots, \ \omega_{nN}^2) \qquad (29)$$

The vector $\underline{\phi}_F$ is of dimension 3Nx1 and is given by

$$\underline{\phi}_F = [\underline{\phi}_1(x_F)^T, \ \underline{0}_N^T, \ \underline{0}_N^T]^T \qquad (30)$$

Since equation (24) implies that only 4 of the β_j's are necessary, $\underline{\beta}$ is a 4 x 1 vector given by

$$\underline{\beta} = [\beta_1, \beta_2, \beta_5, \beta_6]^T \qquad (31)$$

Finally, the matrix [B] is of dimension 3Nx4 and is given explicitly as

$$[B] = \begin{bmatrix} \underline{\phi}_1(L) & \underline{\phi}_1'(L) & \underline{0}_N & \underline{0}_N \\ -\underline{\phi}_2(0) & -\underline{\phi}_2'(0) & \underline{\phi}_2(L) & \underline{\phi}_2'(L) \\ \underline{0}_N & \underline{0}_N & -\underline{\phi}_3(0) & -\underline{\phi}_3'(0) \end{bmatrix} \qquad (32)$$

At this point, we can introduce the damping forces associated with the joints. In equations (22) and (23), the Lagrange multipliers were identified as the forces and moments transmitted by the joints. Hence, we can add joint damping by modifying the expressions for F_i and M_i to include both spring and damping forces. The spring forces

and moments are given by

$$F_{S1} = \begin{cases} k_1(p_2-p_1-e_1) & ; \ p_2-p_1 > e_1 \\ k_1(p_2-p_1+e_1) & ; \ p_2-p_1 < -e_1 \\ 0 & ; \ \text{otherwise} \end{cases} \qquad (33)$$

$$F_{S2} = \begin{cases} k_1(p_4-p_3-e_1) & ; \ p_4-p_3 > e_1 \\ k_1(p_4-p_3+e_1) & ; \ p_4-p_3 < -e_1 \\ 0 & ; \ \text{otherwise} \end{cases} \qquad (34)$$

$$M_{S1} = \begin{cases} k_2(r_2-r_1-e_2) & ; \ r_2-r_1 > e_2 \\ k_2(r_2-r_1+e_2) & ; \ r_2-r_1 < -e_2 \\ 0 & ; \ \text{otherwise} \end{cases} \qquad (35)$$

$$M_{S2} = \begin{cases} k_2(r_4-r_3-e_2) & ; \ r_4-r_3 > e_2 \\ k_2(r_4-r_3+e_2) & ; \ r_4-r_3 < -e_2 \\ 0 & ; \ \text{otherwise} \end{cases} \qquad (36)$$

where k_1 is the lateral or transverse stiffness constant, e_1 is the clearance distance, k_2 is a rotational stiffness and e_2 is the "rotational clearance". The damping forces and moments are given by

$$F_{D1} = \begin{cases} c_1(\dot{p}_2-\dot{p}_1) & ; \ p_2-p_1 > e_1 \ \text{and} \ \dot{p}_2-\dot{p}_1 > 0 \\ c_1(\dot{p}_2-\dot{p}_1) & ; \ p_2-p_1 < -e_1 \ \text{and} \ \dot{p}_2-\dot{p}_1 < 0 \\ 0 & ; \ \text{otherwise} \end{cases} \qquad (37)$$

$$F_{D2} = \begin{cases} c_1(\dot{p}_4-\dot{p}_3) & ; \ p_4-p_3 > e_1 \ \text{and} \ \dot{p}_4-\dot{p}_3 > 0 \\ c_1(\dot{p}_4-\dot{p}_3) & ; \ p_4-p_3 < -e_1 \ \text{and} \ \dot{p}_4-\dot{p}_3 < 0 \\ 0 & ; \ \text{otherwise} \end{cases} \qquad (38)$$

$$M_{D1} = \begin{cases} c_2(\dot{r}_2-\dot{r}_1) & ; \ r_2-r_1 > e_2 \ \text{and} \ \dot{r}_2-\dot{r}_1 > 0 \\ c_2(\dot{r}_2-\dot{r}_1) & ; \ r_2-r_1 < -e_2 \ \text{and} \ \dot{r}_2-\dot{r}_1 < 0 \\ 0 & ; \ \text{otherwise} \end{cases} \qquad (39)$$

$$M_{D2} = \begin{cases} c_2(\dot{r}_4-\dot{r}_3) & ; \ r_4-r_3 > e_2 \ \text{and} \ \dot{r}_4-\dot{r}_3 > 0 \\ c_2(\dot{r}_4-\dot{r}_3) & ; \ r_4-r_3 < -e_2 \ \text{and} \ \dot{r}_4-\dot{r}_3 < 0 \\ 0 & ; \ \text{otherwise} \end{cases} \qquad (40)$$

where c_1 and c_2 are the lateral and torsional damping constants, respectively. Note that the damping forces and moments are active only when contact has occurred *and* the relative velocity is such that further joint deformation takes place. These so called "one-way" viscous dampers are used to emulate the effects of friction and impact damping.

The total joint forces and moments are given by

$$F_i = F_{Si} + F_{Di} \quad ; \quad i = 1,2 \tag{41}$$

$$M_i = M_{Si} + M_{Di} \quad ; \quad i = 1,2 \tag{42}$$

Equations (22), (23) and (33)-(42) can now be combined in the form

$$\underline{\beta} = \begin{Bmatrix} \beta_1 \\ \beta_2 \\ \beta_5 \\ \beta_6 \end{Bmatrix} = \begin{Bmatrix} F_1 \\ M_1 \\ F_2 \\ M_2 \end{Bmatrix} = \underline{f}\,(\underline{q},\,\underline{\dot{q}}) \tag{43}$$

Equations (17), (25) and (43) can be combined into two first-order vector differential equations. Substituting (17) into (43) yields

$$\underline{\beta} = \underline{f}\,([G]\,\underline{\eta},\,[G]\,\underline{\dot{\eta}}) = \underline{f}_1(\underline{\eta},\,\underline{\dot{\eta}}) \tag{44}$$

Substituting (44) into (25) gives

$$[M]\underline{\ddot{\eta}} + [C]\underline{\dot{\eta}} + [K]\underline{\eta} = \underline{\phi}_F F(t) + [B]\underline{f}_1(\underline{\eta},\,\underline{\dot{\eta}}) \tag{45}$$

Defining $\underline{\eta}_1 = \underline{\eta}$ and $\underline{\eta}_2 = \underline{\dot{\eta}}$, equation (45) becomes

$$\underline{\dot{\eta}}_1 = \underline{\eta}_2 \tag{46}$$

$$\underline{\dot{\eta}}_2 = [M]^{-1}\left\{-[C]\underline{\eta}_2 - [K]\underline{\eta}_1 + \underline{\phi}_F F(t) + [B]\underline{f}_1(\underline{\eta}_1,\,\underline{\eta}_2)\right\} \tag{47}$$

Equations (46) and (47) are coupled, nonlinear, ordinary differential equations of first order. In this form, they are easily analyzed using standard time integration software packages. In the next section, this model is used to generate parametric results relating system damping and system response frequencies to joint properties.

RESULTS

In this section, results are presented and discussed for the system consisting of three linear, elastic beams connected by two nonlinear joints. The baseline system parameters are listed in Table 1. The beams are approximately 1 inch (2.54 cm) in diameter and 1 meter in length. Baseline damping for each flexible beam was chosen to be 0.1% in all (component) beam modes.

A sample impulse response is shown in Figure 3 for the baseline system. The impulse is approximated by a constant amplitude force, $F = 25$ N, applied at the midpoint of the first beam ($x_F = 0.5$) for a duration of $T = 0.036$ sec. Three beam modes are used for each of the three beams, giving the combined system nine degrees of freedom. The displayed outputs correspond to the transverse displacements at the midpoints of the first and second beams. Beam displacements are normalized by the beam outer diameter, d_o. It is seen that the second beam responds with a higher amplitude than the first beam, due to the shape of the first "mode" of the three-beam system.

The two displacements show good qualitative agreement. Damping calculations can be made from the free and impulse response curves using the log decrement approach as was done in References [7] and [8]. To investigate the dependence of damping on amplitude, the damping ratio was calculated at several different points along the free response curves. It was found that, as in the rigid beam system studied in References [7] and [8], the damping is inversely proportional to the amplitude. Also evident from an examination of the free response is the dependence of the fundamental response frequency with amplitude. As with all systems having "hardening-spring" type nonlinearities, the response frequencies tend to increase with amplitude.

Forced response to harmonic excitation, $F(t) = F\cos(\omega t)$, was also studied. Figure 4 shows the frequency response curves for two levels of forcing $F = 1.0$ and $F = 0.3$. In each case the forcing is applied to the midpoint of the first beam ($x_F = 0.5$), coincident with the point at which the displacement is calculated. The natural frequency of the system is approximately $\omega = 5.5$ rad/s. This is approximately 1/3 of the first natural frequency of a pinned-pinned beam with identical cross-sectional properties and having length of 3 meters ($\omega_1 = 16.7$ rad/s). Note that the curves exhibit marked hardening spring characteristics, with the response curves "bending to the right" as the amplitude is increased. Associated with this hardening spring characteristic is the presence of "multiple-valued" steady-state response. The standard hardening spring frequency response curve has a range of frequencies for which there are three possible amplitudes of response. It usually is the case that only the highest and lowest amplitude solutions are stable; the middle amplitude solution is unstable [13]. For both levels of excitation, Figure 4 shows that, over a limited range of frequency, multiple steady-state solutions are possible. The unstable solution branches are denoted by the dashed lines in Figure 4. Note that if the hardening spring characteristics were cubic in nature, the frequency response curves would continue to bow to the right as the amplitude is increased. However, with piecewise linear systems, as the amplitude increases, the effective spring stiffness asymptotically approaches the stiffness associated with large amplitude response.

As with the rigid beam model studied in References [7] and [8], the three-beam model experienced a variety of different types of nonlinear behavior. When forced below its natural frequency, the system often exhibited super-harmonic response. At frequencies of excitation higher than the natural frequency of the system, the response often exhibited subharmonic motion. Since most joints have clearances and/or hardening spring characteristics, the influence of nonlinear behavior on the performance of linear controllers and estimators for flexible space structures should be investigated.

CONCLUSIONS

A simplified model of a flexible space structure consisting of three visco-elastic beams and two nonlinear sleeve joints was studied. The equations of motion were derived using component mode analysis. These equations were time simulated to investigate the dependence of system damping

and system behavior on various joint properties. It is found that the damping appears to be directly dependent on amplitude. Larger amplitudes tended to give rise to larger "damping ratios" than small amplitudes. It was also found that even a small amount of play in the sleeve joints caused nonlinear, hardening spring behavior to become evident. The presence of sub- and super-harmonics under sinusoidal excitation was observed.

REFERENCES

1. Balas, M.J., "Active Control of Flexible Systems," Journal of Optimization Theory and Applications, Vol. 25, No. 3, 1978, pp. 415-436.

2. Alberts, T.E., Hastings, G.G., Book, W.J., and Dickerson, S.L., "Experiments in Optimal Control of a Flexible Arm with Passive Damping," Fifth VPI&SU/AIAA Symposium on Dynamics and Control of Large Structures, 12-14 June 1985, Blacksburg, VA.

3. Alberts, T.E., "Augmenting the Control of a Flexible Manipulator with Passive Mechanical Damping," Ph.D. Thesis, School of Mechanical Engineering, Georgia Institute of Technology, Atlanta, GA, September 1986.

4. Hertz, T.J., and Crawley, E.F., "Damping in Space Structure Joints," AIAA Dynamics Specialists Conference, 17-18 May 1984, Palm Springs, CA.

5. Hertz, T.J. and Crawley, E.F., "The Effects of Scale on the Dynamics of Flexible Space Structures," Report No. SSL 18-83, Space Systems Laboratory, Department of Aeronautics and Astronautics, Massachusetts Institute of Technology, Cambridge, MA, September 1983.

6. Crawley, E.F., Sarver, G.L., and Mohr, D.G., "Experimental Measurement of Passive Material and Structural Damping for Flexible Space Structures," Acta Astronautica, Vol. 10, No. 5-6, 1983, pp. 381-393.

7. Ferri, A.A., "Modelling and Analysis of Nonlinear Sleeve Joints of Large Space Structures," To appear in the AIAA Journal of Spacecraft and Rockets.

8. Ferri, A.A., "Investigation of Damping from Nonlinear Sleeve Joints of Large Space Structures," Proceedings of the 11th Biennial Conference on Mechanical Vibrations and Noise, Boston, MA, September 27-30, 1987.

9. Dowell, E.H., "Component Mode Analysis of Nonlinear and Nonconservative Systems," ASME Journal of Applied Mechanics, Vol. 47, March 1980, pp. 172-176.

10. Tongue, B.H. and Dowell, E.H., "Component Mode Analysis of Nonlinear, Nonconservative Systems," ASME Journal of Applied Mechanics, Vol. 50, March 1983, pp. 204-209.

11. Dowell, E.H., "The Behavior of a Linear, Damped Modal System with a Nonlinear Spring-Mass-Dry Friction Damper System Attached," J. of Sound and Vibration, Vol. 89, No. 1, 1983, pp. 65-84.

12. Ferri, A.A., and Dowell, E. H., "The Behavior of a Linear, Damped Modal System with a Nonlinear Spring-Mass-Dry Friction Damper System Attached, Part II," Journal of Sound Vibration, Vol. 101, No. 1, 1985, pp. 55-74.

13. Meirovitch, L., Elements of Vibration Analysis, McGraw-Hill, New York, 1975.

Table 1. Baseline Parameter Values

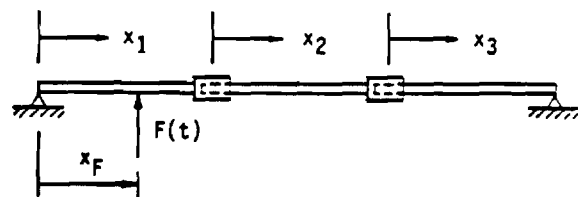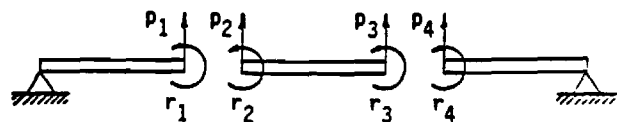| Item	Baseline Value	Units
m	3.2552	kg/m
E	7.4464×10^{10}	N/m^2
I	1.014×10^{-8}	m^4
L	1	m
k_1	20,000	N/m
k_2	100	N·m/rad
c_1	50	N·s/m
c_2	0.75	N·m·s/rad
e_1	0.0001	m
e_2	0.0035	rad
ς	0.001	-

Figure 1. Three-beam system.

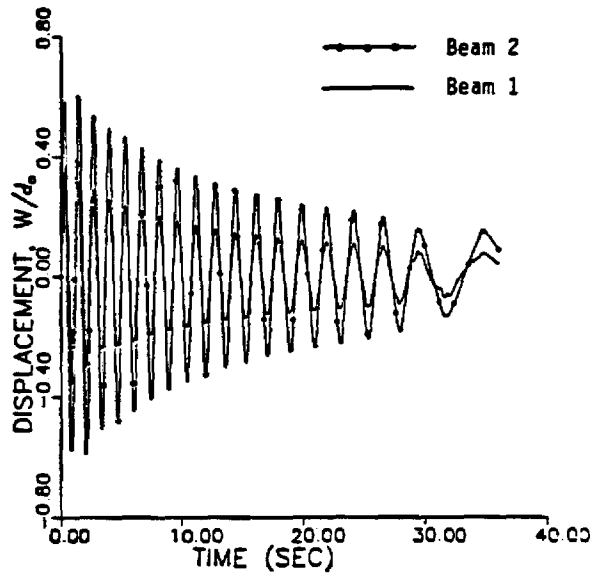Figure 2. Definition of beam-end coordinates.

Figure 3. Impulse response. Transverse displacements at the midpoints of beams 1 and 2 (normalized by beam outer diameter, d_o).
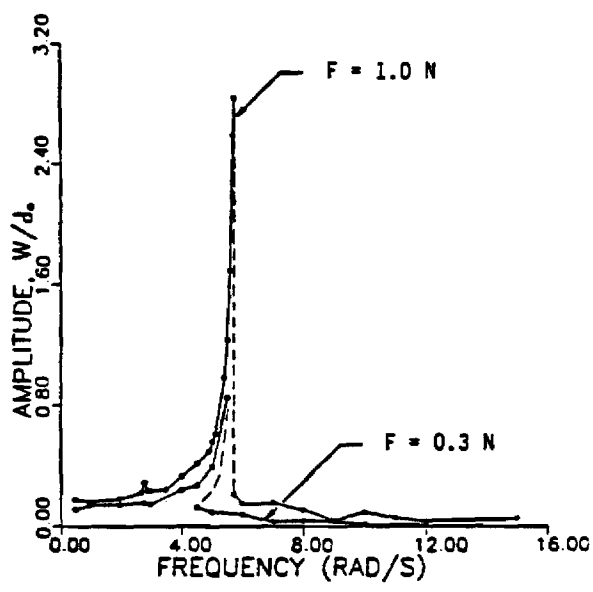

Figure 4. Amplitude w/d_o vs frequency of excitation; two levels of excitation amplitude.

Appendix B

Analysis of Flexible Structures with Nonlinear Joints

1.   Ferri, A.A., "An Improved Algorithm for Galerkin Solutions to Nonlinear Systems," Presented at the ASME/SES Applied Mechanics and Engineering Sciences Conference, Berkeley, CA, June 20-22, 1988.

2.   Ferri, A.A., "A-Posteriori Error Estimates for Harmonic Balance Solution Techniques," In preparation, to be submitted to the ASME Journal of Vibration and Acoustics.

An Improved Algorithm for Galerkin Solutions to Nonlinear Systems

Aldo A. Ferri
School of Mechanical Engineering
Georgia Institute of Technology
Atlanta, Georgia 30332-0405

Galerkin and Harmonic Balance solution routines have been used extensively to find approximate solutions to the governing equations of nonlinear systems. Typically, these solutions are approximated by a finite number of basis functions. In order to check the accuracy of the Galerkin approximate solution, a few approaches can be used. First, an N term Galerkin solution can be checked against an N+1 term solution to see whether an appropriate level of convergence is obtained. A second approach is to compute the solution using an alternate technique and compare it to the Galerkin solution. For example, time integration or finite element techniques can be used to provide an independent check on the Galerkin solution. Of course, both of these approaches have the disadvantage of requiring significantly more computation. An alternative accuracy indicator is developed here and incorporated in a Galerkin solution algorithm. The method is applied to find the steady state time response to harmonically forced nonlinear systems. In this case, the error criterion turns out to be proportional to the higher harmonic content in the output of the nonlinearity. The algorithm is computer implemented and tested on a forced Duffing equation and a Coulomb damped system. It is found that the behavior of the error parameter can be used to judge quantitatively the suitability of Galerkin solution routines to various types of nonlinear systems. In addition, the use of this error criterion to form an algorithm that automatically picks the correct number of basis functions and the efficiency of implementation of this error criterion is discussed.

A-Posteriori Error Estimates for Harmonic Balance
Solution Techniques

Aldo A. Ferri
Assistant Professor
School of Mechanical Engineering
Georgia Institute of Technology
Atlanta, Georgia 30332-0405

Abstract:

The harmonic balance method is commonly applied to linear and nonlinear systems to approximate their steady-state response to periodic excitation. This paper presents two different a-posteriori error estimates for harmonic balance solution techniques. The first is computationally easy to calculate, but is less reliable as an indication of accuracy. The second is more difficult to calculate, but provides a better indication of solution accuracy. Numerical results for a Duffing-type oscillator are presented for each error estimate.

Introduction:

The Harmonic Balance (HB) method is commonly applied to linear and nonlinear systems to approximate their steady-state response to periodic excitation. Unlike time integration and other time domain techniques, the harmonic balance technique does not involve consideration of a transient response, therefore it is very well suited to those systems that have low levels of damping. Another advantage over time domain methods is the ease with which it can handle systems with widely differing response frequencies. Such systems are termed numerically "stiff" [1,2]. This characteristic seriously impedes the efficiency and accuracy of time integration schemes but does not significantly affect the performance of HB algorithms. Systems such as large flexible space structures, flexible robotic manipulators and turbomachinery systems can have both low damping levels and

widely differing response frequencies and, so, are ideal applications for the harmonic balance technique.

An "exact" steady-state solution of a nonlinear system to periodic excitation will, in general, be composed of an infinite set of frequencies. In the case of period-1 solutions; i.e., solutions that repeat with the fundamental period of the excitation, the solution is generally composed of the fundamental excitation frequency plus a countable number of harmonics of the excitation frequency. In practice, the amplitude of the "higher harmonics" will be substantially lower than the "first few" harmonics, hence, it is justified to include only a finite number of harmonics in the analysis. In most cases, however, it is not known apriori how many harmonics will constitute a good approximation to the exact solution. In some cases, a single harmonic provides a very accurate approximation. Other situations may require many harmonics to adequately represent their steady-state response; for example, systems with relay nonlinearities and hard limiters. The most difficult systems to analyze from a practical standpoint are those for which the appropriate number of harmonics change with the frequency or the amplitude of excitation or with initial conditions. Good examples of this may be found in dry friction damped systems [3,4]. When forced harmonically near a resonant frequency, a dry friction damped system will generally respond with the frequency of excitation and negligible amounts of higher harmonics. However, in those frequency ranges where stick-slip motion occurs, a larger number of harmonics are needed to obtain the desired level of accuracy. When frequency

response curves are desired over a range of excitation frequencies, an estimate of solution accuracy is necessary to ensure that the desired level of accuracy is maintained.

This paper addresses a-posteriori estimates of accuracy. Such an accuracy estimate is essential in being able to develop adaptive solution techniques which automatically determine the numbers of harmonics that are sufficient to obtain a specified level of accuracy. The problem is similar to that encountered in the Finite Element Method. See the papers on adaptive mesh refinement [5-8]. In the following sections, two error parameters are developed that can be used to assess the accuracy of the frequency domain solution in a computationally efficient way. Their interpretation will be discussed and each will be calculated for a harmonically forced Duffing-type oscillator. These error parameters will also be compared to a more conventional measure of solution accuracy, namely the root mean square (RMS) difference between the HB and the time integration solutions.

Development of Error Estimates

The simplest form of a-posteriori accuracy check is to compare the HB solutions against other solutions which are known to be more accurate. For example, one could compare the HB solution to the solution obtained through time integration. This, however, presents three problems. The first is the excessive computation time required to obtain the time integrated result. The second is that it is difficult to know whether the time integration solution is indeed accurate. A choice of time step that is too large may lead to a numerically unstable computation. The third problem is that the periodic

solution that is desired may, in fact, be an unstable equilibrium. Finding this steady-state solution using time integration may be quite difficult, especially when the periodic solution has saddle-type stability.

A second approach to checking a multi-harmonic solution is to compare an n harmonic result to a n+m harmonic result, $m \geq 1$. The primary drawback to this approach is that of computation time; it requires at least twice the computation time to calculate the accuracy check as to calculate the original answer. Furthermore, the accuracy check itself is guaranteed to produce at least as accurate a result [9] negating to some extent the need for the original solution. Here, the objective is to develop efficient ways of determining the accuracy of a HB result after it has been obtained.

The two error estimates presented here are developed for a general, nonlinear second-order system, although the method is easily extended to multi-degree-of-freedom systems. Consider the following system:

$$m\ddot{z} + c\dot{z} + kz + h(z,\dot{z}) = F(\omega t) \qquad (1)$$

where $\cdot$ represents a derivative with respect to time and h is a general nonlinear function of z and $\dot{z}$ which need not be continuous. Using the standard definitions for viscous damping ratio and natural frequency for the linear part of (1) gives

$$m(\ddot{z} + 2\varsigma\omega_n \dot{z} + \omega_n^2 z) + h(z,\dot{z}) = F(\omega t) \qquad (2)$$

Defining $\tau = \omega t$ and denoting derivatives with respect to τ with a prime gives

$$m(\omega^2 z'' + 2\varsigma\omega_n\omega z' + \omega_n^2 z) + g(z,z') = F(\tau) \qquad (3)$$

where

$$g(z,z') = h(z,\omega z')$$

Finally, defining $\epsilon = 1/k$, $f(\tau) = F(\tau)/k$ and $\Omega = \omega/\omega_n$, equation (3) becomes

$$\Omega^2 z'' + 2\varsigma\Omega z' + z + \epsilon g(z,z') = f(\tau) \qquad (4)$$

For the remainder of this paper, it will be assumed that $f(\tau)$ is simply harmonic; i.e., $f(\tau)$ = $f^c\cos(\tau) + f^s\sin(\tau)$. The extension to the case of two or more harmonics is straightforward. The first step in any HB solution is to assume that the solution $z(\tau)$ is period-1 with the following form:

$$\hat{z}(\tau) = \sum_{i=1}^{n} z_i^c \cos i\tau + z_i^s \sin i\tau \qquad (5)$$

Note that the constant or "bias" term has been omitted but can be included without difficulty. Substituting (5) into (4) yields

$$\Omega^2 \hat{z}'' + 2\varsigma\Omega\hat{z}' + \hat{z} + \epsilon g(\hat{z},\hat{z}') - f(\tau) = e(\tau) \qquad (6)$$

where $e(\tau)$ is a residual term which arises because (5) satisfies (4) only approximately. Following the Galerkin procedure, the coefficients z_i^c and z_i^s in (5) are chosen to render $e(\tau)$ orthogonal to each of the temporal harmonics in (5). Thus the following 2n scalar equations are obtained:

$$\left.\begin{array}{l} \langle e(\tau), \cos i\tau \rangle = 0 \\[1em] \langle e(\tau), \sin i\tau \rangle = 0 \end{array}\right\} \qquad i = 1, 2, \ldots n \qquad (7)$$

where the inner product is defined as

$$\langle a(\tau), b(\tau) \rangle = \frac{1}{\pi} \int_0^{2\pi} a(\tau)b(\tau) \ d\tau \qquad (8)$$

These 2n equations can be written in the vector form

$$\underline{R}_n(\underline{z}_n) = [CL_n]\underline{z}_n + \{\underline{RNL}_n\} = \underline{0} \qquad (9)$$

where

$$\underline{z}_n = [z_1^c, z_2^c, \ldots, z_n^c, z_1^s, \ldots, z_n^s]^T \qquad (10)$$

$$[CL_n] = \begin{bmatrix} [A] & [B] \\ -[B] & [A] \end{bmatrix} \qquad (11)$$

$$[A] = -\Omega^2 \text{Diag}(1, 4, \ldots, n^2) + I_n \qquad (12)$$

$$[B] = 2\varsigma\Omega \ \text{Diag}(1, 2, \ldots, n) \qquad (13)$$

$$\{\underline{RNL}_n\} = \epsilon \left\{ \begin{array}{c} \langle g(\hat{z}, \hat{z}'), \cos 1\tau \rangle - f^c \\ \langle g(\hat{z}, \hat{z}'), \cos 2\tau \rangle \\ \vdots \\ \langle g(\hat{z}, \hat{z}'), \cos n\tau \rangle \\ \langle g(\hat{z}, \hat{z}'), \sin 1\tau \rangle - f^s \\ \langle g(\hat{z}, \hat{z}'), \sin 2\tau \rangle \\ \vdots \\ \langle g(\hat{z}, \hat{z}'), \sin n\tau \rangle \end{array} \right\} \qquad (14)$$

Note that I_n is an nxn identity matrix. When numerical solutions to (9) (or, equivalently (7)) are sought, it is customary to use some norm of R_n as a measure of the accuracy of the solution vector z. Often, in iterative solution techniques, iteration is continued until the norm of R_n is smaller than some specified convergence parameter.

Now, consider a m-harmonic residue vector, with m > n.

$$\underline{R}_m(\underline{z}_m) \tag{15}$$

where z_m is based on the previously found n-harmonic result:

$$\underline{z}_m = [z_1^c, z_2^c, \ldots, z_n^c, 0, 0, \ldots, 0, z_1^s, z_2^s, \ldots, z_n^s, 0, 0, \ldots, 0]^T \tag{16}$$

Note that if the n-harmonic result is accurate compared to an m-harmonic solution (m > n), then the coefficients of the cosine and sine components of frequencies $n+1, n+2, \ldots, m$ should be "small" in some appropriate sense. Thus, one check on the accuracy of z_n is given by the norm of $R_m(z_m)$. It is desirable to find a computationally efficient way of expressing the norm of R_m. The 2m scalar equations comprising R_m can be separated into four groups.

$$\langle e(\tau), \cos i\tau \rangle \qquad i=1,\ldots,n \tag{17a}$$

$$\langle e(\tau), \cos j\tau \rangle \qquad j=n+1,\ldots,m \tag{17b}$$

$$\langle e(\tau), \sin i\tau \rangle \qquad i=1,\ldots,n \tag{17c}$$

$$\langle e(\tau), \sin j\tau \rangle \qquad j=n+1,\ldots,m \tag{17d}$$

It is important to recognize that the solution vectors z_n and z_m imply the same expression for $\hat{z}(\tau)$, since the coefficients of the harmonics $n+1$ through m are identically zero in

both cases. Therefore, $e(\tau)$ appearing in (17a)-(17d) is the exact same function as that appearing in equation (7) and consequently, (17a) and (17c) form the elements of R_n. It is also apparent that, since the linear portion of (6) does not contain any harmonics greater than n, (17b) and (17d) depend only on the nonlinearity, g. If the Euclidean or l_2 norm is considered, the following expression is found

$$\left\| R_m(z_m) \right\|_2 = \left\| R_n(z_n) \right\|_2 + \mu^2 \tag{18}$$

where

$$\mu = \epsilon \left[\sum_{j=n+1}^{m} \langle g(\hat{z},\hat{z}'), \cos j\tau \rangle^2 + \langle g(\hat{z},\hat{z}'), \sin j\tau \rangle^2 \right]^{1/2} \tag{19}$$

It may be noted that the inner-product terms in (19) are simply the Fourier coefficients of g for the frequencies $n+1$ through m. Thus an interesting interpretation of μ is that it is proportional to the RMS spillover of g into the harmonics $n+1$ through m. As will be discussed later, μ is computationally very easy to calculate. This is especially true if an FFT is used to evaluate the Fourier coefficients appearing in (19). Furthermore, if an FFT algorithm is used to evaluate the inner-product terms in (14), then the terms appearing in (19) are already available for use.

Looking at (18) it is clear that $|R_m|$ will be equal to $|R_n|$ when μ is identically zero. If z_n is a sufficiently accurate solution then $|R_n|$ is approximately zero. Thus the size of R_m is mostly dependent on the size of μ. A "large" value of μ indicates that the n-harmonic solution does not represent a very accurate m-harmonic result. One drawback of using μ

solution does not represent a very accurate m-harmonic result. One drawback of using μ as an indicator of solution accuracy is that it tends to increase with increasing amplitude. This is most readily seen when one considers that μ is proportional to the RMS spillover in the higher harmonics. As the amplitude increases, so must μ. In order to remove some of this amplitude dependence, μ can be normalized with respect to a quantity that also grows with amplitude. The following normalization scheme is used

$$\hat{\mu} = \frac{\mu}{\epsilon} \left[\sum_{j=1}^{n} <g(\hat{z},\hat{z}'),\cos j\tau>^2 + <g(\hat{z},\hat{z}'),\sin j\tau>^2 \right]^{-1/2} \quad (20)$$

The error parameters μ and $\hat{\mu}$ have the deficiency that they do not utilize any of the information associated with the linear portion of the differential equation. Furthermore, they do not directly reflect the error in the solution vector. To examine this further, consider the true solution to the m-harmonic residue vector z_m^* and determine an expression for the error between it and z_m:

$$\underline{R}_m(\underline{z}_m^*) = \underline{0} = \underline{R}_m(\underline{z}_m + \Delta \underline{z}_m) \approx \underline{R}_m(\underline{z}_m) + \left. \frac{\partial \underline{R}_m}{\partial \underline{z}_m} \right|_{\underline{z}=\underline{z}_m} \Delta \underline{z}_m \quad (21)$$

where $\Delta z_m = z_m^* - z_m$. Defining $[C_m]$ to be the 2mx2m dimensioned Jacobian matrix, equation (20) can be solved for Δz_m

$$\Delta \underline{z}_m = -[C_m]^{-1} \underline{R}_m(\underline{z}_m) \quad (22)$$

The error parameter ν is defined to be the error in the norm of the solution vector divided by the norm of the solution vector

$$\nu = \frac{|\Delta z_m|}{|z_m|} = \frac{|\,[C_m]^{-1} R_m(z_m)\,|}{|z_n|} \tag{23}$$

Note that ν requires more computation than μ, but that it more correctly reflects the error in the solution vector. It is interesting to study equation (21). A well known property of induced norms is that [10]

$$\frac{|R_m(z_m)|}{|[C_m]|} \leq |\Delta z_m| \leq |[C_m]^{-1}| |R_m(z_m)| \tag{24}$$

It is seen that the relationship of $|R_m|$ to $|\Delta z_m|$ is dependent on the Jacobian matrix $[C_m]$. If $[C_m]^{-1}$ is small (indicating that R is "steep" in the vicinity of z_m) large values of $|R_m|$ do not necessarily imply large errors in the solution vector. Alternatively, if $[C_m]^{-1}$ is large (indicating that R is "shallow" in the neighborhood of z_m) then a small value of $|R_m|$ does not necessarily imply a small error in the solution vector.

References

1. Conte, S.D. and deBoor, C., <u>Elementary Numerical Analysis: An Algorithmic Approach</u>, McGraw-Hill Book Co., New York, 1980.

2. Gear, C.W., <u>Numerical Initial Value Problems in Ordinary Differential Equations</u>, Prentice-Hall, New Jersey, 1971.

3. Pierre, C., Ferri, A.A. and Dowell, E.H., "Multi-Harmonic Analysis of Dry Friction Damped Systems using an Incremental Harmonic Balance Method," ASME Journal of Applied Mechanics, Vol. 52, No. 4, December 1985, pp.958-964.

4. Ferri, A.A. and Dowell, E.H., "Frequency Domain Solutions to Multi-Degree-of-Freedom, Dry Friction Damped Systems," Journal of Sound and Vibration, Vol. 124, No. 2, 1988, pp. 207-224.

5. Zienkiewicz, O.C., "The Generalized Finite Element Method-State of the Art and Future Directions," ASME Journal of Applied Mechanics, Vol. 50, No. 4b, December 1983, pp. 1210-1217.

6. Babuska, I. and Rheinboldt, W.C., "A-Posteriori Error Estimates for the Finite Element Method," International Journal for Numerical Methods in Engineering, Vol. 12, 1978, pp. 1597-1615.

7. Babuska, I. and Rheinboldt, W.C., "Adaptive Approaches and Reliability Estimations in Finite Element Analysis," Computer Methods in Applied Mechanics and Engineering, 17/18, 1979, pp. 519-540.

8. Zienkiewicz, O.C. and Zhu, J.Z., "A Simple Error Estimator and Adaptive Procedure for Practical Engineering Analysis," International Journal for Numerical Methods in Engineering, Vol. 24, 1987, pp. 337-357.

9. Urabe, M., "Galerkin's Procedure for Nonlinear Periodic Systems," Archive for Rational Mechanics and Analysis, Vol. 20, No. 2, 1965, pp. 120-152.

10. Noble, B. and Daniel, J.W., <u>Applied Linear Algebra, Second Edition</u>, Prentice-Hall, Inc., New Jersey, 1977.

Appendix C

Design of Flexible Structures with Nonlinear Joints

1.   Anderson, J.R. and Ferri, A.A., "Behavior of a Single-Degree-of-Freedom System With a Generalized Friction Law," To appear in the Journal of Sound and Vibration.

2.   Anderson, J.R. and Ferri, A.A., "Behavior of a Nonlinear System with an Amplitude-Dependent Coulomb Friction Law," Presented at the 26th Annual Meeting of the Society of Engineering Science, Ann Arbor, MI, Sept. 18-20, 1989.

3.   Ferri, A.A., "Damping and Vibration of Beams with Various Types of Frictional Support Conditions," Proceedings of the 30th AIAA/ASME/ASCE/AHS/ASC Structures, Structural Dynamics and Materials Conference, Mobile, AL, April 3-5, 1989.

4.   Ferri, A.A. and Heck, B.S., "Active and Passive Joints for Damping Augmentation of Large Space Structures," Accepted as a full paper for the 1990 American Control Conference. Also, submitted to the AIAA Journal of Guidance, Control and Dynamics.

BEHAVIOR OF A SINGLE-DEGREE-OF-FREEDOM SYSTEM
WITH A GENERALIZED FRICTION LAW

James R. Anderson
Graduate Research Assistant

Aldo A. Ferri
Assistant Professor

School of Mechanical Engineering
Georgia Institute of Technology
Atlanta, GA 30332-0405

Abstract

Though single-degree-of-freedom systems with classical dry (Coulombic) friction have been studied extensively, the properties of systems damped with generalized friction laws have not been thoroughly examined. This paper investigates the properties of a system damped by a combination of viscous damping, dry friction with constant normal force, dry friction with amplitude-dependent normal force, and dry friction with rate-dependent normal force. This system is studied first using an "exact" time domain method and using first-order harmonic balance. The stick-slip behavior of the system is also studied. It is seen that amplitude-dependent normal force gives rise to a viscous-like damping characteristic. It is also seen that the response amplitude can be decreased or increased by the addition of amplitude-dependent friction.

1. Introduction

Dry friction is an important source of mechanical damping in many physical systems. In fact, in systems such as turbomachinery rotors and large flexible space structures, dry friction may be the most important source of energy dissipation. In turbine blade systems, many researchers have studied the dynamic behavior of dry friction damped rigid and/or elastic blades [1–11]. In most of these studies, it is assumed that the normal force to the sliding interface is constant. This may be termed the "classic" dry friction damped case. In the few studies where the normal force was allowed to vary with blade amplitude, it was found that the system exhibited a viscous-like damping characteristic; see, for example, Bielawa [11]. In the field of large space structures (LSS) the inclusion of amplitude-dependent normal forces have also produced viscous-like damping properties [12–14]. In most frictionally damped physical systems, some amplitude dependence is natural, although at times the amplitude-dependent component of the total friction force may be small compared to that of the constant normal force.

The viscous-like damping property suggests that many mechanical designs can be improved by configuring frictional interfaces in ways that allow normal forces to vary with displacement. In some applications, classic dry friction is inadequate to suppress vibration. For example, turbine blade systems experiencing flutter cannot be globally stabilized with classic dry friction. See, for example, Ferri [15] and Griffin and Sinha [8]. The deficiency stems from the well known property

of classically damped systems that the effective damping varies inversely with the amplitude of the response. Hence, for a sufficiently large disturbance, it is possible for the energy input to the system by aerodynamic forces to overcome the energy dissipation provided by dry friction. By designing turbine blade systems so that the friction forces are dependent on blade displacement, it may be possible to greatly increase the stable operating region of turbine blades. Taking advantage of amplitude-dependent friction forces in the design of LSS joints may also significantly increase the passive damping level of spacecraft.

This paper systematically examines the dynamic behavior of a single-degree-of-freedom system with amplitude- and rate-dependent friction forces. As will be shown, a system with amplitude-dependent friction is much more likely to experience intermittent sticking. If the system sticks a significant amount of time, the energy disssipation capability may be seriously degraded. Hence, special care is taken in this analysis to examine sticking conditions. In the following sections, the model and subsequent equations of motion are developed. Approximate solutions are presented to gain qualitative insight to the problem. Sticking conditions are determined for different ranges of parameter values. Finally, the exact solution to the equation of motion is developed. Representitive results are also presented.

2. Model Development and Analysis

The extended friction law considered in this paper is given by

$$F_f = \mu(K_0 + K_1|x| + K_2|\dot{x}|)\text{sgn}(\dot{x}) \tag{1}$$

where x represents the relative slip displacement, $\dot{x}$ represents the relative slip velocity, K_0 is the constant portion of the normal force, K_1 is the friction interface amplitude "gain", K_2 is the friction interface velocity "gain", and μ is the coefficient of friction. In general, the friction coefficient, μ, should be written as a static coefficient, μ_s, when $\dot{x} = 0$ and a dynamic coefficient,

μ_d, when $\dot{x} \neq 0$. However, in this paper, it will be assumed that $\mu_s = \mu_d = \mu$.

Two possible systems having a generalized friction law are shown in Figures 1a and 1b. The device in Figure 1a is purely "passive" while Figure 1b represents an "active" device. The equation of motion for either system forced harmonically is given by

$$m\ddot{x} + c\dot{x} + kx + \mu(K_0 + K_1|x| + K_2|\dot{x}|)\text{sgn}(\dot{x}) = F \cos \omega t \tag{2}$$

Introducing the following nondimensional quantities:

$$z = \frac{kx}{\mu K_0} \quad \Omega = \frac{\omega}{\sqrt{k/m}} \quad f = \frac{F}{\mu K_0} \quad \zeta = \frac{c + \mu K_2}{2\sqrt{km}} \quad \kappa_1 = \frac{\mu K_1}{k} \quad \tau = \omega t \quad ' \equiv \frac{d}{d\tau} \tag{3}$$

Eq. (2) becomes

$$\Omega^2 z'' + 2\zeta\Omega z' + z + \text{sgn}(z') + \kappa_1|z|\text{sgn}(z') = f \cos \tau \tag{4}$$

Note that the μK_2 parameter is mathematically equivalent to a viscous damping coefficient. For this reason the effect of K_2 is contained in the viscous damping ratio ζ.

Unfortunately, this nondimensionalization scheme does not permit the study of the case $K_0 = 0$; therefore, a second nondimensionalization scheme is also considered. For this situation the following dimensionless variable is introduced:

$$\bar{z} = \frac{kx}{F} \tag{5}$$

This leads to the equation of motion

$$\Omega^2 \bar{z}'' + 2\zeta\Omega \bar{z}' + \bar{z} + \kappa_1|\bar{z}|\text{sgn}(\bar{z}') = \cos \tau \tag{6}$$

where Ω, ζ, κ_1 are as defined in (3). It may be noted that there is a strong similarity between equations (4) and (6). The equations differ only in the exclusion of the $\text{sgn}(\bar{z}')$ term in (6) and the forcing term, f scaled to unity in (6). It is important to note, however, that these equations

are cast in terms of variables scaled to different parameters. Approximate solutions to (4) and (6), will now be sought.

2.1 Approximate Solutions

First order harmonic balance will be used to form an approximate solution to (4) and (6). The response is first assumed to be composed of a single harmonic

$$z(t) = Z_c \cos \tau + Z_s \sin \tau. \tag{7}$$

The amplitude of the response is given by

$$Z = \sqrt{Z_c^2 + Z_s^2}. \tag{8}$$

Obviously, this approximation will be best for the case of stick-free motion. At low frequencies, it may be expected that this approximation will be less accurate as sticking is known to occur more often there [16]. Next, the assumed response (7) is substituted into the equation of motion, (4) or (6). The equation is then multiplied by $\cos \tau$ and integrated over one period. Multiplying the equation of motion by $\sin \tau$ and integrating provides another relation. These two equations, along with (8), lead to the response functions given by (9) and (10), for the governing equations (4) and (6), respectively.

$$\frac{Z}{f} = \frac{1}{\sqrt{(1 - \Omega^2)^2 + (2\zeta\Omega + 4/(\pi Z) + 2\kappa_1/\pi)^2}} \tag{9}$$

$$\tilde{Z} = \frac{1}{\sqrt{(1 - \Omega^2)^2 + (2\zeta\Omega + 2\kappa_1/\pi)^2}} \tag{10}$$

From equations (9) and (10) approximate frequency response plots can be generated. Also, equivalent viscous damping can be found by equating the second term under the square-root sign in (9) and (10) with the quantity $(2\zeta_{eq}\Omega)^2$. This yields

$$\zeta_{eq} = \zeta + \zeta_0 + \zeta_1 \tag{11}$$

where

$$\zeta_0 = \frac{2}{\pi \Omega Z} \tag{12}$$

$$\zeta_1 = \frac{\kappa_1}{\pi \Omega} \tag{13}$$

and ζ is defined in (3). For the $K_0 = 0$ case, $\zeta_0 = 0$. For $K_0 \neq 0$ at resonance, $\zeta_0 = 2/\pi Z$ which means that damping decreases with increasing amplitude. In the absence of ζ and ζ_1, it is theoretically possible to get an unbounded response at resonance (provided that $f > 4/\pi$)[17]. Both ζ and ζ_1 have the effect of bounding the response at resonance. Note that at resonance, $\zeta_1 = \text{constant} = \kappa_1/\pi$, resembling the linear viscous damping ratio ζ. It should be emphasized that relations (12) and (13) are approximate relations which reveal the qualitative trends in the type of damping resulting from the constant component of the normal force and the amplitude-dependent portion of the normal force. Also, this approximation is not very accurate for the case of stick-slip motion, which is known to be more prevalent at low amplitudes and low frequencies of excitation.

2.2 Sticking Regions in Phase Space

Much insight to the behavior of the system can be gained by studying the sticking regions in phase space. Since, sticking can occur only when the velocity is zero, all regions discussed below are presented in the $z' = 0$ plane; i.e., the z–τ plane. Sticking regions are obtained by studying the acceleration vector field as z' approaches zero. For sticking to occur, both relations (14) and (15) must be satisfied.

$$\lim_{z' \to 0^+} z'' \leq 0 \tag{14}$$

$$\lim_{z' \to 0^-} z'' \geq 0 \tag{15}$$

The sticking regions are those combinations of z and τ that satisfy (14) and (15). Substituting

z'' from equation (4) into (14) and (15), the following sticking regions are obtained for the case $K_0 \neq 0$:

for $\kappa_1 < 1$,

$$\frac{f \cos \tau - 1}{1 + \kappa_1} \leq z \leq \frac{f \cos \tau + 1}{1 - \kappa_1} \qquad \text{for } z > 0$$

$$\frac{f \cos \tau - 1}{1 - \kappa_1} \leq z \leq \frac{f \cos \tau + 1}{1 + \kappa_1} \qquad \text{for } z < 0 \tag{16}$$

for $\kappa_1 > 1$,

$$\left\{ \begin{array}{c} z > 0 \\[2mm] z \geq \dfrac{f \cos \tau - 1}{1 + \kappa_1} \\[4mm] z \geq \dfrac{-(f \cos \tau + 1)}{\kappa_1 - 1} \end{array} \right\} \quad \text{or} \quad \left\{ \begin{array}{c} z < 0 \\[2mm] z \leq \dfrac{1 - f \cos \tau}{\kappa_1 - 1} \\[4mm] z \leq \dfrac{f \cos \tau + 1}{1 + \kappa_1} \end{array} \right\} \tag{17}$$

for $\kappa_1 = 1$,

$$\left\{ \begin{array}{c} z > 0 \\[2mm] z \geq \dfrac{f \cos \tau - 1}{2} \\[4mm] f \cos \tau \geq -1 \end{array} \right\} \quad \text{or} \quad \left\{ \begin{array}{c} z < 0 \\[2mm] z \leq \dfrac{f \cos \tau + 1}{2} \\[4mm] f \cos \tau \leq 1 \end{array} \right\} \tag{18}$$

Regardless of the value of κ_1, sticking occurs at $z = 0$ when $-1 \leq f \cos \tau \leq +1$.

For the case $K_0 = 0$, $\ddot{z}''$ from equation (6) can be substituted into equations (14) and (15), yielding the following sticking regions:

for $\kappa_1 < 1$,

$$\frac{\cos \tau}{1 + \kappa_1} \leq \dot{z} \leq \frac{\cos \tau}{1 - \kappa_1} \qquad \text{for } \dot{z} > 0$$

$$\frac{\cos \tau}{1 - \kappa_1} \leq \dot{z} \leq \frac{\cos \tau}{1 + \kappa_1} \qquad \text{for } \dot{z} < 0 \tag{19}$$

for $\kappa_1 > 1$,

$$\left\{ \begin{array}{c} \dot{z} > 0 \\[2mm] \dot{z} \geq \dfrac{\cos \tau}{1 + \kappa_1} \\[4mm] \dot{z} \geq \dfrac{-\cos \tau}{\kappa_1 - 1} \end{array} \right\} \quad \text{or} \quad \left\{ \begin{array}{c} \dot{z} < 0 \\[2mm] \dot{z} \leq \dfrac{-\cos \tau}{\kappa_1 - 1} \\[4mm] \dot{z} \leq \dfrac{\cos \tau}{1 + \kappa_1} \end{array} \right\} \tag{20}$$

for $\kappa_1 = 1$,

$$\left\{ \begin{array}{c} \ddot{z} > 0 \\[8pt] \dot{z} \geq \dfrac{\cos \tau}{2} \\[8pt] \cos \tau \geq 0 \end{array} \right\} \quad \text{or} \quad \left\{ \begin{array}{c} \ddot{z} < 0 \\[8pt] \dot{z} \leq \dfrac{\cos \tau}{2} \\[8pt] \cos \tau \leq 0 \end{array} \right\} \tag{21}$$

Sticking cannot be sustained at $\ddot{z} = 0$ as the sticking condition here reduces to $\cos \tau = 0$ which does not occur over a finite time interval.

Figures 2–7 show the sticking regions for various parameter values. The ordinate label 'Position' refers to the relative slip displacement, z. The hatched regions refer to those combinations of z and τ for which sticking occurs when the system is subjected to harmonic excitation. It should be mentioned here that for the case $K_0 \neq 0$ the forcing ratio, f, must be greater than unity for sustained motion to occur as $f < 1$ implies that the constant portion of the friction force is greater than the input force. Obviously, the sticking regions depend strongly on κ_1. For $\kappa_1 > 1$ sticking is much more likely to occur than for $\kappa_1 < 1$. Note that on Figures 4 and 7, values of z exist through which a horizontal line can be drawn which remains entirely in the sticking region for all time. At these z permanent lockup takes place. For $\kappa_1 > 1$ (Figures 4 and 7) sticking, as well as permanent lockup, occurs over a far greater area of the z–τ plane than for $\kappa_1 < 1$ (Figures 2 and 5). This can be explained by examining (3). For $\kappa_1 > 1$ the interface "stiffness" is greater than the spring stiffness. Thus, at any position, the friction force is greater than the spring force. When far enough away from the zero position, the input force cannot overcome the friction force and sticking occurs.

If $\kappa_1 = 1$ (Figures 3 and 6), the spring and interfacial stiffnesses are exactly equal. Now sticking can only take place far from the origin at times when the spring force acts in the opposite direction of the input force. When the spring and input force act in the same direction, sticking can only occur when $|f \cos \tau| < 1$ for $K_0 \neq 0$ and only when $\cos \tau = 0$ for $K_0 = 0$. When $\kappa_1 = 0$

the sticking region reduces to that presented by Shaw [18]. For $0 < \kappa_1 < 1$ the sticking region expands as a function of z as one would expect; see Figure 2. Also, notice that ζ, and therefore K_2, has no effect on the sticking regions.

Finally, stability of the free response is studied. The system is positively damped at all times and is clearly stable in the sense of Lyapunov. However, the system is not asymptotically stable for $K_0 \neq 0$. This is most easily seen by considering the sticking regions given by expressions (16), (17), and (18) with the external force amplitude f set equal to zero. It is seen that for the classically damped dry friction system ($\kappa_1 = 0$) the sticking region reduces to $-1 \leq z \leq +1$. Thus, the motion would die down until the velocity becomes zero while $|z| \leq 1$. At that point, permanent lockup would take place. Note that, in general, permanent lockup would not occur at $z = 0$, hence the system could not be classified as asymptotically stable. As κ_1 becomes larger ($0 < \kappa_1 < 1$) the sticking region grows to $\frac{-1}{1-\kappa_1} < z < \frac{1}{1-\kappa_1}$. This implies that permanent lockup can now occur further from the origin. Finally, for $\kappa_1 \geq 1$, the sticking region becomes the entire $z{-}\tau$ plane. In this case, motion would continue only until the first time that the velocity becomes zero.

For the case $K_0 = 0$, the dimensional form of equations (19), (20), and (21) reveal that the sticking region collapses to the line $x = 0$ as long as $0 \leq \kappa_1 \leq 1$. Thus asymptotic stability is guaranteed. However, for $\kappa_1 \geq 1$, the sticking region becomes the entire $x{-}\tau$ plane and the system loses asymptotic stability.

It is interesting to note that while the generalized friction law can improve the passive damping of a mechanical system, it may do so at the expense of asymptotic stability.

2.3 Exact Solution

A straightforward approach to solving (4) and (6) is simply to numerically integrate the

equations. However, attemps to time integrate the equations using a sixth-order Runga-Kutta techinque met with considerable difficulty. The source of the problem was the unusually high numerical "stiffness" of the equations for small velocities. Another problem with this approach lies in the determination of sticking, which can only occur when the velocity becomes zero. Since time integration can only produce the time interval over which the velocity changes sign, determination of the exact time that the velocity becomes zero is difficult. This drawback, combined with the system's high numerical stiffness for small velocities, made the results quite sensitive to the time step of integration. Consequently, time integration solutions required an unusually small time step which, in turn, gave rise to requirements of substantial computation to obtain the results. To circumvent these difficulties, a second time domain approach that utilized the piecewise linear nature of the governing equations was developed.

Composite analytical solutions can be found to (4) and (6) as both equations are piecewise linear. Like the sticking regions, the solution is highly dependent on κ_1. Equations (4) and (6) are put in the following form:

$$\Omega^2 z'' + 2\zeta\Omega z' + \omega_n^2 z = f \cos \tau - \text{sgn}(z') \tag{22}$$

$$\Omega^2 \bar{z}'' + 2\zeta\Omega \bar{z}' + \omega_n^2 \bar{z} = \cos \tau \tag{23}$$

where

$$\omega_n^2 = 1 + \kappa_1 \text{sgn}(zz'). \tag{24}$$

From (24) one can see that ω_n^2 takes on two possible values depending on whether the magnitude of the displacement is increasing or decreasing. In terms of the z–z' phase plane, ω_n^2 will be constant within each quadrant and will change value when an axis is crossed. In one cycle of motion (if no sticking occurs), ω_n^2 will change value four times. In quadrants I and III, ω_n^2 will take on a positive value regardless of the value of κ_1. In quadrants II and IV, ω_n^2 will be positive,

zero, or negative for $\kappa_1 < 1$, $\kappa_1 = 1$, or $\kappa_1 > 1$ respectively.

For a given value of ω_n^2, an analytic solution can be obtained which is valid until either z or z' becomes zero. Each solution consists of a homogeneous part that involves two unknown constants and a particular part that depends exclusively on the "inputs" to the system. By matching "initial" conditions (position, velocity) of the new solution to the "final" conditions of the old solution to satisfy continuity, one can solve for the unknown constants and uniquely determine the solution in each quadrant of phase space.

Homogeneous solutions are obtained by first assuming an exponential response and solving for the roots of the resulting characteristic equation. One of five different homogeneous solutions is possible depending on the values of ω_n^2 and ζ. For $\omega_n^2 > 0$, the solution form is simply that for a single-degree-of-freedom, spring-mass-damper system. Three solution types are possible:

$$\text{underdamped} \qquad \omega_n^2 > \zeta^2$$

$$\text{overdamped} \qquad \omega_n^2 < \zeta^2$$

$$\text{critically damped} \qquad \omega_n^2 = \zeta^2.$$

All of these solutions are stable for positive ζ and the solution can be found in numerous texts. See, for example, [19].

The fourth possibility is $\omega_n^2 = 0$. This solution contains an eigenvalue that is negative and real as well as a zero eigenvalue. This situation is analogous to that of a mass-damper system. However, as mentioned earlier, this will only be the case during two "quarters" of the forcing period. The other two intervals will produce solutions of type with $\omega_n^2 > 0$. As expected, the net behavior over a complete cycle of forcing is that of a spring-mass-damper system.

Finally, it is possible for ω_n^2 to take on negative values. In this solution one root is positive real and the other is negative real (saddle-type stability). The positive real root will produce an exponential growth in the response. Using physical reasoning, one might expect that increasing

κ_1 would always result in smaller amplitudes of response. However, ω_n^2 can become negative (in two separate quarter-cycles) only when $\kappa_1 > 1$. Therefore, it is possible for an increase in κ_1 to produce an increase in the amplitude. As will be seen later, this type of behavior is observed especially at low frequencies of excitation.

By observing (22) and (23), it appears that there are two unique "inputs" to the system. Particular solutions to each of the two "inputs" must be found. First, the cosine input is studied. The particular solution for a linear system forced sinusoidally is harmonic, with the same frequency as the input. The amplitudes of the sine and cosine response are easily obtained through, for example, harmonic balance. Next, the solution to the $\text{sgn}(z')$ input is assumed to be made up of two terms; one which is linear in time, and one which is constant in time. Except for the case of $\omega_n^2 = 0$, the linear solution in time is zero. Note that when $\omega_n^2 = 0$, the portion of the response which is linear with time is present only over every other quarter-cycle, therefore, the total response may still be bounded. The magnitude of the constant solution depends only on the value of ω_n^2. The magnitude of the solution which is linear in time for $\omega_n^2 = 0$ depends on both ζ and Ω.

Thus for any set of parameter values, it is possible to find a closed-form expression which, based on the position and velocity at the entry to a particular quadrant in phase space, determines the system trajectory throughout that quadrant. The position and velocity at the trajectory's exit from the quadrant then becomes the initial condition for the next quadrant of phase space. A stick-free nonlinear motion over a period of forcing can be viewed as the composition of four linear maps [18]. This fact can be used to determine an "exact" steady-state solution for harmonic excitation. However, unlike the "exact" solutions developed by Den Hartog and Shaw, the determination of the stick-free periodic motion requires the solution of a system of transcendental equations. This anaylsis procedure is outlined in Appendix A.

As mentioned above, each solution applies only until z or z' becomes zero. Each time $z' = 0$, a check must be made to determine if sticking occurs. The spring force and input force are algebraically summed and termed the external force. The total friction force required to initiate sticking is determined and if the magnitude of this force is less than or equal to the maximum possible friction force, $\mu_s N$, sticking is said to occur. If sticking does occur, time is stepped forward until the input force and, hence, the external force, becomes large enough to exceed the maximum possible friction force magnitude and produce motion. Based on the direction of the external force just before the motion resumes, one can determine the direction of the motion (in particular, $\text{sgn}(zz')$ can be obtained) and use that information to compute the value of ω_n^2 needed for the next solution segment. If the magnitude of the external force is greater than the maximum possible friction force, no sticking occurs. In this case, a new value of ω_n^2 is calculated based on the impending direction of motion and the next "piecewise-valid" solution is found. Alternatively, sticking can be determined by checking to see if the trajectory has "landed" in a sticking region when $z' = 0$. If sticking occurs, one can move along the z–τ plane at the same z value until reaching a sticking boundary at which time motion will resume.

With the solution types known and using the above algorithm to deal with sticking, a computer program was written to solve the single-degree-of-freedom system with a generalized friction law. Results obtained are presented and disscussed in the next section.

3. Numerical Results

As mentioned throughout this paper, the value of κ_1 is extremely important in determining the system response. In particular, the sticking regions and response depend on whether $\kappa_1 < 1$, $\kappa_1 = 1$, or $\kappa_1 > 1$. For this reason, six representative cases are presented in this section. These are for $\kappa_1 = 0.4$, 1.0, and 1.2 each with K_0 zero and nonzero. In all six cases $\zeta = .1$, and for

the nonzero K_0 cases, the forcing ratio, f, was chosen to be 5. The sticking regions for these six cases can be seen in Figures 2–7 and were discussed previously.

We will begin by discussing equivalent viscous damping. For small values of κ_1 and ζ, the log decrement method can be used to calculate an approximate value for the viscous damping ratio. For small values of κ_1, the damping ratios calculated from this method agree somewhat with the one harmonic approximation, however, the correlation degenerates as the degree of sticking increases. Also for small ζ_{eq}, the half-power method can be applied to the frequency response plot to approximate viscous damping. Values obtained from the above method compared favorably to those given by equation (11) for small κ_1. For higher values of κ_1 where sticking is prevalent no good approximation for viscous damping was found. It appears that the viscous-like behavior is almost entirely eliminated when a substantial amount of sticking occurs.

Approximate frequency response curves drawn from equations (9) and (10) are compared to the "exact" response curves in Figures 8 and 9. The upper curves in both plots corespond to $\kappa_1 = 0.4$, with the lower curves drawn for $\kappa_1 = 1.2$. For high frequencies, the approximate and true curves approach the same values, however, for low frequencies there is very poor agreement as stick-slip motion occurs. Recall that the one-harmonic approximations (9) and (10) do not account for sticking. At low values of κ_1, there is good agreement between the single harmonic frequency response results and results from the "exact" time domain analysis. For higher values of κ_1, the single harmonic approximation is poor as sticking, which produces higher harmonics, occurs more often. A better approximation could be obtained by considering a multi-harmonic solution. However, these approximations require solving a system of nonlinear alegbraic equations.

Figures 10 and 11 show true frequency response curves for values of $\kappa_1 > 1$, $\kappa_1 < 1$, and $\kappa_1 = 1$. In Figure 10 the forcing ratio, f, as well as ζ, is the same for all curves. The special case of $K_0 = 0$ is drawn in Figure 11. Note that in Figures 10 and 11, the curves of different

κ_1 intersect, which means that for different levels of amplitude-dependent friction, the same amplitude response can occur for a given frequency of excitation. Perhaps more important is the fact that for frequencies of excitation slightly lower than $\Omega \approx 0.4$, small increases in κ_1 can actually increase the amplitude of the response. Further investigation reveals that as κ_1 is increased further, a maximum amplitude is eventually reached; as κ_1 approaches infinity, the amplitude goes to zero. Also note that the approximate curves drawn from equations (9) and (10) do not exhibit this behavior. This suggests that stick-slip motion is largely responsible for the intersection of the frequency response curves. This can be verified somewhat by examining Figure 12, where time traces are shown for a frequency of excitation $\Omega = 0.369$ and for two different levels of κ_1 (0.4 and 1.2). Although the amplitude of the responses is the same, the sticking time and phase of the responses is different. Obviously, the percentage of time per cycle that the mass spends fully stuck is a very important design consideration as no energy is dissipated during those times.

Figures 13 and 14 show the percentage of time per cycle that the mass is stuck. Parameter values for Figures 13 and 14 are the same as for Figures 10 and 11, respectively. As the frequency, Ω, approaches zero, all of the curves tend to drop off from approaching complete lockup and instead cascade with decreasing amplitude. For these low frequencies, the local minima in the percent time sticking curves correspond to bifurcations in the number of stops per cycle. As the frequency is decreased, each time a local minimum is encountered, the number of stops per cycle increases by two. The curves in Figures 13 and 14 then can be used to determine the number of stops per cycle as well as the frequency at which sticking begins to occur in Figures 10 and 11 respectively. Note that the percent of time sticking curves for different values of κ_1 do not intersect. Therefore, increasing the level of amplitude-dependent friction for a given frequency of excitation appears to always produce a greater amount of sticking.

It should be mentioned that for the cases presented here, numerical integration of the equations of motion as dissused earlier successfully determines the responses to a good degree of accuracy. However, the computer time required was often substantially greater. Also, some parameter values were found which resulted in erroneous results until a very fine time step was used. Therefore, the "exact" solution is recommended.

4. Conclusions

A single-degree-of-freedom dry friction damped system with a generalized friction law was studied. It was shown that the system is strongly affected by the presence of amplitude-dependent frictional forces. A critical parameter governing the system response is κ_1, the ratio of the "frictional spring constant" μK_1 to the elastic spring constant k. In particular, the system response and the sticking regions depend on whether κ_1 is less than, equal to, or greater than unity. For low values of κ_1, the damping characteristics of the system show a strong resemblance to those of a viscous damped system. It is also found that for small values of κ_1, there is good agreement between the single harmonic approximate solutions and solutions found using a time-domain "exact" solution technique. Equivalent viscous damping ratios found from the single harmonic analysis are also found to have their best correlation with the "exact" method for small values of κ_1. For larger values of κ_1, the agreement between the single harmonic results and results from the "exact" solution method deteriorates. This is due primarily to the increased occurrence of sticking. It is shown that the amount of time per cycle that the system spends stuck grows monotomically with κ_1. However, a somewhat surprising result is that at certain frequencies of excitation, increasing the level of amplitude-dependent friction can increase the amplitude of the response.

In contrast to a single-degree-of-freedom dry friction damped system with a constant normal

force, it is found that unbounded response at resonance can be prevented by the addition of either amplitude-dependent or velocity-dependent frictional forces. Thus, it may be possible to greatly enhance the performance of dry friction damped systems which are prone to low damping levels at high response amplitudes. This is especially important in applications where viscous damping augmentation is difficult or impractical, for example large flexible space structures and turbomachinery bladed disks. In systems of this type, the present work suggests that beneficial damping properties may be achieved through the re-design of frictional interfaces.

Acknowledgement

References

1. Muszynska, A. and Jones, D.I.G.,"On Tuned Bladed Disk Dynamics: Some Aspects of Friction Related Mistuning," J. of Sound and Vibration, Vol. 86, No. 1, 1983, pp. 107–128.

2. Muszynska, A. and Jones, D.I.G.,"Bladed Disk Dynamics Investigated by a Discrete Model: Effects of Traveling Wave Excitation, Friction, and Mistuning," Proceedings, Machine Vibration Monitoring and Analysis Meeting, Oak Brook, Illinois, 30 March – 1 April 1982.

3. Muszynska, A. and Jones, D.I.G.,"A Parametric Study of Dynamic Response of a Discrete Model of Turbomachinery Bladed Disk," ASME J. of Vibration, Acoustics, Stress, and Reliability in Design, Vol. 105, October 1983, pp. 434–443.

4. Jones, D.I.G.,"Vibrations of a Compressor Blade with Slip at the Root," Air Force Wright Aeronautical Laboratories Report AFWAL-TR-80-4003, April 1980.

5. Beards, C.F.,"The Damping of Structural Vibration by Controlled Interfacial Slip in Joints," ASME J. of Vibration, Acoustics, Stress, and Reliability in Design, Vol. 105, July 1983, pp. 369–373.

6. Beards, C.F., and Woonat, A.,"The Control of Frame Vibration by Friction Damping in Joints," ASME J. of Vibration, Acoustics, Stress, and Reliability in Design, Vol. 106, January 1985, pp. 26–32.

7. Griffin, J.H.,"Friction Damping of Resonant Stresses in Gas Turbine Engine Airfoils," ASME J. of Engineering for Power, Vol. 102, April 1980, pp. 329–333.

8. Griffin, J.H., and Sinha, A.,"Friction Damping of Flutter in Gas Turbine Engine Airfoils," AIAA J. Aircraft, Vol. 20, No. 4, pp. 372–376.

9. Menq, C-H., Griffin, J.H., and Bielak, J., "The Forced Response of Shrouded Fan Stages," Tenth Biennial ASME Design Engineering Division Conference on Mechanical Vibration and Noise, September 1985, Cincinnati, Ohio.

10. Srinivasan, A.V., Cutts, D.G., and Sridhar, S., "Turbojet Engine Blade Damping," NASA CR-165406, July 1981.

11. Bielawa, R.L., "An Analytic Study of the Energy Dissipation of Turbomachinery Bladed-Disk Assemblies due to Inter-Shroud Segment Rubbing," ASME Journal of Machine Design, Vol. 100, April 1978, pp. 222–228.

12. Hertz, T.J., and Crawley, E.F., "Damping in Space Structure Joints," AIAA Dynamics Specialists Conference, 17-18 May 1984, Palm Springs, California.

13. Hertz, T.J., and Crawley, E.F., "The Effects of Scale on the Dynamics of Flexible Space Structures," Report No. SSL 18-83, Space Systems Laboratory, Department of Aeronautics and Astronautics, Massachusetts Institute of Technology, Cambridge, MA, September 1983.

14. Ferri, A.A., "Investigation of Damping from Nonlinear Sleeve Joints of Large Space Structures," Proceedings of the 11th Biennial Conference on Mechanical Vibrations and Noise, Boston, MA, September 27-30, 1987.

15. Ferri, A.A., and Dowell, E.H., "The Behavior of a Linear, Damped Modal System with a Nonlinear Spring-Mass-Dry Friction Damped System Attached, Part II," J. of Sound and Vibration, Vol. 101, No. 1, 1985, pp. 55–74.

16. Pratt, T.K., and Williams, R., "Non-Linear Analysis of Stick/Slip Motion," J. of Sound and Vibration, Vol. 74, No. 4, 1981, pp. 531–542.

17. Den Hartog, J.P., "Forced Vibrations with Combined Coulomb and Viscous Friction," Trans. ASME, APM-53-9, 1931, pp. 107–115.

18. Shaw, S.W., "On the Dynaimc Response of a System with Dry Friction," J. of Sound and Vibration, Vol. 108, No. 2., 1986, pp. 305–325.

19. Den Hartog, J.P., **Mechanical Vibrations**, McGraw-Hill, New York, Fourth Edition, 1956.

Appendix A

The "exact" solution technique used by Den Hartog [17] and Shaw [18] for the classic dry friction damped system under harmonic excitation may be extended to the generalized friction case. The basic technique consists of deriving expressions for the solution in various linear regions of the piecewise-linear system and enforcing continuity and periodicity relations. Continuity simply implies that the displacement and velocity are matched across the boundary of linear regions. The degree-of-difficulty involved in this solution technique depends directly on the number of piecewise-linear intervals encountered in a fundamental period of the motion. To yield a tractable solution, the following assumption is usually made:

$$z(\tau \pm \pi) = -z(\tau) \qquad (A.1)$$

Note that this assumption not only enforces period-1 motion, but also restricts the solution space to motions which have "similar" behavior in each half-cycle of forcing. Thus, only a single half-cycle needs to be considered.

In theory, there is no limit to the number of piecewise-linear regions that a system can encounter in each half-cycle, however, the technique is limited in practice to systems with a relatively small number of regions. In the classic dry friction damped case, $\kappa_1 = 0$, the number of regions in phase space encountered per half-cycle of forcing is just one for stick-free motion. In the generalized dry friction damped case, $\kappa_1 > 0$, the number of regions encountered is *two* for stick free motion. In both cases, the number of regions per half-cycle of forcing increases by one with every addition of a stick per half-cycle.

As discussed in the paper, the generalized friction nonlinearity results in there being four piecewise-linear regions in phase space corresponding to the four quadrants of the z–z' plane. In addition, when sticking occurs, the trajectory can spend a finite amount of time on the line $z' = 0$.

In each quadrant, the following linear, nonhomogeneous differential equations apply:

Region I $(z > 0, z' > 0)$: $\Omega^2 z'' + 2\zeta\Omega z' + (1 + \kappa_1)z = f\cos(\tau + \phi) - 1$ $(A.2)$

Region II $(z < 0, z' > 0)$: $\Omega^2 z'' + 2\zeta\Omega z' + (1 - \kappa_1)z = f\cos(\tau + \phi) - 1$ $(A.3)$

Region III $(z < 0, z' < 0)$: $\Omega^2 z'' + 2\zeta\Omega z' + (1 + \kappa_1)z = f\cos(\tau + \phi) + 1$ $(A.4)$

Region IV $(z > 0, z' < 0)$: $\Omega^2 z'' + 2\zeta\Omega z' + (1 - \kappa_1)z = f\cos(\tau + \phi) + 1$ $(A.5)$

In each case, the general solution involves two unknown constants associated with the homogeneous portion of the solution.

For definiteness, consider the period-1 trajectory shown in Figure A1. The motion begins at the point $(z_0, 0)$ in the z–z' plane at time $\tau = 0$. (Note that choosing this time to be zero makes the phase of the harmonic forcing, ϕ, an unknown.) The initial conditions together with (A.1) yield the following four equations:

$$z(0) = z_0 \qquad\qquad (A.6)$$

$$z'(0) = 0 \qquad\qquad (A.7)$$

$$z(\pi) = -z_0 \qquad\qquad (A.8)$$

$$z'(\pi) = 0 \qquad\qquad (A.9)$$

As shown in Figure A1, the trajectory starts in Region IV and, at time τ_1, crosses into Region III. A solution for the motion in Region IV, $z(\tau)$, can be obtained using the initial conditions specified by (A.6) and (A.7). The general functional form is

$$z(\tau) = Z_4(z_0, \phi, \tau) \qquad 0 \leq \tau \leq \tau_1 \qquad\qquad (A.10)$$

At time $\tau = \tau_1$, the trajectory crosses into the next piecewise-linear region, Region III. A solution in this region can be found using the terminal conditions specified by (A.8) and (A.9).

$$z(\tau) = Z_3(z_0, \phi, \tau) \qquad \tau_1 \leq \tau \leq \pi \qquad\qquad (A.11)$$

The unknowns, z_0, ϕ, and τ_1 are found by enforcing continuity and requiring that the boundary point lie on the line $z = 0$.

$$Z_4(z_0, \phi, \tau_1) = Z_3(z_0, \phi, \tau_1) \qquad (A.12)$$

$$Z_4'(z_0, \phi, \tau_1) = Z_3'(z_0, \phi, \tau_1) \qquad (A.13)$$

$$Z_4(z_0, \phi, \tau_1) = 0 \qquad (A.14)$$

Equations (A.12), (A.13), and (A.14) constitute three transcendental equations in three unknowns. The solution must be found numerically, using for example a multi-dimensional root solver.

This procedure must be modified somewhat to account for sticking. As a consequence of (A.1), the number of stops per cycle must be even, thus, the simplest case of stick-slip motion is one that has two stops per cycle. It is assumed that the mass becomes unstuck at time $\tau = 0$ and that it sticks again at a time τ_2, $\tau_1 < \tau_2 < \pi$. In this case, the time τ_2 at which $z' = 0$ must be added as a fourth unknown. An additional equation to be considered is a force balance just prior to slipping, at time $\tau = 0^-$.

It is interesting to contrast the generalized friction case with the classic dry friction damped case. As seen in [17] and [18], the classic dry friction damped case yields a closed-form solution for stick-free motion, while motion with two stops per cycle requires the solution of a single transcendental equation. For the generalized friction case, stick-free motion involves the solution of *three* coupled transcendental equations, while motion with two stops per cycle involves the solution of *four* coupled transcendental equations. In both the classic and the generalized friction cases, each additional pair of stops per cycle (past two) adds three more equations. Therefore, as the number of stops per cycle grows, the degree of complexity in obtaining the solution grows.

The time domain solution method presented in this paper presents several advantages over

the "exact" method described above. First, the time domain method does not restrict the solution to be period-1, and makes no assumption regarding the "anti-symmetry" of the first and second half-cycles. Secondly, it is no more difficult to study stick-free motion than to study stick-slip motion with any number of stops per cycle. The advantages come at the expense of having to first solve for the transient response, while the "exact" method presented here avoids the determination of the transient response.

Figure 1: Single-degree-of-freedom system with generalized friction damping. (a) Passive system.
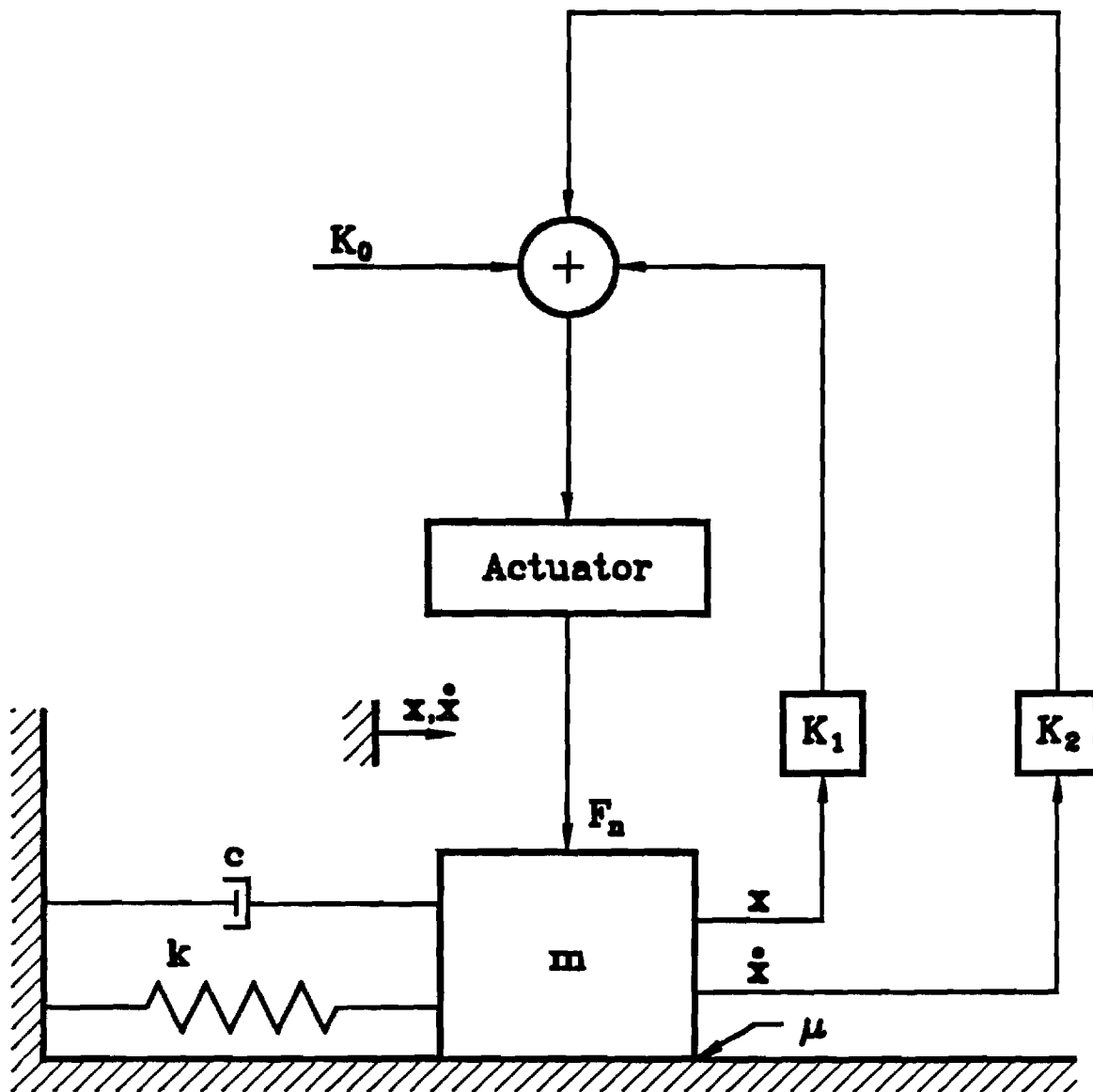
Figure 1: Single-degree-of-freedom system with generalized friction damping. (b) Active system.
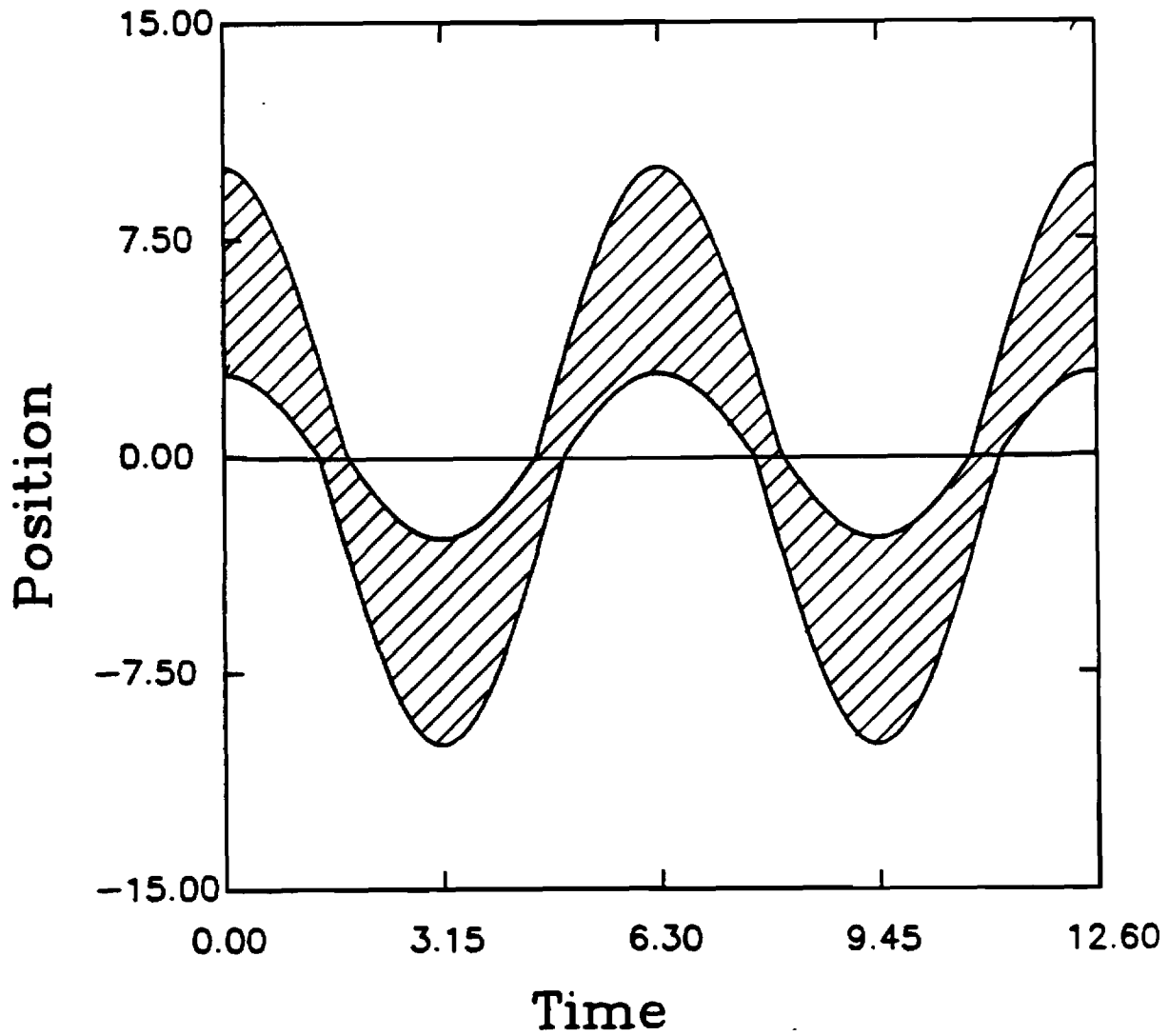
Figure 2: Sticking region for $\kappa_1 = 0.4$ with $K_0 \neq 0$, $f = 5$, and $\zeta = 0.1$. Region where sticking occurs is shown hatched.
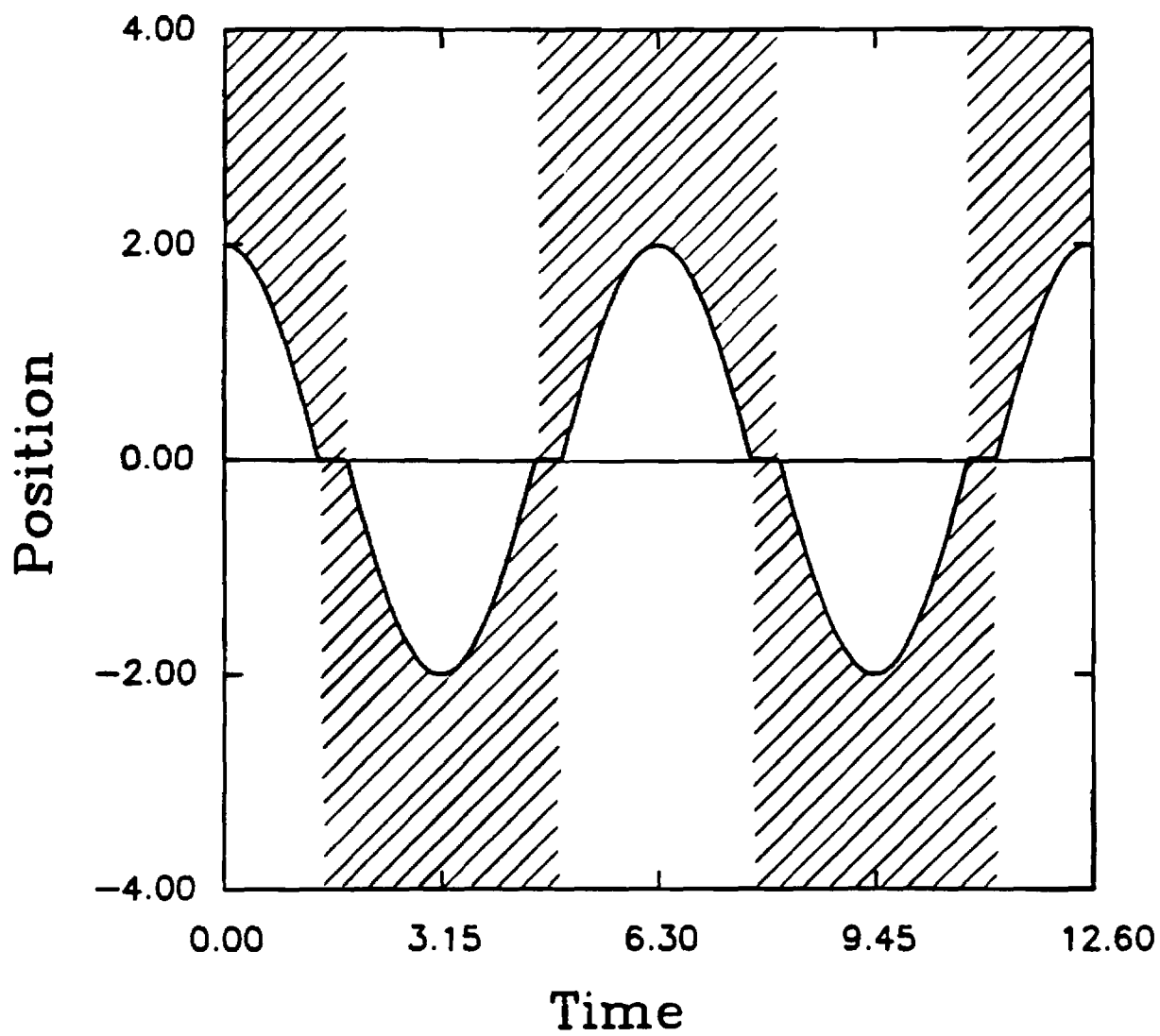
Figure 3: Sticking region for $\kappa_1 = 1.0$ with $K_0 \neq 0$, $f = 5$, and $\zeta = 0.1$. Region where sticking occurs is shown hatched.
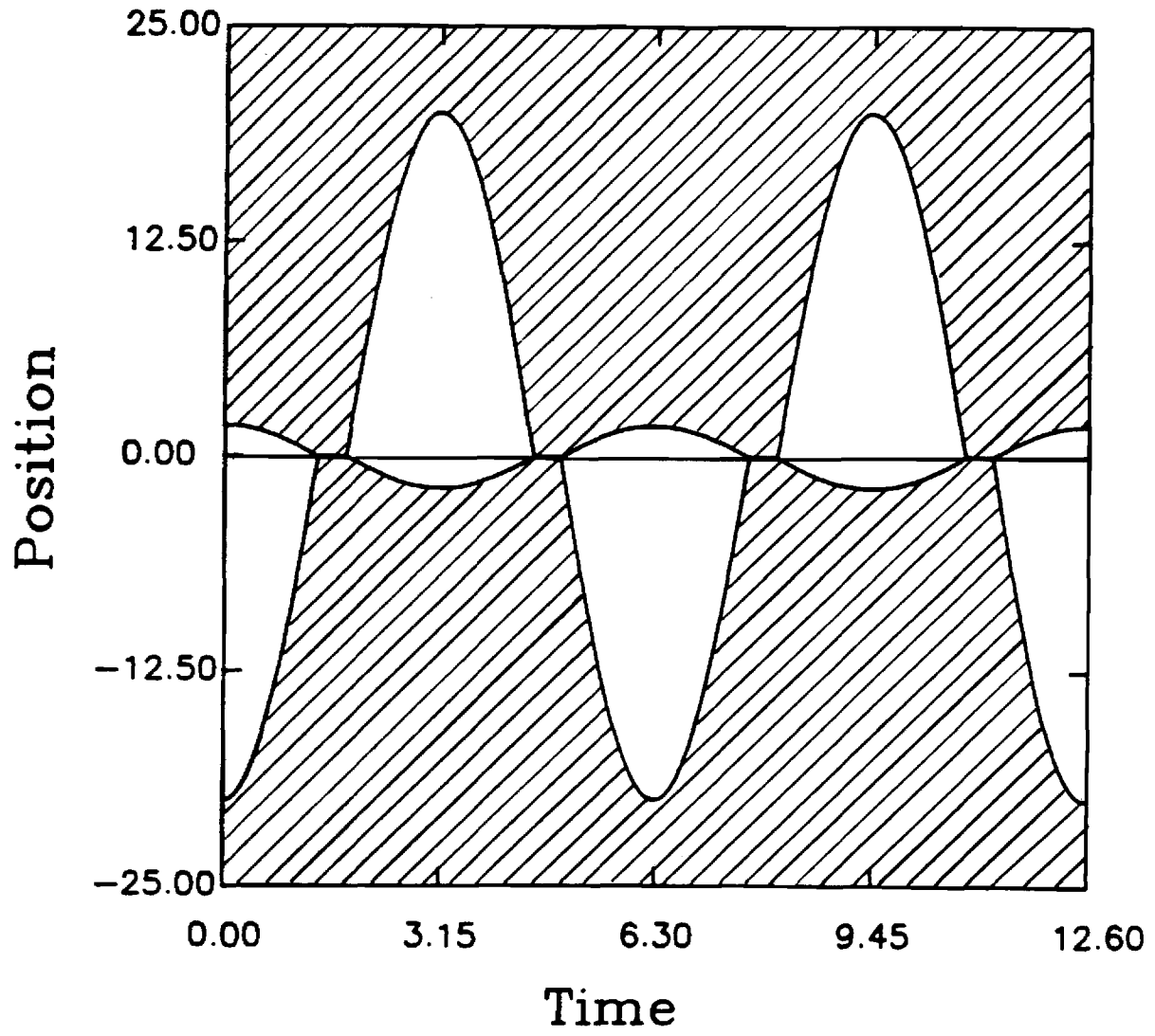
Figure 4: Sticking region for $\kappa_1 = 1.2$ with $K_0 \neq 0$, $f = 5$, and $\zeta = 0.1$. Region where sticking occurs is shown hatched.
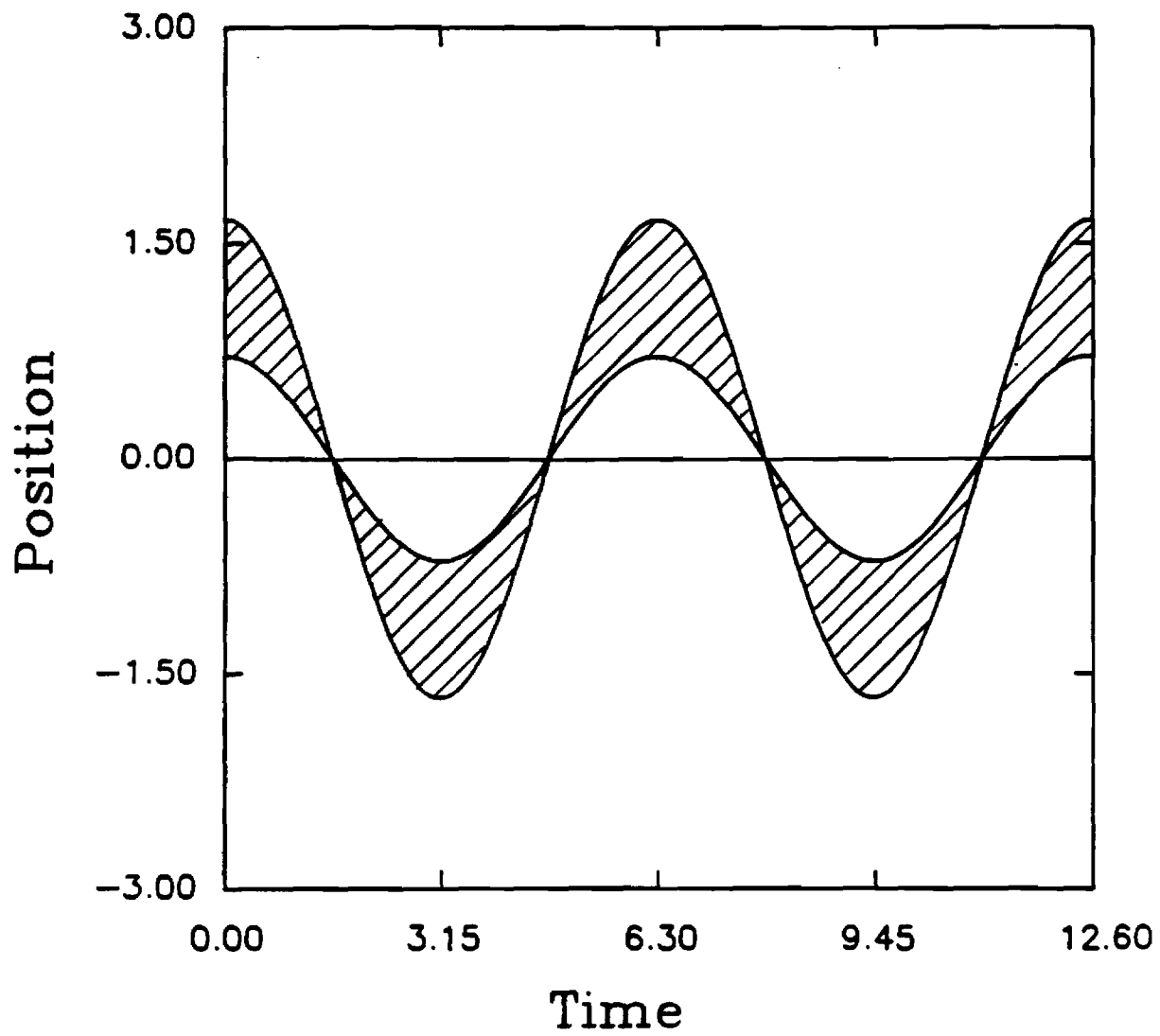
Figure 5: Sticking regions for $\kappa_1 = 0.4$ with $K_0 = 0$ and $\zeta = 0.1$. Regions where sticking occurs are shown hatched.
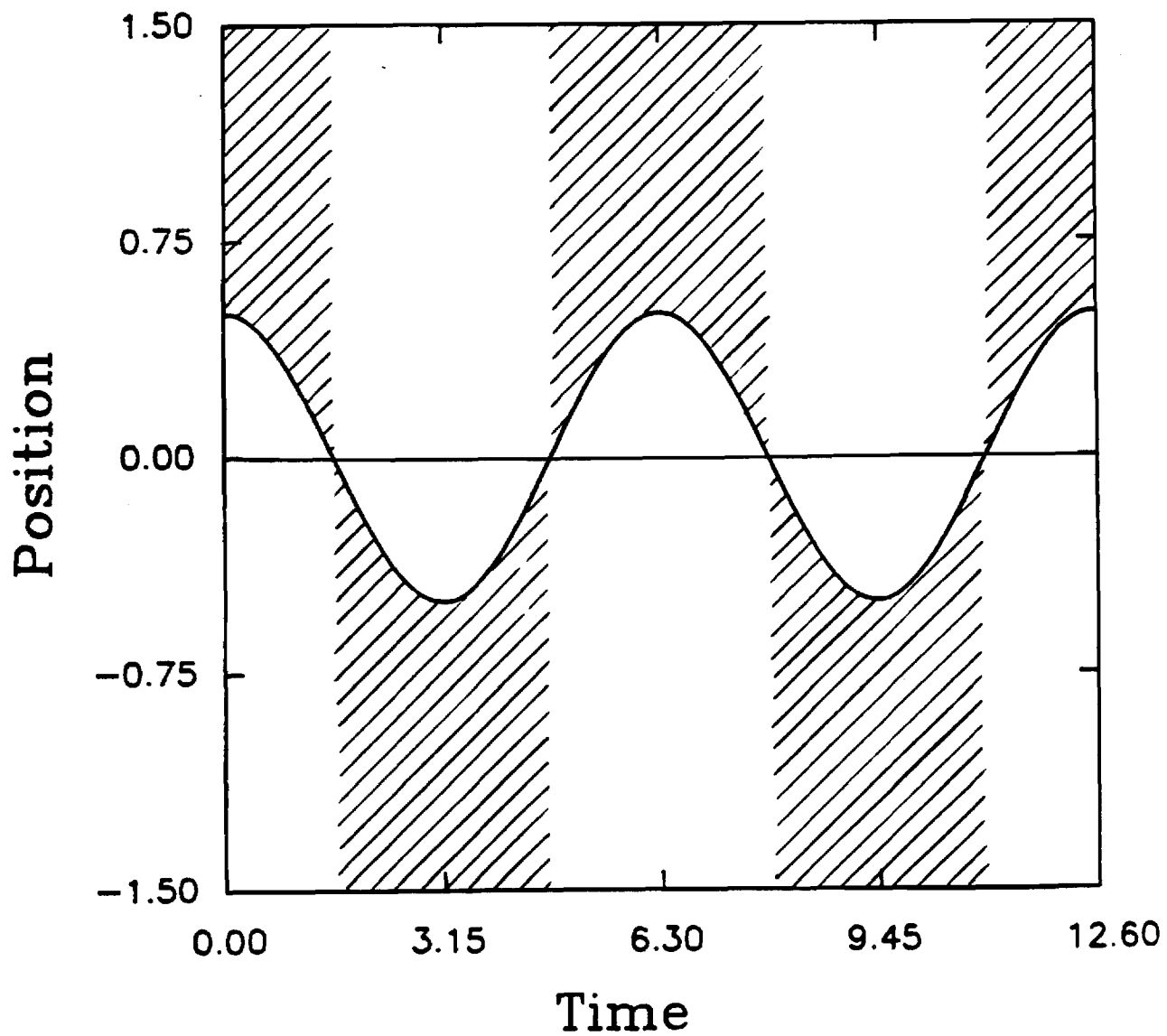
Figure 6: Sticking regions for $\kappa_1 = 1.0$ with $K_0 = 0$ and $\zeta = 0.1$. Regions where sticking occurs are shown hatched.
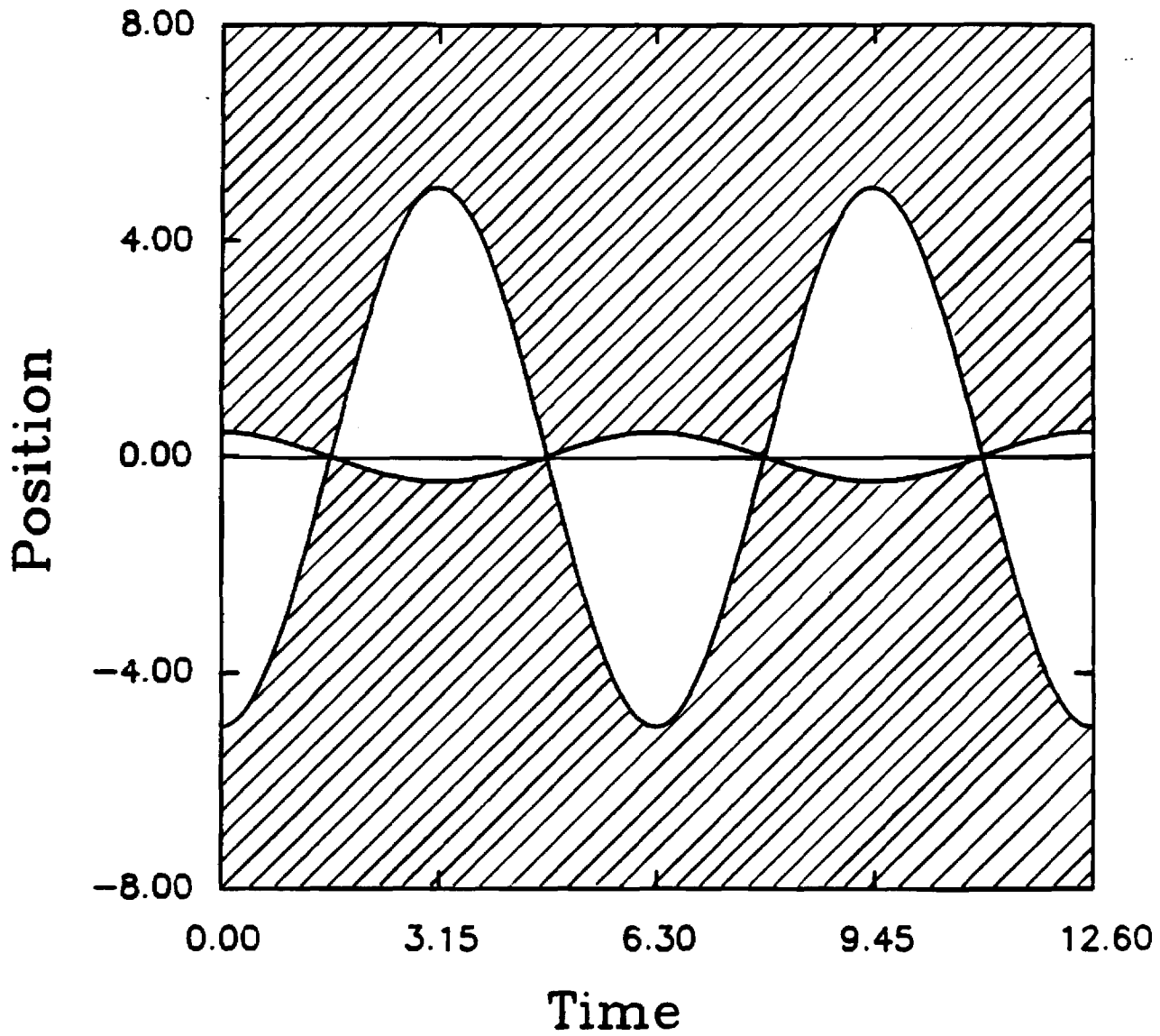
Figure 7: Sticking regions for $\kappa_1 = 1.2$ with $K_0 = 0$ and $\zeta = 0.1$. Regions where sticking occurs are shown hatched.
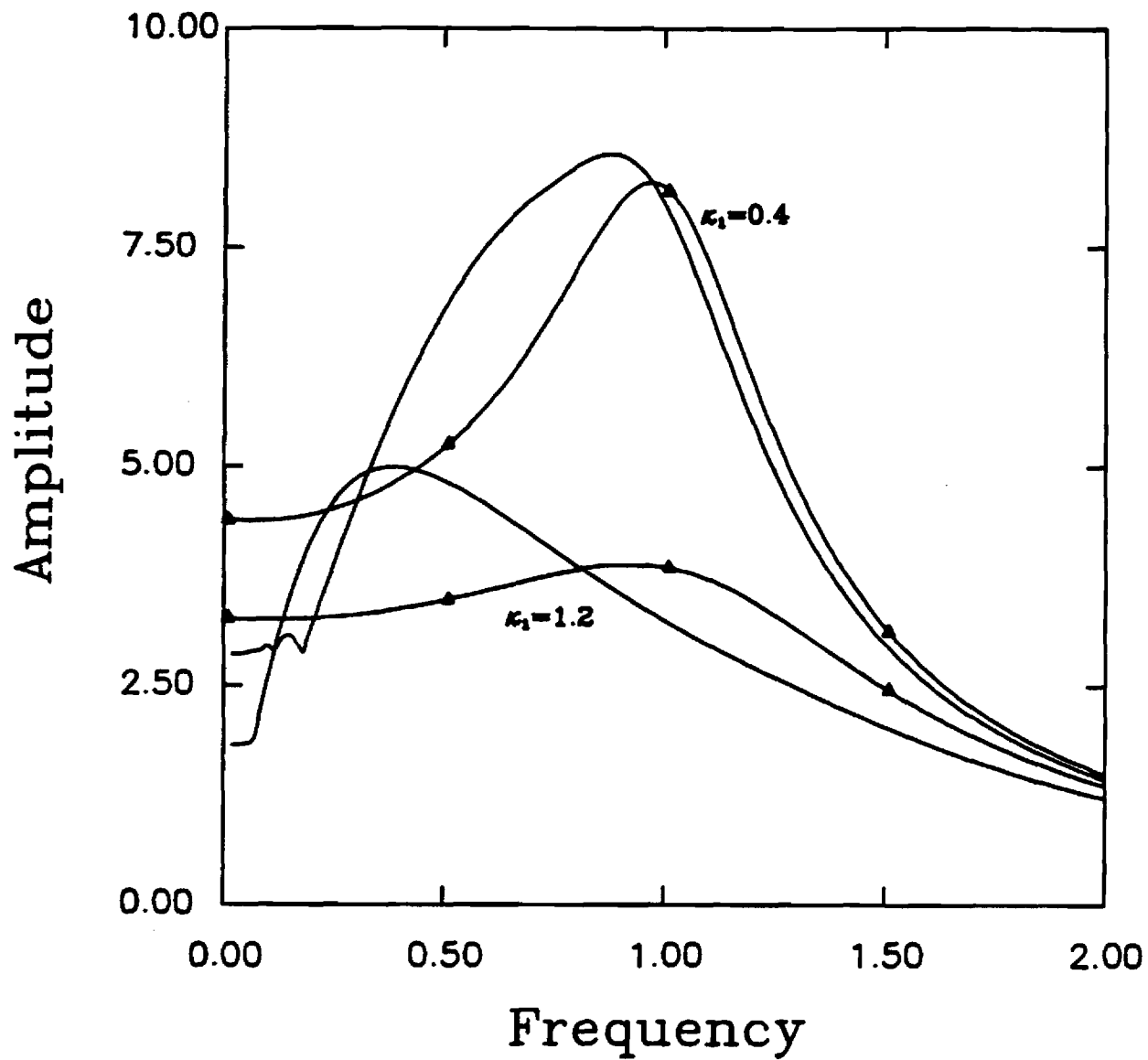
Figure 8: Frequency response for the case $K_0 \neq 0$: $f = 5$, $\zeta = 0.1$. $\triangle$ First order harmonic balance: — Solution from "exact" method.
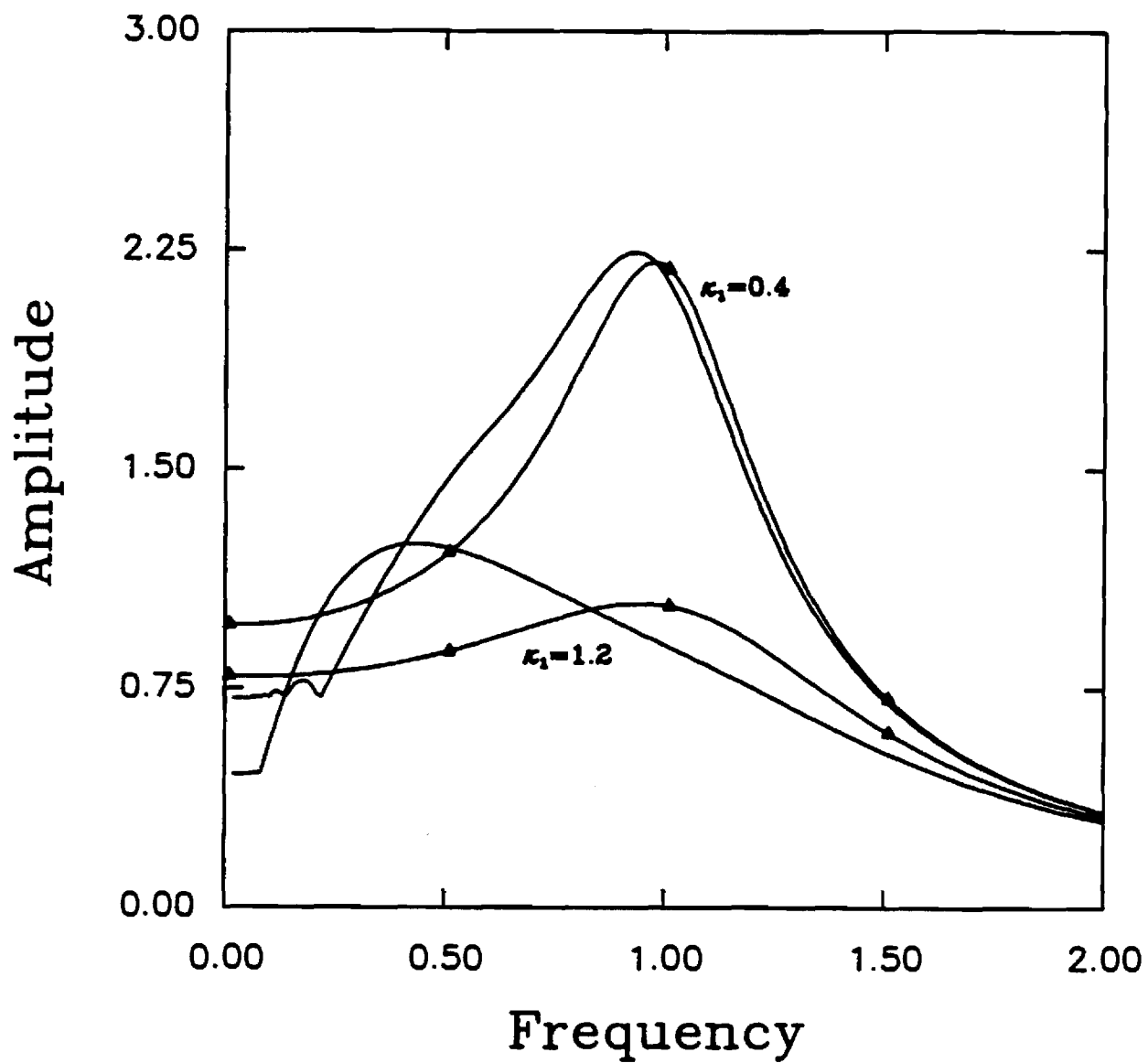
Figure 9: Frequency response for the case $K_0 = 0$; $\zeta = 0.1$. $\triangle$ First order harmonic balance; — Solution from "exact" method.
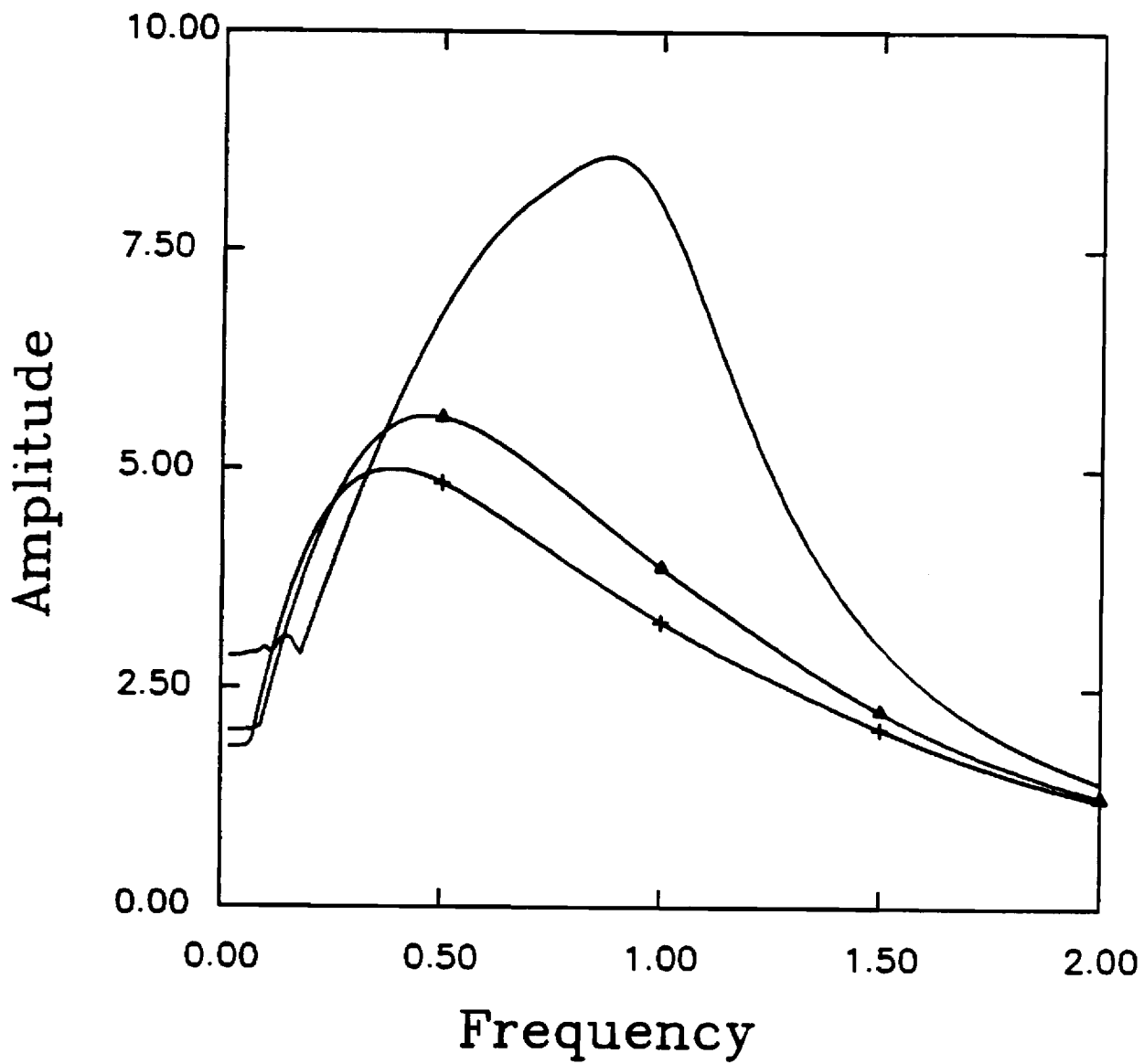
Figure 10: "Exact" frequency response for the case $K_0 \neq 0$, $f = 5$, $\zeta = 0.1$. — $\kappa_1 = 0.4$; $\triangle$ $\kappa_1 = 1.0$; $+$ $\kappa_1 = 1.2$.
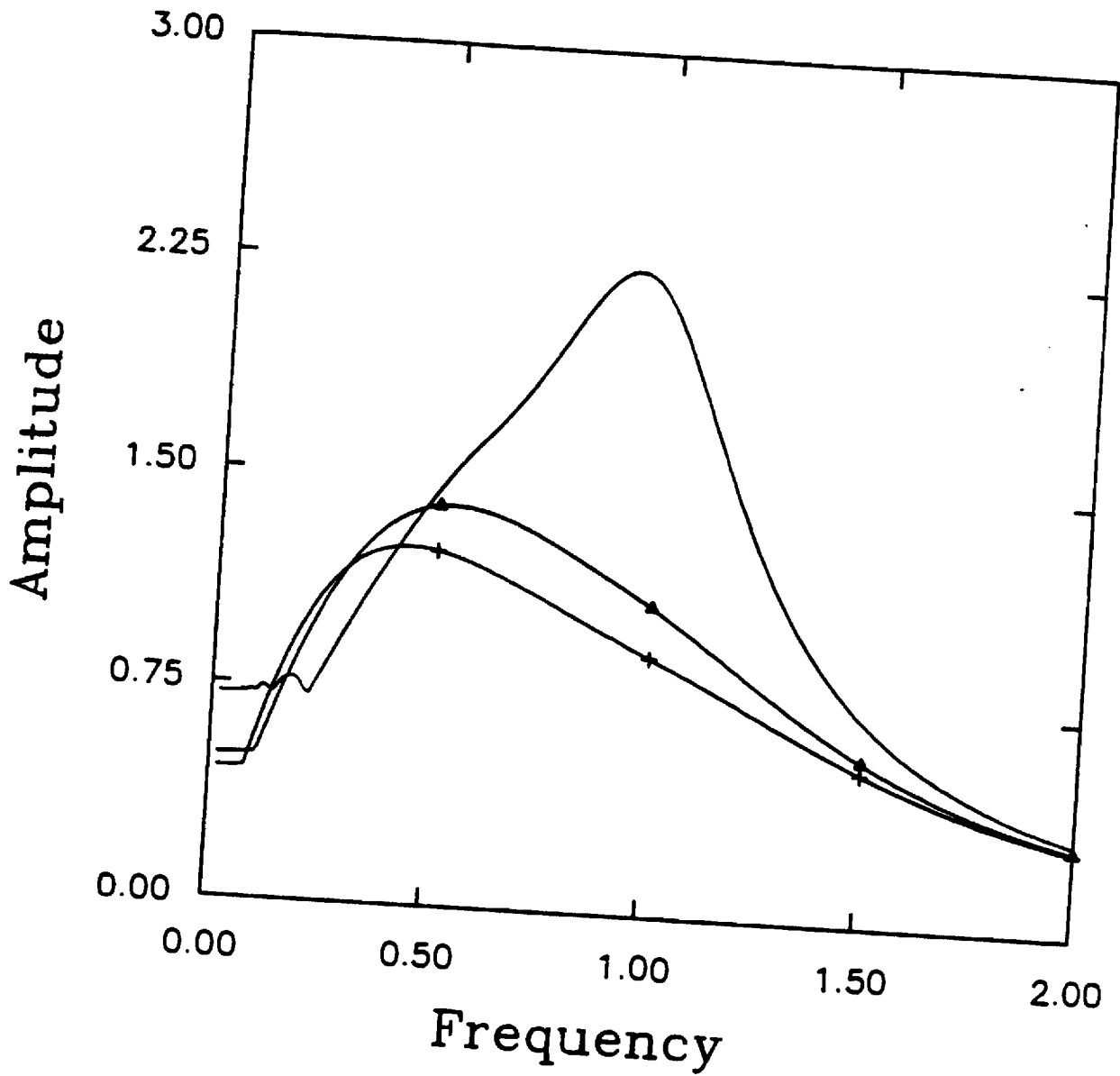
Figure 11: "Exact" frequency response for the case $K_0 = 0$, $\zeta = 0.1$. — $\kappa_1 = 0.4$; △ $\kappa_1 = 1.0$; ÷ $\kappa_1 = 1.2$.
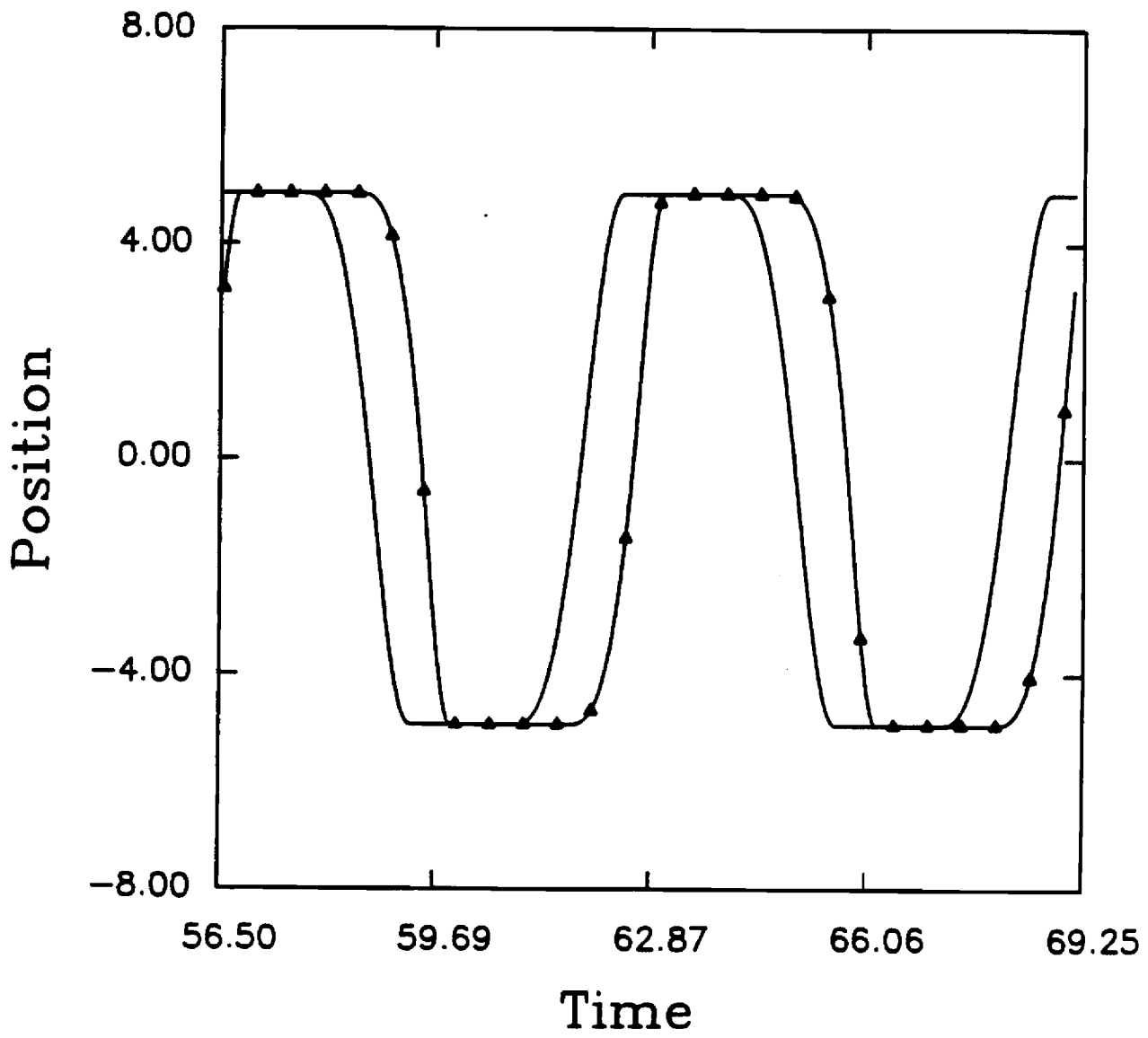
Figure 12: Time histories, $z(\tau)$ vs. τ for $\Omega = 0.369$. — $\kappa_1 = 0.4$; △ $\kappa_1 = 1.2$.
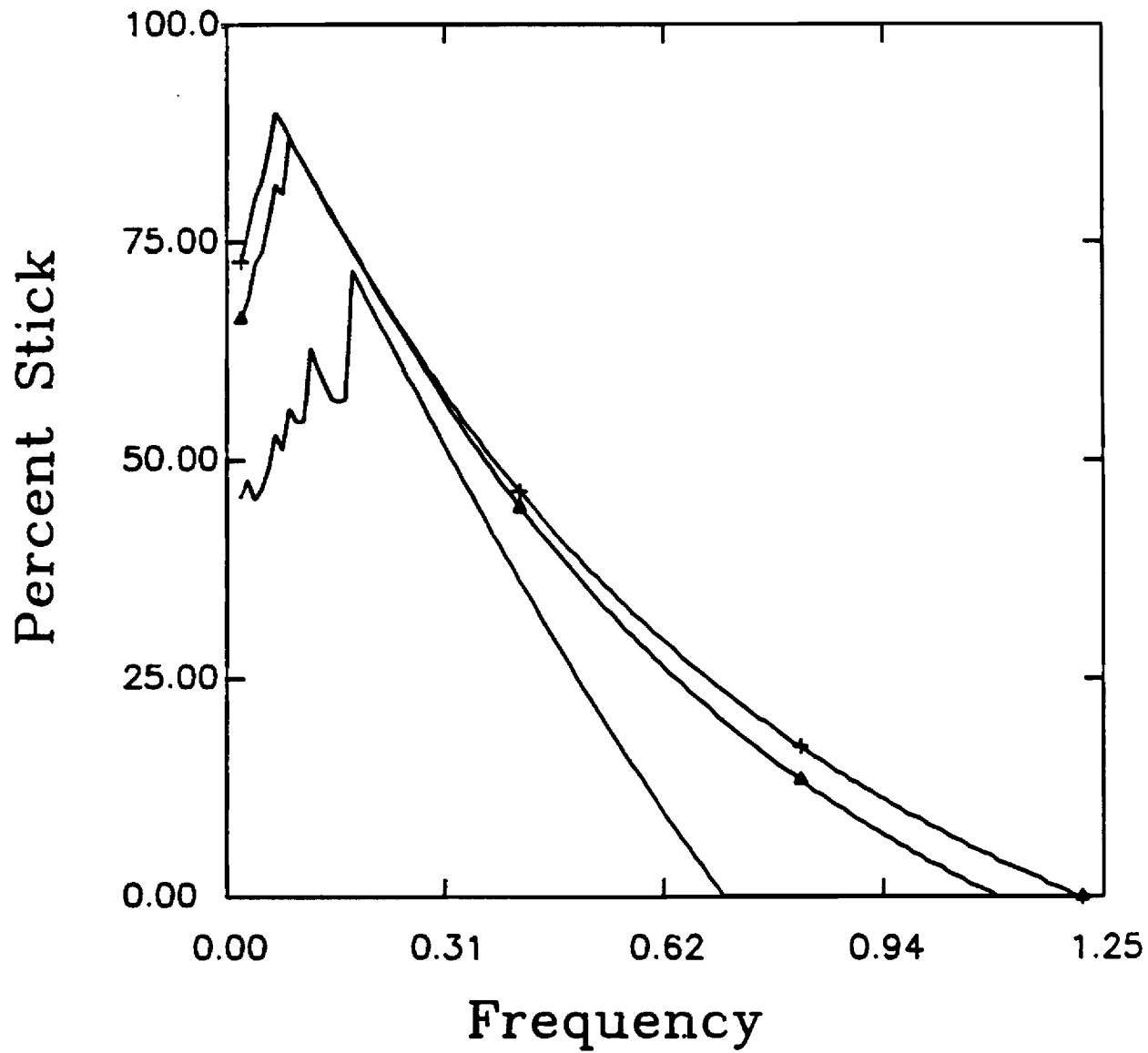
Figure 13: Percent-time of sticking per cycle of excitation vs Ω for $K_0 \neq 0$, $f = 5$, $\zeta = 0.1$. — $\kappa_1 = 0.4$; $\triangle$ $\kappa_1 = 1.0$; $+$ $\kappa_1 = 1.2$.
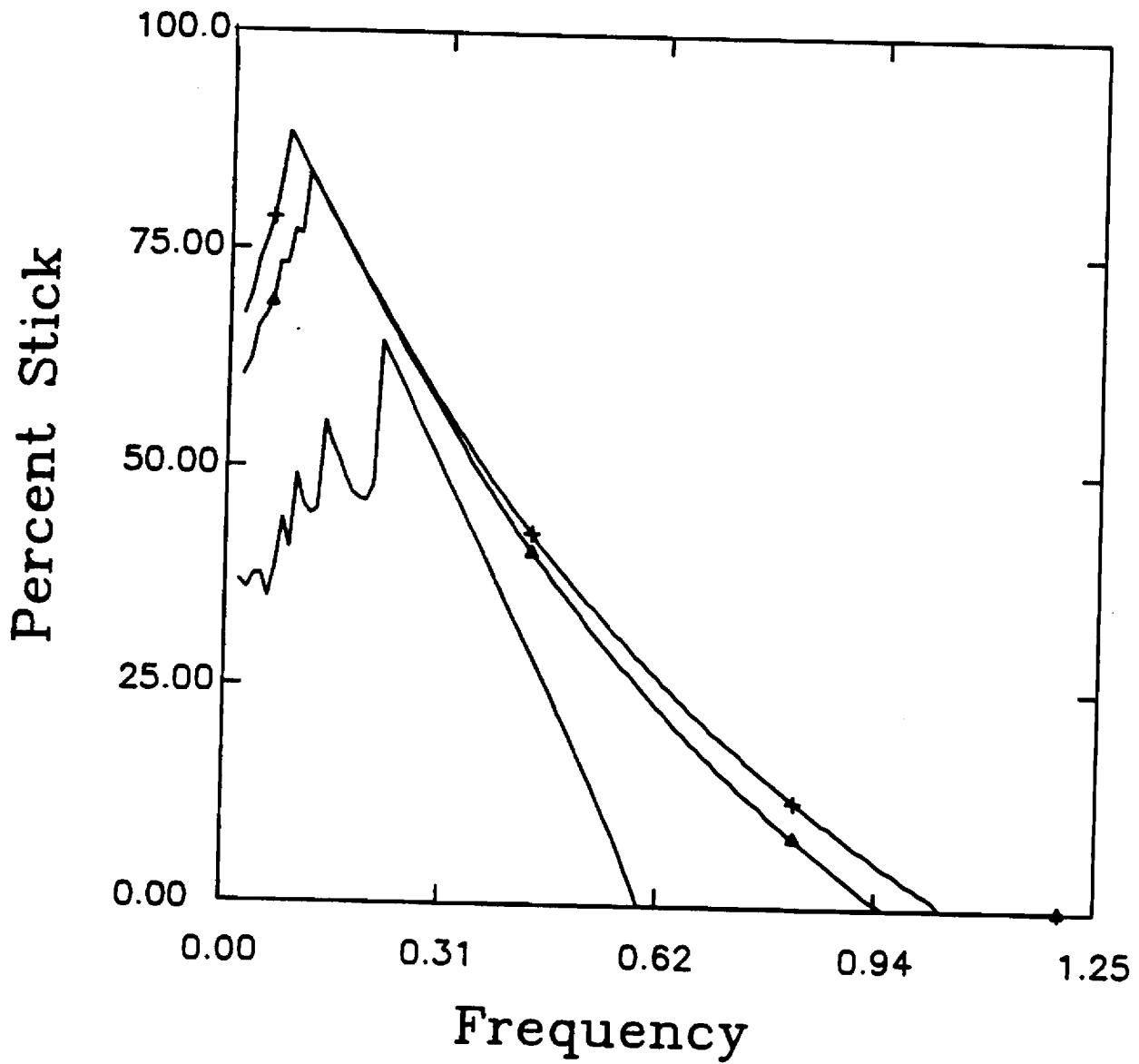
Figure 14: Percent-time of sticking per cycle of excitation vs Ω for $K_0 = 0$, $\zeta = 0.1$. — $\kappa_1 = 0.4$: $\triangle \ \kappa_1 = 1.0$; + $\kappa_1 = 1.2$.
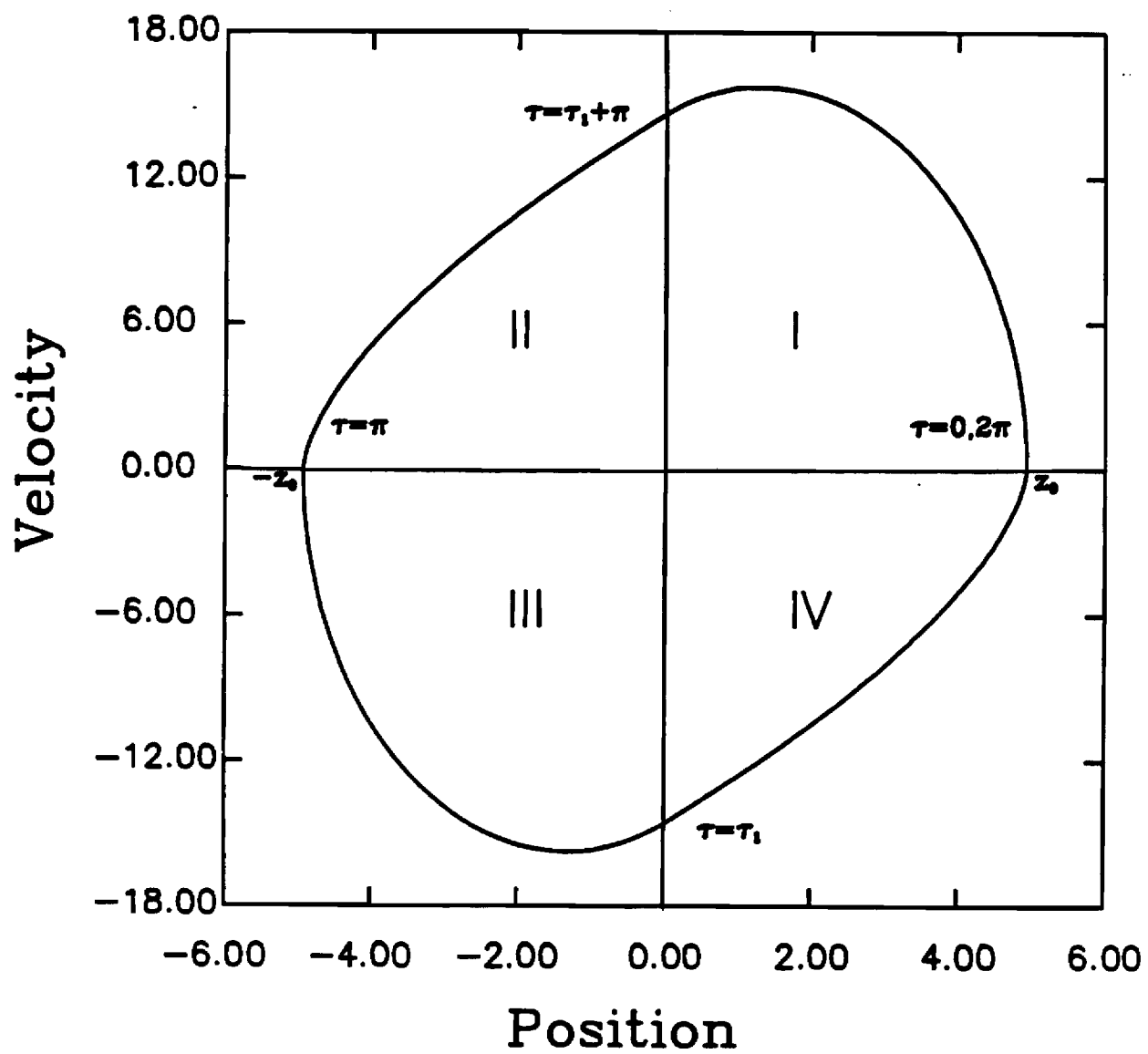
Figure A1: Phase-Plot for a typical periodic steady state response.

Behavior of a Nonlinear System With an Amplitude-Dependent Coulomb Friction Law

James R. Anderson
Graduate Research Assistant

Aldo A. Ferri
Assistant Professor

School of Mechanical Engineering
Georgia Institute of Technology
Atlanta, Georgia 30332-0405

Abstract

Dry friction is an important source of mechanical damping in many physical systems. In fact, in systems such as turbomachinery rotors and large flexible space structures, dry friction may be the most important source of energy dissipation. Though systems with classical dry (Coulombic) friction have been studied extensively, the properties of systems damped with generalized friction laws have not been thoroughly examined. This paper investigates the properties of a single-degree-of-freedom system damped by a combination of viscous damping, dry friction with a constant normal force and dry friction with an amplitude dependent normal force. This system is studied using an "exact" time integration method and using first-order harmonic balance. The stick-slip behavior of the system is also examined.

It is seen that the system is strongly affected by the presence of amplitude dependent frictional forces. A critical parameter governing the system response is κ_1 defined to be the ratio of amplitude dependent frictional forces to elastic spring forces. In particular, the system response and the sticking regions depend on whether κ_1 is less than, equal to or greater than unity. For low values of κ_1, the damping characteristics of the system show a strong resemblance to those of a viscously damped system. It is also found that for small values of κ_1, there is good agreement between the single harmonic approximate solutions and solutions found using a time-domain "exact" solution technique. For larger values of κ_1, the agreement between the single harmonic results and results from the "exact" solution method deteriorates. This is due primarily to the increased occurrence of sticking. A somewhat surprising result is that at certain frequencies of excitation, small increases in the level of amplitude dependent friction can *increase* the amplitude of response. As one might expect, though, as the level of amplitude dependent friction approaches infinity, the response amplitude goes to zero. The results suggest that the passive damping of many mechanical systems can be enhanced by the addition of amplitude-dependent friction forces.

DAMPING AND VIBRATION OF BEAMS WITH VARIOUS TYPES OF FRICTIONAL SUPPORT CONDITIONS

Aldo A. Ferri *
Georgia Institute of Technology
Atlanta, GA 30332-0405

Abstract

The damping characteristics of a flexible beam with various types of frictional supports is considered. For each configuration studied, the only source of damping is dry friction at one support. The study considers supports with constant normal forces and supports for which the normal force varies with beam displacement. It is seen that the nature of the damping depends on whether the frictional interface is transverse to or in line with the beam. It is also seen that the equivalent viscous damping of the system can be inversely proportional to, invariant with respect to, directly proportional to, or directly proportional to the square of the displacement amplitude.

Introduction

Built-up and fastened structures are of considerable interest due to their many applications in the aerospace industry. In particular, aircraft frames and large space structures (LSS) are typically composed of large numbers of monolithic beams and plates which are fastened together by various means. In the case of LSS, the structures are usually composed of truss elements interconnected by joints. The connecting joints are a vital source of energy dissipation for LSS and, consequently, much interest has been directed towards the design of joints that provide a maximum amount of passive damping. A survey of some popular joint configurations may be found in references 1 and 2. Many studies have been conducted to determine analytically and/or experimentally the damping properties of built-up and fastened structures [1-4]. Unfortunately, the studies have often produced contradictory conclusions regarding the type and the amount of damping that can be expected from built-up structures. See, for example Ungar [7,8]. The purpose of this paper is to examine the influence of the nature of the fastening device on the type of damping that the structure exhibits. In particular, the damping characteristics of structures damped solely by dry friction are investigated.

A flexible elastic beam is studied with four different types of frictional interfaces. The four cases are shown schematically in Figures 1 through 4. In each case, the only source of damping is a frictional interface on the right-hand side, $x = L$. Case I incorporates a transverse

frictional interface while Cases II, III and IV contain longitudinal or "in-plane" frictional interfaces. Examination of these four cases provides insight into the amount and the type of damping that can be obtained in built-up structures through dry friction.

Case I: Transverse Slipping

Figure 1 shows a linear elastic beam with a transverse frictional interface on the right-hand side. This type of system has been studied by a number of authors. [9-12] The governing equation for this system is

$$EI \frac{\partial^4 w(x,t)}{\partial x^4} + m \frac{\partial^2 w(x,t)}{\partial t^2}$$

$$= F(x,t) - \mu N Sgn(\frac{\partial w(x=L,t)}{\partial t}) \delta(x-L) \quad (1)$$

where $w(x,t)$ is the transverse flexural displacement, EI is the beam's flexural rigidity, m is the mass per unit length, $F(x,t)$ is a distributed time varying external force and μ is the coefficient of sliding friction. N is the normal force to the sliding interface and it is assumed that it does not vary with time or with the beam's end deflection. The Sgn nonlinearity is defined to be equal to +1 when the argument is greater than zero, -1 when the argument is less than zero and equal to zero when the argument is identically zero. This can be viewed as a simplified version of the classic Coulomb damping law. (In this study, only steady slipping will be considered. In the case of stick-slip motion [13,14], it is necessary to modify equation (1) to explicitly define the friction force when the beam tip velocity is identically zero.)

In order to simplify the analysis, an approximate system model is considered, making use of a Galerkin projection of (1) onto a single spacial beam mode. The flexural beam displacement, $w(x,t)$ is approximated by a single beam mode $\phi_n(x)$ (perhaps a cantilevered-free uniform beam mode) and a single modal amplitude, $a_n(t)$:

$$w(x,t) = a_n(t) \phi_n(x) \quad (2)$$

Substituting (2) into (1) and performing the Galerkin procedure yields:

$$a_n(t) \int_0^L EI(\phi_n''(x))^2 dx$$

$$+ \ddot{a}_n(t) \int_0^L m\,\phi_n(x)^2 dx = \int_0^L F(x,t)\phi_n(x)dx$$

$$- \mu N\, Sgn(\dot{a}_n(t)\phi_n(L)) \int_0^L \delta(x-L)\phi_n(x)dx \qquad (3)$$

where ' and $\cdot$ denote differentiation with respect to x and t respectively. Note that, in keeping with the theory of Rayleigh-Ritz techniques, $\phi_n(x)$ need only satisfy the geometric boundary conditions for (3) to yield a "weak" solution [15]. Defining

$$m_n = \int_0^L m\phi_n(x)^2 dx \qquad (4a)$$

$$m_n \omega_n^2 = \int_0^L EI(\phi_n''(x))^2 dx \qquad (4b)$$

$$f_n(t) = \int_0^L F(x,t)\phi_n(x)dx \qquad (4c)$$

and assuming that $\phi_n(L)>0$, equation (3) can be written

$$m_n \left[\ddot{a}_n(t) + \omega_n^2\, a_n(t) \right]$$

$$= f_n(t) - \mu N Sgn(\dot{a}_n(t))\phi_n(L) \qquad (5)$$

First-order harmonic balance is now used to examine the qualitative behavior of the single-mode model governed by equation (5). The modal amplitude and the modal forcing are assumed to be simply harmonic in the form

$$a_n(t) = A \cos(\omega t) \qquad (6a)$$

$$f_n(t) = f_c \cos(\omega t) + f_s \sin(\omega t) \qquad (6b)$$

Note that the simple harmonic motion assumption rules out the possibility of stick-slip motion. Substituting (6a) and (6b) into (5) and balancing harmonics yields

$$m_n (\omega_n^2 - \omega^2) A = f_c \qquad (7)$$

$$-\mu N\phi_n(L)\frac{4}{\pi} = f_s \qquad (8)$$

where use has been made of the relation:

$$Sgn(-A\omega \sin(\omega t)) = -\frac{4}{\pi} \sin(\omega t) \qquad (9)$$

Noting that the amplitude of the harmonic excitation force f is given by $f^2 = f_c^2 + f_s^2$, equations (7) and (8) can be solved for the amplitude A.

$$f^2 = f_c^2 + f_s^2 = m_n^2(\omega_n^2 - \omega^2)^2 A^2 + (\mu N\phi_n(L)\frac{4}{\pi})^2$$

or

$$A = \cfrac{\cfrac{f}{m_n \omega_n^2}}{\left[(1-(\frac{\omega}{\omega_n})^2)^2 + \left[\frac{4\mu N\phi_n(L)}{\pi A m_n \omega_n^2} \right]^2 \right]^{1/2}} \qquad (10)$$

The equivalent viscous damping ratio is found by equating the damping term in equation (10) with the equivalent viscous damping term $2\varsigma_n \omega/\omega_n$:

$$2\varsigma_n \frac{\omega}{\omega_n} = \frac{4\mu N\phi_n(L)}{\pi A m_n \omega_n^2}$$

Solving for ς_n gives

$$\varsigma_n = \frac{2\mu N\phi_n(L)}{\pi A m_n \omega_n \omega} \qquad (11)$$

It may be noted that, except for the modal quantity, expression (11) is the classic result for a single-degree-of-freedom dry friction damped system [16]. At resonance, $\omega = \omega_n$ and expression (11) reduces to

$$\varsigma_n = \frac{2\mu N\phi_n(L)}{\pi A m_n \omega_n^2} \qquad (12)$$

Case II: Longitudinal Slipping, Constant Normal Force

The system shown in Figure 2 is studied next. The major difference between the procedure carried out for the case of transverse slipping and longitudinal slipping is that the latter requires the inclusion of a beam foreshortening. This problem was studied by Dowell [17], and the analysis is included here only for completeness. The governing equation for the system of Figure 2 is

$$EI \frac{\partial^4 w(x,t)}{\partial x^4} - N_x \frac{\partial^2 w(x,t)}{\partial x^2}$$

$$+ m \frac{\partial^2 w(x,t)}{\partial t^2} = F(x,t) \qquad (13)$$

$$N_x = -\mu N Sgn(\dot{u}) \qquad (14)$$

where N_x is the axial tension in the beam, and u is the longitudinal displacement of the beam tip (defined to be positive when in the positive x direction). Neglecting the axial deformation of the beam, the longitudinal tip displacement is due entirely to foreshortening:

$$u = -\frac{1}{2}\int_0^L (\frac{\partial w(x,t)}{\partial x})^2 dx \qquad (15)$$

Again, approximating the flexural displacement w(x,t) by the single mode expression (2), and performing a single mode Galerkin projection of equation (13) yields

$$a_n(t)\int_0^L EI(\phi_n''(x))^2 dx + N_x\, a_n(t)\int_0^L (\phi_n'(x))^2 dx$$

$$+ \ddot{a}_n(t)\int_0^L m\,\phi_n(x)^2 dx = \int_0^L F(x,t)\phi_n(x)dx \qquad (16)$$

Similarly, substituting (2) into (15) yields

$$u = -\frac{1}{2}a_n(t)^2\int_0^L (\phi_n'(x))^2 dx \qquad (17)$$

Since the integral term in (17) is guaranteed to be positive, substitution of (17) into (14) gives

$$N_x = \mu N\, Sgn(a_n(t)\dot{a}_n(t)) \qquad (18)$$

Defining

$$s_n = \int_0^L (\phi_n'(x))^2 dx \qquad (19)$$

and using the definitions given previously in (4a)-(4c), equations (16) and (18) can be combined in the form

$$m_n\left[\ddot{a}_n(t) + \omega_n^2\, a_n(t)\right]$$

$$+ \mu N\, Sgn(a_n(t)\dot{a}_n(t))s_n a_n(t) = f_n(t) \qquad (20)$$

An approximate solution to (20) is sought, as before, using first order harmonic balance. Substituting the relations (6a) and (6b) into (20) and balancing harmonics yields:

$$m_n (\omega_n^2 - \omega^2) A = f_c \qquad (21)$$

$$-\frac{2}{\pi}\mu N s_n A = f_s \qquad (22)$$

As before, these two equations may be combined to determine an expression for the equivalent viscous damping ratio at resonance:

$$\varsigma_n = \frac{\mu N s_n}{\pi m_n \omega_n^2} \qquad (23)$$

Case III: Longitudinal Slipping, Amplitude- Dependent Normal Force

The analysis for the system of Figure 3 is in most respects the same as that described for Case II. Equations (13), (15), (16) and (17) still apply. The primary difference is the governing law for the axial tension force, N_x

$$N_x = -\mu K\, |w(L-\epsilon,t)|\, Sgn(\dot{u})$$

where K is the clamping stiffness and ϵ is a small length parameter indicating that the clamping force is applied close to the beam's end. (It is assumed that there is no preload in the clamp.) Substituting the one-mode approximation (2) into the expression above yields

$$N_x = \mu k |a_n(t)| Sgn(a_n(t)\dot{a}_n(t)) \qquad (24)$$

where $k = K|\phi_n(L-\epsilon)|$ combines the effects of the clamping stiffness K and the mode shape near the beam tip. Substituting (24) into (16) and performing first order harmonic balance yields the following expression for equivalent viscous damping ratio at resonance:

$$\varsigma_n = \frac{2A\mu k s_n}{3\pi m_n \omega_n^2} \qquad (25)$$

Case IV: Longitudinal Slipping, Normal Force Dependent on Slip Displacement

Examining Figure 4, it is seen that the normal force is now dependent on the absolute value of the slip displacement, u. The axial tension in the beam can be expressed as

$$N_x = -\mu K \gamma |u|\, Sgn\,(\dot{u})$$

where γ is the "slope" of the beam profile at the right end of the beam. As for Case III, it is assumed that the preload of the clamp is zero. Using the one-mode approximation for u(t) given by (17), the expression above becomes

$$N_x = \mu k |\frac{1}{2} s_n a_n(t)^2|\, Sgn(a_n(t)\dot{a}_n(t)) \qquad (26)$$

where now, $k = K\gamma$ includes the effects of the clamping stiffness and the beam profile at the clamp. Expression (26) can be substituted into (16) yielding the single mode approximation for this system. Again, an equivalent viscous damping ratio can be found through the application of first order harmonic balance:

$$\varsigma_n = \frac{A^2 \mu k s_n^2}{4\pi m_n \omega_n^2} \qquad (27)$$

Discussion

The nature and the amount of damping that each of the frictional interfaces contribute to the flexible beam system can now be discussed. It is instructive to examine the influence of various physical parameters on the equivalent viscous damping ratio.

From equation (12), it is seen that the equivalent viscous damping at resonance for Case I is inversely proportional to the amplitude. Thus, high amplitude motion is more lightly damped than low amplitude motion. Such systems are prone to unbounded response at resonance and exhibit free time response with linear envelopes of decay. The system is also seen to depend directly on the magnitude of the friction force, μN. Finally, it is seen that the damping is inversely proportional to the modal stiffness, $m_n \omega_n^2$.

In order to examine the damping characteristics of the systems in Cases II, III and IV in terms of physical quantities, the mode shapes for a simply-supported uniform beam are used. The nth such mode is given by

$$\phi_n(x) = \sin(\frac{n\pi x}{L}) \qquad (28)$$

Using this expression in equations (4a), (4b) and (19) gives:

$$m_n = m\frac{L}{2} \qquad (29a)$$

$$\omega_n^2 = \frac{EI}{m} (\frac{n\pi}{L})^4 \qquad (29b)$$

$$s_n = \frac{L}{2}(\frac{n\pi}{L})^2 \qquad (29c)$$

Substitution of the relations (29a)-(29c) into (23) gives the equivalent damping ratio for Case II in terms of the physical parameters of the system:

$$\varsigma_n = \frac{\mu N L^2}{\pi^3 EI n^2} \qquad (30)$$

It is seen that the equivalent viscous damping is inversely proportional to EI and to the square of the mode number. Thus it is expected that for a particular beam material and geometry, dry friction contributes less damping to the higher modes than to the lower modes. It can also be seen that the viscous damping is directly proportional to μN and to L^2. Note that, in contrast to the transverse slipping case, the damping ratio is not dependent on amplitude and, as noted in reference 17, the damping is similar to viscous damping.

It may be noted that the equivalent viscous damping ratio derived by Hertz and Crawley [1] was also found to be independent of amplitude. The system studied there did not include beam foreshortening, but did include a amplitude-dependent normal force. It appears that a number of different systems damped only by dry friction can exhibit a viscous-like damping characteristic. This type of behavior is seen in references 18 and 19 as well.

In terms of physical quantities, the equivalent viscous damping for Case III can be obtained by substituting expressions (29a)-(29c) into (25):

$$\varsigma_n = \frac{2\mu k A L^2}{3\pi^3 EI n^2} \qquad (31)$$

Again it is seen that the equivalent viscous damping ratio in the nth mode is inversely proportional to EI and to the square of the mode number. It is also found to be directly proportional to L^2, to μN, and to the clamping stiffness. Most importantly, it is seen to be directly proportional to the transverse amplitude of response, A. Thus the damping increases as the amplitude of vibration increases. This type of behavior is similar to that of a system with hydraulic damping. [16] It should be mentioned that the value of k is also tied to the mode number n. As seen in equation (24), k depends on the mode shape $\phi_n(x)$ evaluated at $x=L-\epsilon$. Thus, the value of k will vary with n unless $n\epsilon/L$ is maintained equal to a constant.

These three cases may be contrasted with that of Case IV. Substituting (29a)-(29c) into (27) gives

$$\varsigma_n = \frac{\mu k L A^2}{8\pi EI} \qquad (32)$$

In this case, the damping ratio is inversely proportional to EI, and is directly proportional to μN, the clamping stiffness and the beam length. Unlike the previous three cases, the damping appears to be independent of mode number. In this respect, it is similar to linear viscous damping. However, unlike viscous damping, the equivalent damping ratio is seen to be directly proportional to the square of the amplitude.

The results suggest that it may be possible for a system damped largely by dry friction to exhibit a number of different types of damping characteristics. The nature of the damping and its dependence on vibration amplitude, mode number, material properties and length dimensions is governed by the geometry of the connecting interfaces. Examining the types of configurations shown in Figures 1 through 4, it is reasonable to assume that a standard truss structure or typical space-frame may have some or all of the clamping conditions shown. Also, one might envision that the connecting joints in some structures may behave like those of Cases I and II for small levels of beam displacement, behave like that of Case III for somewhat larger beam displacement amplitudes, and behave like that of Case IV for still larger

amplitudes. Moreover, a joint or interface could have the characteristic of two or more of the above cases *in the same amplitude or frequency range.* For example, including the effect of clamp preload in Cases III and IV will result in different expressions for the equivalent viscous damping ratio. Therefore, the amount and the nature of the damping exhibited by a structure may be highly dependent on the frequency of excitation and on the amplitude of response. It is perhaps for this reason that experiments that have attempted to measure the damping of built-up structures have yielded surprising and, at times, contradictory results.

Finally, it should be emphasized that these results are most accurate at system resonant frequencies. However, even at a resonant frequency, the presence of stick-slip motion or permanent interface "lockup" will undoubtedly affect the damping characteristics. When the system is forced off of a resonant frequency, two or more "modes" will respond. The analysis of stick-slip and multi-modal response requires a more refined analysis, and is planned as future work.

Conclusions

The analysis shows that a system damped solely by dry friction can exhibit many different types of damping characteristics. The nature of the damping for a particular structure is tied both to the amplitude dependence of the normal forces and to the orientation of the frictional interface in the structure. It is seen that it is possible for dry-friction damped systems to exhibit equivalent viscous damping properties that are inversely proportional to the response amplitude, invariant with respect to the response amplitude, directly proportional to the response amplitude or directly proportional to the square of the response amplitude.

The results also suggest that those systems that suffer from an inadequate level of passive damping might benefit from a redesign of the connecting interfaces. In particular, it may be possible to tailor frictional interfaces in turbomachinery bladed disks and in large space structure joints to enhance the overall structural damping level.

References

1. Hertz, T.J., and Crawley, E.F., "Damping in Space Structure Joints," AIAA Dynamics Specialists Conference, 17-18 May 1984, Palm Springs, California.

2. Hertz, T.J. and Crawley, E.F., "The Effects of Scale on the Dynamics of Flexible Space Structures," Report No. SSL 18-83, Space Systems Laboratory, Department of Aeronautics and Astronautics, Massachusetts Institute of Technology, Cambridge, MA, September 1983.

3. Ashley, H., "On Passive Damping Mechanisms in Large Space Structures," AIAA J. of Spacecraft and Rockets, Vol. 21, No. 5, 1984, pp. 448-455.

4. Crawley, E.F., Sarver, G.L., and Mohr, D.G., "Experimental Measurement of Passive Material and Structural Damping for Flexible Space Structures," Acta Astronautica, Vol. 10, No. 5-6, 1983, pp. 381-393.

5. Crawley, E.F. and Aubert, A.C., "Identification of Nonlinear Structural Elements by Force-State Mapping," AIAA Journal, Vol. 24, No. 1, 1986, pp. 155-162.

6. Sun, C.T. and Juang, J.N., "Modeling Global Structural Damping in Trusses Using Simple Continuum Models," AIAA Journal, Vol. 24, No. 1, 1986, pp. 144-150.

7. Ungar, E.E. and Carbonell, J.R., "On Panel Vibration Damping Due to Structural Joints," AIAA Journal, Vol. 4, No. 8, August, 1966, pp. 1385-1390.

8. Ungar, E.E., "The Status of Engineering Knowledge Concerning the Damping of Built-Up Structures," Journal of Sound and Vibration, Vol. 26, No. 1, 1973, pp. 141-154.

9. Dowell, E.H., "The Behavior of a Linear, Damped Modal System with a Nonlinear Spring-Mass-Dry Friction Damper System Attached," J. of Sound and Vibration, Vol. 89, No. 1, 1983, pp. 65-84.

10. Dowell, E.H., and Schwartz, H.B., "Forced Response of a Cantilever Beam with a Dry Friction Damper Attached, Part I: Theory," J. of Sound and Vibration, Vol. 91, No. 2, 1983, pp. 255-267.

11. Dowell, E.H., and Schwartz, H.B., "Forced Response of a Cantilever Beam with a Dry Friction Damper Attached, Part II: Experiment," J. of Sound and Vibration, Vol. 91, No. 2, 1983, pp. 269-291.

12. Ferri, A.A., and Dowell, E.H., "Frequency Domain Solutions to Multi-Degree-of-Freedom, Dry Friction Damped Systems," Journal of Sound and Vibration, Vol. 124, No. 2, 1988, pp. 207-224.

13. Pratt, T.K. and Williams, R., "Non-Linear Analysis of Stick/Slip Motion," Journal of Sound and Vibration, Vol. 74, No. 4, 1981, pp. 531-542.

14. Shaw, S.W., "On the Dynamic Response of a System with Dry Friction," Journal of Sound and Vibration, Vol. 108, No. 2, 1986, pp. 305-325.

15. Hughes, T.J.R., The Finite Element Method: Linear Static and Dynamic Finite Element Analysis, Prentice-Hall, Englewood Cliffs, New Jersey, 1987.

16. Den Hartog, J.P., **Mechanical Vibrations**, McGraw-Hill, New York, Fourth Edition, 1956.

17. Dowell, E.H., "Damping in Beams and Plates due to Slipping at the Support Boundaries," Journal of Sound and Vibration, Vol. 105, No. 2, 1986, pp. 243-254.

18. Jezequel, L., "Structural Damping by Slip in Joints," ASME Journal of Vibration, Acoustics, Stress, and Reliability in Design, Vol. 105, 1983, pp. 497-504.

19. Bielawa, R.L., "An Analytic Study of the Energy Dissipation of Turbomachinery Bladed-Disk Assemblies due to Inter-Shroud Segment Rubbing," ASME Journal of Mechanical Design, Vol. 100, April 1978, pp. 222-228.
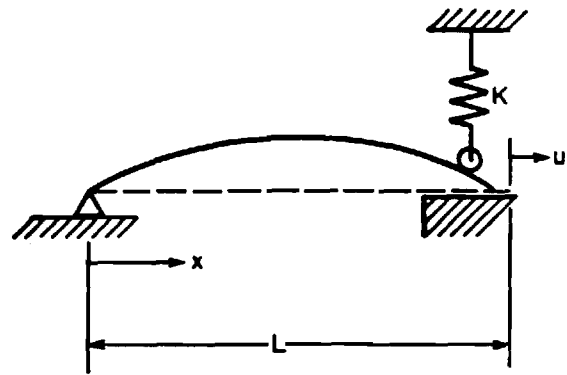
Figure 3:   Case III, longitudinal slipping, normal force proportional to beam flexural displacement
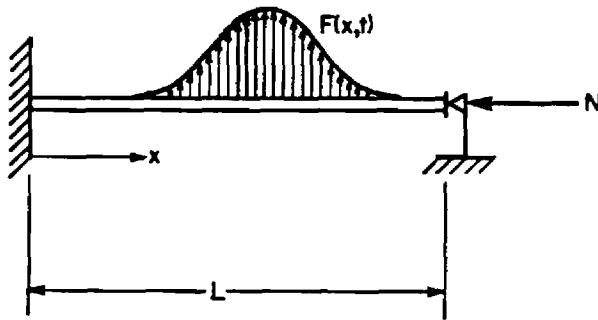
Figure 1:   Case I, transverse frictional interface
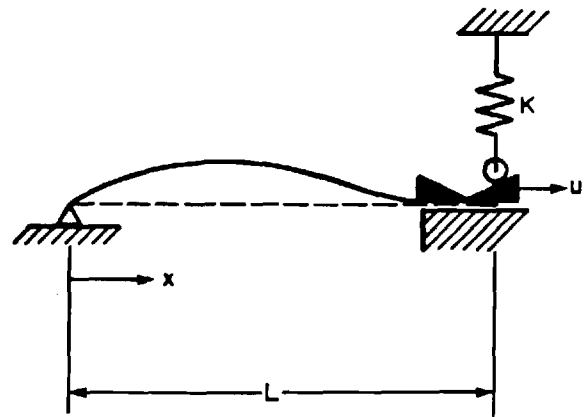
Figure 4:   Case IV, longitudinal slipping, normal force proportional to beam in-plane tip displacement
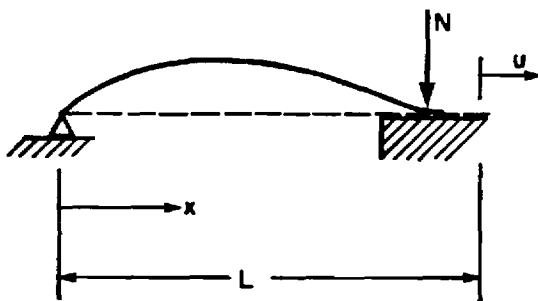
Figure 2:   Case II, longitudinal slipping, constant normal force

Active and Passive Joints for Damping Augmentation of Large Space Structures

Aldo A. Ferri
School of Mechanical Engineering

Bonnie S. Heck
School of Electrical Engineering

Georgia Institute of Technology
Atlanta, Georgia

Abstract

The low inherent damping of large space structures (LSS) has prompted considerable research into active and passive damping augmentation. This paper discusses the development and analysis of improved joints for large space structures. These joints are able to give LSS higher levels of passive damping without significantly increasing the structure's weight or complexity. Two types of joint designs will be considered: passive joints and active joints. In each case, the normal force to a frictional interface is varied yielding a connecting joint with increased damping performance. A single-degree-of-freedom joint and a system consisting of two elastic beams connected by a single active/passive joint are considered. It is shown that these new joint designs are able to enhance the energy dissipation from LSS in a relatively simple and robust way. Numerical simulation results are presented and discussed.

1. Introduction

One of the major problems remaining in the development of large space structures (LSS) is the anticipated low level of passive damping. This low level of damping impacts the feasibility of placing large flexible space structures in orbit for a number of reasons. Perhaps the most important reason is that it is difficult to design attitude and shape controllers for lightly damped flexible structures. Since the open-loop system has low relative stability, it is quite possible that perturbations to the control scheme, such as observation spillover or plant uncertainty, can drive the closed-loop system unstable [1]. Many researchers have aimed to circumvent this problem by designing better (often more complicated and sophisticated) control systems. A review of the literature up until 1984 can be found in reference [2]. An alternate approach is to design structures to have a

greater passive damping capacity. It has been shown that the addition of passive damping to a flexible structure can greatly facilitate the model reduction and control design of flexible structures [3,4]. This paper addresses the possibility of increasing the passive damping of truss-like structures by enhancing the energy dissipating capability of connecting joints.

It has been suggested that an important contributor to the overall passive damping of traditional flexible truss-like structures is the connecting joints [5,6]. One of the major dissipative mechanisms in joints is dry (Coulombic) friction. The analysis of structures with dry friction has received considerable attention. See, for example, Ferri [7] or the references cited therein. In most of these studies, it is assumed that the normal force to the sliding interface is constant. This may be termed the "classic" dry friction damped case. In the few studies where the normal force was allowed to vary with the relative slip amplitude, it was found that the system exhibited a viscous-like damping characteristic; see, for example, Hertz and Crawley [6] and Ferri [8-10].

The viscous-like damping property suggests that many mechanical designs can be improved by configuring frictional interfaces in ways that allow the normal forces to vary with displacement. In some applications, classic dry friction is inadequate to suppress vibration. For example, turbine blade systems experiencing flutter cannot be globally stabilized with classic dry friction. See for example Ferri [11] and Griffin and Sinha [12]. The deficiency stems from the fact that the damping level of dry friction damped systems with constant normal forces varies inversely with the amplitude of response. Hence, for a sufficiently large disturbance, it is possible for the energy input to the system by aerodynamic forces to overcome the energy dissipation provided by dry friction. In the field of LSS dynamics and control, the instabilities resulting from uncertainties and inaccuracies in the system model also result in forces which are in-phase with displacements and/or velocities. In these cases however, the external forces are provided by the force and torque actuators which are driven by a feedback control law. By designing connecting joints to have frictional forces which are dependent on relative joint displacements and velocities, it may be possible to greatly increase the stable operating range of an LSS attitude or shape controller.

It should be noted that viscous damping augmentation, especially in the form of viscoelastic materials such as those used in constrained layer damping, are subject to problems of "outgassing" in space environments [13]. This causes the material properties of the viscoelastic material to change with time, resulting in a degradation of the effectiveness of the damping treatment. An active or passive joint design which is based on energy dissipation from dry friction could provide a viscous-like damping, but still be well suited to a space environment.

The outline of the remainder of this paper follows. Section 2 discusses background material related to the dynamics of a dry friction damped system and introduces the design of passive and active joints as a method of damping augmentation. Section 3 first describes

the model development for single-degree-of-freedom joint systems. These models are then incorporated into a two-span flexible beam system. Sticking conditions for the joints are also obtained. Numerical studies are presented in Section 4 and Section 5 contains concluding remarks.

2. Background Material

As mentioned above, one of the major dissipative mechanisms in joints is dry (Coulombic) friction. It has been shown that dry friction can cause some significantly nonlinear behavior in an otherwise linear structure. The major nonlinear characteristics of classic dry friction damped systems are threshold force levels, "unbounded response" at resonance and "stick-slip" motion. A threshold force phenomenon implies that there exist different types of behavior for a flexible system with sliding interfaces. If the sum of the external forces acting tangent to the contact surface are not large enough to overcome the friction force then the sliding interface will "stick". At some critical value of disturbance or excitation level, the interface may break loose, causing a dramatic change in the system's behavior. "Unbounded response" at resonance refers to the fact that a structure damped only by dry friction can exhibit unbounded response when forced at a system natural frequency. As mentioned previously, this is due to the inverse dependence of damping on the amplitude of response in classic dry friction damped systems. Thus large levels of slip will decrease the damping contribution from the friction interface. "Stick-slip" motion refers to the fact that for some levels of excitation and/or for some frequencies of excitation, the sliding interface may stick and slip intermittently. One consequence of this is a net decrease in the amount of damping from the frictional interface. A second consequence is that the stick-slip motion will tend to excite other structural modes, making purely harmonic one-mode response unattainable.

It appears that the undesirable nonlinear effects of classic dry friction can be greatly reduced by the introduction of either an active or a passive mechanism by which the normal forces (and, hence the frictional forces) can be allowed to vary. At the same time, the beneficial contribution of dry friction to the overall damping of the structure can be retained or enhanced. For example, when permanent "lockup" occurs or when intermittent sticking occurs, the normal force can be reduced allowing motion (and, hence energy dissipation) to resume. On the other hand, the undesirable decrease in Coulombic damping with relative slip amplitude can be alleviated by allowing energy dissipation to be proportional to the square of the relative slip displacement.

The passive and active types of joints are discussed separately below.

1. Passive Joint: A passive connecting joint has been developed that has amplitude dependent friction forces. Although many types of truss connecting joints possess this property to varying degrees, the principle has not yet been fully exploited. One possible

joint configuration is the modified pin-type joint shown in Figure 1. (Though the connected members are shown as being simply curved, the actual geometry remains to be determined.) The curved contacting surfaces will allow the normal force to vary with the relative rotation angle. To re-iterate, this type of design will cause the overall damping to be nearly viscous, without the use of visco-elastic materials or "dash-pots". The passive joint design must also be well-suited to automated or human space platform construction, and must not adversely affect the structural integrity or the weight of the structure.

2. Active Joint: One of the limitations of the passive joint design is that the initial tension on the joint and the curvature of the connected elements must be chosen a priori. However, different vibration environments may require different normal forces. An active joint can be designed to choose the proper normal force to optimize the energy dissipation based on sensor feedback from colocated or distributed sensors. Many of the sensors used in an attitude or shape control system can also be used for the active joint control system. A preliminary design is shown in Figure 2. Note that the active control system acts solely to enhance the overall damping of the joints. One might therefore consider the strategy to be an "active-passive" damping augmentation technique, where active control is used to increase the effectiveness of a passive damping source. One advantage of this active control strategy is that the required actuator can be as simple as a commercially available electromagnetic clamp. Unlike other active damping schemes, the method is not based on momentum management techniques such as thruster rockets and control moment gyros. A general disadvantage of momentum management techniques is a weight penalty and, in the case of thruster rockets, a contamination of the local environment of the spacecraft.

There are several tradeoffs between active and passive joint types. The passive joint appears to be much less expensive and much lighter than the active joint, especially if one takes into account the total expense and weight associated with the power harness required for the active case. In fact, the passive joint requires no external energy source. A disadvantage of the passive joint is that it is non-adjustable. A particular geometry and pre-load must be chosen apriori and cannot be varied to accommodate changes in frictional properties or changes in the structural vibration environment. The active joint, on the other hand, is easily modified in real time, is more robust due to feedback, and can even be designed to behave linearly, like an ideal viscous damping element (see discussion below). The passive joint may be prone to steady-state error due to sticking whereas the active joint can be made asymptotically stable. Still, the passive joints proposed here are superior to those previously considered (e.g., [14]) where normal forces to frictional interfaces were pre-set and not allowed to vary with displacement.

It should also be mentioned that there is a similarity between the active joint and "semi-active" suspension elements for rail and road vehicles [15,16]. Semi-active suspensions are ones in which an orifice in a hydraulic dashpot is actively varied to produce different amounts and types of damping. Systems containing either a semi-active

suspension element or an active joint are not fully controllable but are only controllable to the origin. Another similarity is that a "failure" of the control system can only result in a degradation of performance, and not in instability since both elements can only remove energy from a system. An important difference, however, is that the mathematical model of the active joint is nonsmooth, making traditional optimal control strategies difficult to apply. Also, as mentioned earlier, a damper based on dry friction would seem to be better-suited to a space environment.

3. Model Development

In this section, models are developed for the active and passive single- degree-of-freedom (SDOF) system and the two-span beam.

SDOF Joint

Figure 3 shows a schematic of a SDOF joint including a frictional interface. The two connecting bodies are represented by the moving mass and the stationary frame. Using the nomenclature defined in Figure 3, a force summation in the direction tangent to the sliding interface yields the following equation of motion for the SDOF system:

$$m\ddot{x} + c\dot{x} + kx + R(x,\dot{x}) = F(t) \tag{1}$$

where $F(t)$ is a disturbance force and $R(x,\dot{x})$ is the nonlinear force which resists relative slip in the joint. In the case of the active joint $R(x,\dot{x})$ will be assumed to have the form

$$R(x,\dot{x}) = \mu\, N_A(x,\dot{x})\, Sgn(\dot{x}) \tag{2}$$

where

$$Sgn(z) = \begin{cases} +1 & ; \quad z>0 \\ 0 & ; \quad z=0 \\ -1 & ; \quad z<0 \end{cases}$$

and $N_A(x,\dot{x})$ is the active force applied normal to the sliding interface and has the form

$$N_A(x,\dot{x}) = K_0 + K_1|x| + K_2|\dot{x}| \tag{3}$$

Although, in practice, nothing limits the functional form of N_A (other than the fact that $N_A \geq 0$), the form shown above was chosen due to its simplicity and ease of implementation. (Optimal control strategies are left to a forthcoming paper. Note that due to the nonsmooth nature of the system dynamics, the optimization process is not trivial.) Note that the term

$$\mu K_2 |\dot{x}| \text{Sgn}(\dot{x}) = \mu K_2 \dot{x} \qquad (4)$$

can be interpreted as an additional *linear, or viscous damping* term. Substituting (2), (3) and (4) into (1) yields the general form for the active SDOF joint.

$$m\ddot{x} + (c + \mu K_2)\dot{x} + kx + \mu(K_0 + K_1 |x|)\text{Sgn}(\dot{x}) = F(t) \qquad (5)$$

A possible design of a passive SDOF joint is shown in Figure 4. In this case, variation in the normal force is achieved through contouring or profiling one of the two bodies and applying the normal force through an elastic spring element. A force summation in the direction tangent to the sliding interface yields the same equation as (1). In this case, however, the nonlinear resisting force is given by:

$$R(x, \dot{x}) = \mu N_p(x)\text{Sgn}(\dot{x}) + N_p(x)\tan\alpha \text{Sgn}(x) \qquad (6)$$

where the second term arises due to the component of the interaction force between the movable body and the roller in the direction tangent to the sliding interface. $N_p(x)$ is the passively applied normal force given by:

$$N_p(x) = k_0 + k_1 \tan\alpha |x| \qquad (7)$$

where k_0 is the preload (force) present in the spring at the point $x=0$. Substituting (6) and (7) into (1) yields:

$$m\ddot{x} + c\dot{x} + kx + \mu(k_0 + k_1 \tan\alpha |x|)\text{Sgn}(\dot{x})$$

$$+ (k_0 + k_1 \tan\alpha |x|)\tan\alpha \, \text{Sgn}(x) = F(t) \qquad (8)$$

or, noting that $|x|\text{Sgn}(x) = x$:

$$m\ddot{x} + c\dot{x} + (k + k_1 \tan^2\alpha)x + \mu(k_0 + k_1 \tan\alpha |x|)\text{Sgn}(\dot{x})$$

$$+ k_0 \tan\alpha \, \text{Sgn}(x) = F(t) \qquad (9)$$

Two-Beam Model

Consider the two-span beam system shown in Figure 5. The mathematical model for this system will be developed using a modal approach. The flexural displacement of the two beams are denoted w_1 and w_2 and are expanded as

$$w_1(x_1,t) = \sum_{i=1}^{N} a_i(t)\,\phi_i(x_1) \tag{10}$$

$$w_2(x_2,t) = \sum_{i=1}^{N} b_i(t)\,\psi_i(x_2) \tag{11}$$

The basis functions ϕ_i and ψ_i are chosen to be the normalized eigenfunctions for pinned-pinned beams of length L_1 and L_2 respectively:

$$\phi_n(x_1) = \left[\frac{2}{m_1 L_1}\right]^{1/2} \sin\left(\frac{n\pi x_1}{L_1}\right) \tag{12}$$

$$\psi_n(x_2) = \left[\frac{2}{m_2 L_2}\right]^{1/2} \sin\left(\frac{n\pi x_2}{L_2}\right) \tag{13}$$

where m_1 and m_2 are the mass/unit length for beams 1 and 2 respectively. Using these eigenfunctions as the basis functions yields the following equations of motion for the combined system.

$$\ddot{a}_i + 2\varsigma_{1i}\omega_{1i}\dot{a}_i + \omega_{1i}^2\,a_i = F_1(t)\,\phi(x_{F_1}) + M(t)\,\phi_i'(L_1) \qquad i=1,N \tag{14}$$

$$\ddot{b}_i + 2\varsigma_{2i}\omega_{2i}\dot{b}_i + \omega_{2i}^2\,b_i = F_2(t)\,\phi(x_{F_2}) - M(t)\,\psi_i'(0) \qquad i=1,N \tag{15}$$

$$M(t) = k_r\theta + rR(\theta,\dot{\theta}) \tag{16}$$

$$\theta(t) = \sum_{i=1}^{N} b_i(t)\,\psi_i'(0) - \sum_{j=1}^{N} a_i(t)\,\phi_i'(L_1) \tag{17}$$

$$\dot{\theta}(t) = \sum_{i=1}^{N} \dot{b}_i(t)\,\psi_i'(0) - \sum_{j=1}^{N} \dot{a}_i(t)\,\phi_i'(L_1) \tag{18}$$

$$' \equiv \frac{d}{dx_j} \qquad j=1 \text{ or } 2 \qquad (19)$$

where $R(\cdot,\cdot)$ is defined for the active joint in equation (2) and for the passive joint in equation (6). The angle θ represents the relative angular displacement between the left end of the second beam and the right end of the first beam. Again, N_A and N_p are the forces applied normal to the plane of relative motion (N_A and N_p correspond to the active and the passive joints, respectively). The quantity r is an appropriate length dimension such that $\mu r N_A$ (or $\mu r N_p$) is the magnitude of the frictional moment transmitted between the two beams. The total moment transmitted between the two beams is composed of the frictional moment, an elastic moment due to a restraining spring (having stiffness coefficient k_r), and for the passive joint an additional moment corresponding to the second term in equation (6). Note that ω_{ij} represents the jth natural frequency of the ith beam, without any coupling between the two beams. These are given by:

$$\omega_{ij} = j^2 \pi^2 \left[\frac{EI_i}{m_i L_i^4} \right]^{1/2} \qquad i=1,2 \qquad j=1,N \qquad (20)$$

Equations (14) and (15) can be placed in state-space form by defining the state vector to be

$$\underline{x} = [a_1, a_2, \ldots, a_N, b_1, \ldots, b_N, \dot{a}_1, \ldots, \dot{a}_N, \dot{b}_1, \ldots, \dot{b}_N]^T \qquad (21)$$

and defining

$$\underline{F}(t) = [F_1(t), F_2(t)]^T \qquad (22)$$

the equations of motion can be written:

$$\dot{\underline{x}} = A \underline{x} + G \underline{F}(t) + B M(t) \qquad (23)$$

where

$$A = \begin{bmatrix} [0]_{2N} & I_{2N} \\ -\text{Diag}(\omega) & -\text{Diag}(\varsigma) \end{bmatrix} \qquad (24)$$

$$G = \begin{bmatrix} \underline{0}_{2N} & \underline{0}_{2N} \\ \underline{\phi}(x_{F_1}) & \underline{0}_N \\ \underline{0}_N & \underline{\psi}(x_{F_2}) \end{bmatrix} \qquad (25)$$

$$B = [\underline{0}_{2N}^T, \quad (\underline{\phi}'(L_1))^T, \quad -(\underline{\psi}'(0))^T]^T \tag{26}$$

where

$$\text{Diag}(\varsigma) = \text{Diag}(2\varsigma_{11}\omega_{11}, \ 2\varsigma_{12}\omega_{12}, \ldots, \ 2\varsigma_{1N}\omega_{1N}, \ 2\varsigma_{21}\omega_{21}, \ldots, \ 2\varsigma_{2N}\omega_{21}) \tag{27}$$

$$\text{Diag}(\omega) = \text{Diag}(\ \omega_{11}^2, \ \omega_{12}^2, \ldots, \ \omega_{1N}^2, \ \omega_{21}^2, \ldots, \ \omega_{21}^2) \tag{28}$$

$$\underline{\phi}(x) = [\phi_1(x), \ \dot{\phi}_2(x), \ldots, \ \phi_N(x)]^T \tag{29}$$

$$\underline{\psi}(x) = [\psi_1(x), \ \psi_2(x), \ldots, \ \psi_N(x)]^T \tag{30}$$

$$\underline{\phi}'(x) = [\phi_1'(x), \ \phi_2'(x), \ldots, \ \phi_N'(x)]^T \tag{31}$$

$$\underline{\psi}'(x) = [\psi_1'(x), \ \psi_2'(x), \ldots, \ \psi_N'(x)]^T \tag{32}$$

$[0]_{2N}$ is a 2Nx2N null matrix, I_{2N} is a 2Nx2N identity matrix, $\underline{0}_{2N}$ is a 2Nx1 null column vector and $\underline{0}_N$ is an Nx1 null column vector. The system outputs y_1 and y_2 are defined to be the flexural displacements of the first beam at $x_1 = 0.25L_1$ and $x_2 = 0.75L_2$, respectively:

$$\underline{y} = C \ \underline{x} \tag{33}$$

where

$$\underline{y} = [y_1, \ y_2]^T \tag{34}$$

$$C = \begin{bmatrix} \underline{\phi}^T(0.25L_1) & \underline{0}_N^T & \underline{0}_{2N}^T \\ \underline{0}_N^T & \underline{\psi}^T(0.75L_2) & \underline{0}_{2N}^T \end{bmatrix} \tag{35}$$

Finally, it is convenient to relate the relative angular displacement θ to the state vector $\underline{x}$:

$$\theta = D_1 \ \underline{x} \tag{36}$$

$$\dot{\theta} = D_1 \ \underline{\dot{x}} = D_2 \ \underline{x} \tag{37}$$

where

$$D_1 = [(\underline{\phi}'(L_1))^T, \ (\underline{\psi}'(0))^T, \ \underline{0}_{2N}^T] \tag{38}$$

$$D_2 = [\underline{0}_{2N}^T, \ (\underline{\phi}'(L_1))^T, \ (\underline{\psi}'(0))^T] \tag{39}$$

are 1x4N constant-valued row vectors.

The two-beam system may be viewed as a general case of two linear, distributed elastic systems coupled with an active/passive joint. The pinned-pinned configuration is chosen solely for the resulting simple form of the modal expansions. The modal formulation is applicable to arbitrary coupled elastic systems by simply replacing the modal eigenfunctions and natural frequencies with those of the actual system.

Sticking Regions

An important consideration in the design of an active or passive joint is joint lock-up or sticking. Sticking degrades the system performance for two reasons. First, since the energy dissipation mechanism is dry friction, slipping is necessary for positive damping to occur. Intermittent sticking results in a degradation of energy dissipation, therefore it should be avoided. Second, permanent lock-up is undesirable because it destroys asymptotic stability.

Sticking conditions can be obtained by examining the impending motion of the system when the relative slip velocity is zero. The body of work in the field of variable structure systems (VSS) [17] can be drawn upon to determine the sticking conditions and the resultant system dynamics when sticking occurs. (In the terminology of VSS, sticking of dry friction damped systems is referred to as *sliding*. In this paper, sticking and sliding will refer to the physical condition of the frictional interface.) For the SDOF system, sticking occurs when the following condition is met:

$$\dot{x} \, \ddot{x}^* < 0 \quad \forall \ (x, \dot{x}) \ \text{such that} \ |\dot{x}| < \epsilon \tag{40}$$

where ϵ is a small positive parameter. Substitution of $\ddot{x}^*$ from equation (1) into (40) yields specific conditions for sticking to occur in both the active SDOF system and the passive SDOF system.

The sticking conditions for the active SDOF system with no external forcing are given as follows:

i) If $\mu K_1 \geq K$, then the system sticks for all x.

(41)

ii) If $\mu K_1 < K$, then the system sticks for all x such that

$$|x| \leq \frac{\mu K_0}{K - \mu K_1}$$

The sticking conditions for the passive SDOF system with no external forcing are given as follows:

i) If $\mu > \tan\alpha$ and $k \leq (\mu - \tan\alpha)k_1 \tan\alpha$,

then sticking occurs for all x.

ii) If $\mu > \tan\alpha$ and $k > (\mu - \tan\alpha)k_1 \tan\alpha$,

then sticking occurs for all x such that

$$|x| < \frac{(\mu - \tan\alpha)k_0}{k - (\mu-\tan\alpha)k_1\tan\alpha}$$

(42)

The sticking conditions for the passive joint are shown graphically in Figure 6. As seen in the figure, when the elastic spring constant, k, is sufficiently small, sticking occurs for all values of x. For larger values of k, sticking occurs for smaller and smaller values of x. In other words, the sticking region grows smaller as the value of the elastic spring constant (or the value of α) increases. Also note that for the case $k_0 = 0$, no sticking occurs for $k > k_1 \tan\alpha(\mu-\tan\alpha)$. These sticking conditions can be used to design a frictional interface so that it does not stick, or is at least ultimately bounded. Note that a sufficient condition for sticking not to occur is

$$\mu \leq \tan\alpha$$

(43)

When sticking occurs, an expression for the system dynamics can be obtained using the equivalent control method [17]. The exression for both the active and the passive SDOF system is given as follows:

$$m\ddot{x} = 0$$

(44)

This system is linear and contains two zero eigenvalues resulting from the constraint that the velocity is zero during sticking. It should be noted that, for the unforced case $F(t)=0$, once the system has stuck, it remains terminally stuck. Thus, while the system is stable in the sense of Lyapunov, it is not necessarily asymptotically stable. Also note that stability is preserved even under a control system failure.

The sticking conditions for the two-beam system with either the passive or the active joints are obtained in the same way as for the SDOF system. The relative slip displacement x must be replaced by the relative angular displacement θ. The first and second derivatives of θ with respect to time can be expressed in terms of the state vector $\underline{x}$ through use of equations (23)-(39).

$$\dot{\theta}\ \dot{\theta}^* = \underline{x}^T D_2^T D_2 \underline{\dot{x}} < 0 \quad \forall\ \underline{x}\ \text{such that}\ |\dot{\theta}| < \epsilon \qquad (45)$$

where, again, ϵ is a small positive parameter. Substitution of (23) into (45) yields:

$$\underline{x}^T D_2^T D_2 \left[A\ \underline{x} + G\ \underline{F}(t) + B\ M(t) \right] < 0 \quad \forall\ \underline{x}\ \text{such that}\ |\dot{\theta}| < \epsilon \qquad (46)$$

An expression for the dynamics of the system during sticking is again found using the equivalent control method [17]. Interestingly, the dynamics of the system during sticking are the same for both the passive and the active joints:

$$\underline{\dot{x}} = (A - B(D_2 B)^{-1} A)\underline{x} + (G - B(D_2 B)^{-1} G)\underline{F} \qquad (47)$$

As in the SDOF case, the dynamics of the system during sticking is linear with two zero eigenvalues corresponding to the constraint that the angular joint velocity must be zero for sticking to occur. Unlike the SDOF system, the unforced two-beam system can still experience motion when the frictional interface is stuck. Thus when sticking occurs, the damping of the system is reduced to that associated with flexural deformation of the beams. It is also interesting that the unforced system can breakloose by itself. Thus, stick-slip motion is possible.

4. Numerical Results

A variety of simulation results are presented next to show the qualitative effect of the various joint design parameters on the free response of the two-beam model. Both active and passive joint configurations are considered. For each case presented, the properties of the A,B,C and D_2 matrices are kept the same. A single beam mode is used to represent each beam. The following numerical values are used: $m_1 = m_2 = 3.25458$ kg/m^3, $L_1 = 1.0$ m, $L_2 = 2.0$ m, $EI_1 = EI_2 = 755.06$ N·m^2, $\mu = 0.1$, $r = 0.01$ m, and $\varsigma_{11} = \varsigma_{21} = 0$. The initial condition for each simulation result is $\underline{x} = [0.0127617, 0, 0, 0]^T$. This corresponds to an initial deflection of 1 cm at the midspan of the first beam.

Figures 7-11 pertain to the two-span beam system connected by the passive joint. Figures 7 and 8 show the relative effect of the transverse spring constant, k_1. (Recall that, for the active joint, K_1 plays a role similar to that of $k_1 \tan\alpha$ in the passive case.) Figure 7 shows the free response of y_1 for $k_1 = 10,000$ N/m. Note that the envelope of decay is

exponential in shape, similar to the case of linear, viscous damping. It is important to note that the only source of damping in this system is dry friction since the beam structural damping has been set equal to zero. As the value of k_1 is increased, the response damps out faster, but the envelopes of decay remain exponential in shape for large values of displacement. For smaller values of displacement, stick-slip motion becomes prevalent as seen in Figure 8 which shows the relative angular displacement in the joint, θ. The constant-valued portions of the curve in Figure 8 correspond to sticking.

Figures 9 and 10 show the relative effect of k_0 on the free response. For these plots, $\alpha = 0$ and $k_1 = 0$, therefore, this corresponds to the case of constant normal force; i.e., the classic dry friction case. Note that the envelopes of decay in these figures are linear like those traditionally associated with dry friction. As the value of k_0 is increased, the oscillations die out more rapidly, however, sticking becomes more noticeable. Observe that in Figure 10, once permanent sticking has occurred ($t \approx 0.2$ sec), no further energy dissipation takes place and a steady-state oscillation results.

Figure 11 shows the free response of y_1 for the passive joint case with $k_0 = 10$, $k_1 = 10,000$ and $\alpha = 10^\circ$. Note that the system exhibits both linear and exponential envelopes of decay. The envelope is more nearly exponential for large values of displacement and more nearly linear for small values of displacement.

The effect of α is seen by comparing Figure 11 (where $\alpha = 10^\circ$) to Figure 12 (where $\alpha = 20^\circ$). Essentially, increasing the value of α has two effects: it increases the natural frequency of the system by adding an apparent stiffness to the joint, and it increases the rate of decay of the free response.

The performance of the active joint is seen in Figure 13. Figure 13 corresponds to the case $K_0 = K_1 = 0$, $K_2 = 399$ N/(m/s). Recall that setting K_0 and K_1 both equal to zero results in the joint characteristics being equivalent to those of a linear viscous damping element. The value $K_2 = 399$ N/(m/s) corresponds to the viscous damping element that gives the highest level of damping to the most lightly-damped linear mode of vibration. As can be seen, excellent performance is obtained. An extensive study was conducted varying K_0, K_1 and K_2 for the system with the parameters defined above. It was found that using non-zero values of K_0 and K_1 in conjunction with $K_2 = 399$ N/(m/s) resulted in the degradation of system performance over that shown in Figure 13.

5. Concluding Remarks

These results suggest that joints designed with amplitude or rate-dependent frictional forces can offer substantial improvements in performance over joints with constant normal forces. One advantage is that the overall damping characteristics can be made to resemble those of a linear viscous damping element. Thus, it may be possible to incorporate the joints in a global structural model as simple linear elements, greatly simplifying the analysis

of the assembled structure. In addition, the modified joints are well-suited to a space environment and do not present a significant weight penalty.

It should be added that both the active and passive joint types can be used together in a single space structure. Although it may be unnecessary (or even impractical) to place active or passive joints at *every truss structure juncture,* it may be possible to achieve good results simply by placing a few active or passive joints at strategic locations throughout the structure. The interaction of the active and passive joints with an overall attitude or pointing control strategy also needs to be addressed.

Acknowledgement

References

1. Balas, M.J., "Active Control of Flexible Systems," Journal of Optimization Theory and Applications, Vol. 25, No. 3, 1978, pp. 415-436.

2. Nurre, G.S., Ryan, R.S., Scofield, H.N. and Sims, J.L., "Dynamics and Control of Large Space Structures," Journal of Guidance and Control, Vol. 7, No. 5, 1984, pp. 514-526.

3. Alberts, T.E., Hastings, G.G., Book, W.J., and Dickerson, S.L., "Experiments in Optimal Control of a Flexible Arm with Passive Damping," Fifth VPI&SU/AIAA Symposium on Dynamics and Control of Large Structures, 12-14 June 1985, Blacksburg, VA.

4. Alberts, T.E., "Augmenting the Control of a Flexible Manipulator with Passive Mechanical Damping," Ph.D. Thesis, School of Mechanical Engineering, Georgia Institute of Technology, Atlanta, GA, September 1986.

5. Hertz, T.J. and Crawley, E.F., "The Effects of Scale on the Dynamics of Flexible Space Structures," Report No. SSL 18-83, Space Systems Laboratory, Department of Aeronautics and Astronautics, Massachusetts Institute of Technology, Cambridge, MA, September 1983.

6. Hertz, T.J., and Crawley, E.F., "Damping in Space Structure Joints," AIAA Dynamics Specialists Conference, 17-18 May 1984, Palm Springs, California.

7. Ferri, A.A., "The Dynamics of Dry Friction Damped Systems," Ph.D. Thesis, Department of Mechanical and Aerospace Engineering, Princeton University, Princeton, NJ, September 1985.

8. Ferri, A.A., "Investigation of Damping From Nonlinear Sleeve Joints of Large Space Structures," Proceedings of the ASME 11th Biennial Conference on Mechanical Vibrations and Noise, Boston, MA, September 27-30, 1987.

9. Ferri, A.A., "Modeling and Analysis of Nonlinear Sleeve Joints of Large Space Structures," AIAA Journal of Spacecraft and Rockets, Vol. 25, No. 5, 1988, pp. 354-360.

10. Ferri, A.A., "Damping and Vibration of Beams with Various types of Frictional Support Conditions," Proceedings of the AIAA/ASME/ASCE/AHS/ASC 30th Structures, Structural Dynamics and Materials Conference, Mobile, AL, April 3-5, 1989.

11. Ferri, A.A., and Dowell, E.H., "The Behavior of a Linear, Damped Modal System with a Nonlinear Spring-Mass-Dry Friction Damper System Attached, Part II," Journal of Sound Vibration, Vol. 101, No. 1, 1985, pp. 55-74.

12. Griffin, J.H. and Sinha, A., "Friction Damping of Flutter in Gas Turbine Engine Airfoils," AIAA J. Aircraft, Vol. 20, No. 4, pp. 372-376.

13. Trudell, R.W., Curley, R.C. and Rogers, L.C., "Passive Damping in Large Space Structures," AIAA Paper No. AIAA-80-0677, 13 pgs.

14. Beards, C.F., "The Damping of Structural Vibration by Controlled Interfacial Slip in Joints," Journal of Vibration, Acoustics, Stress, and Reliability in Design, Vol. 105, July 1983, pp. 369-373.

15. Hrovat, D., Margolis, D.L. and Hubbard, M., "An Approach Toward the Optimal Semi-Active Suspension," ASME Journal of Dynamic Systems, Measurement, and Control, Vol. 110, September 1988, pp. 288-296.

16. Graf, P.L. and Shoureshi, R., "Modeling and Implementation of Semi-Active Hydraulic Engine Mounts," ASME Journal of Dynamic Systems, Measurement, and Control, Vol. 110, December 1988, pp. 422-429.

17. Utkin, V.I., "Variable Structure Systems with Sliding Modes," IEEE Transactions on Automatic Control, Vol. AC-22, April 1977, pp. 212-222.
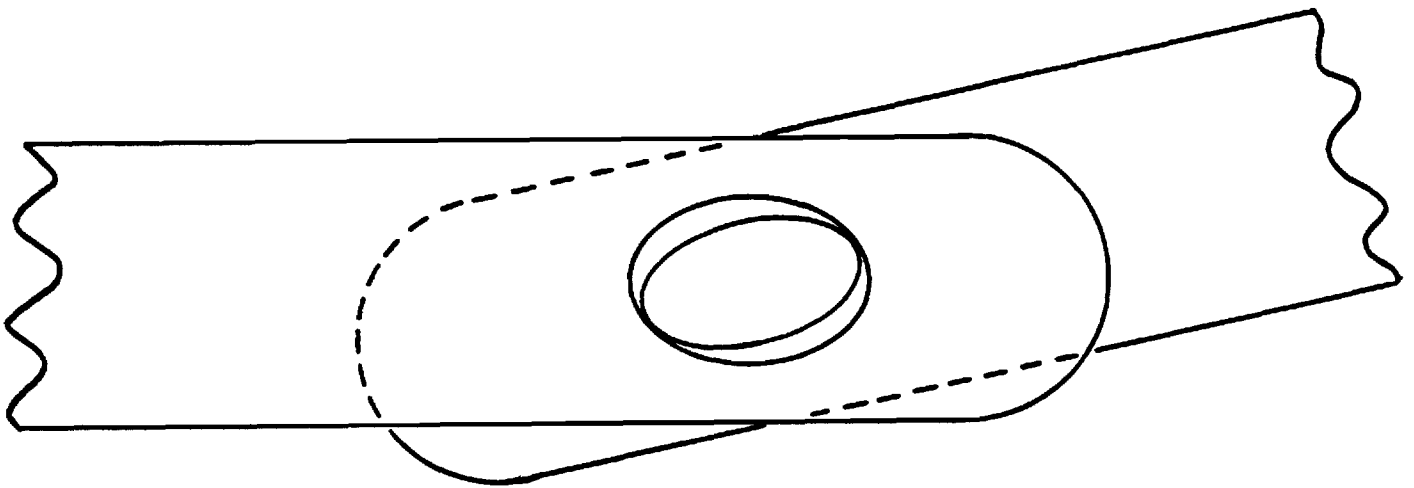
Figure 1: Passive revolute joint geometry.
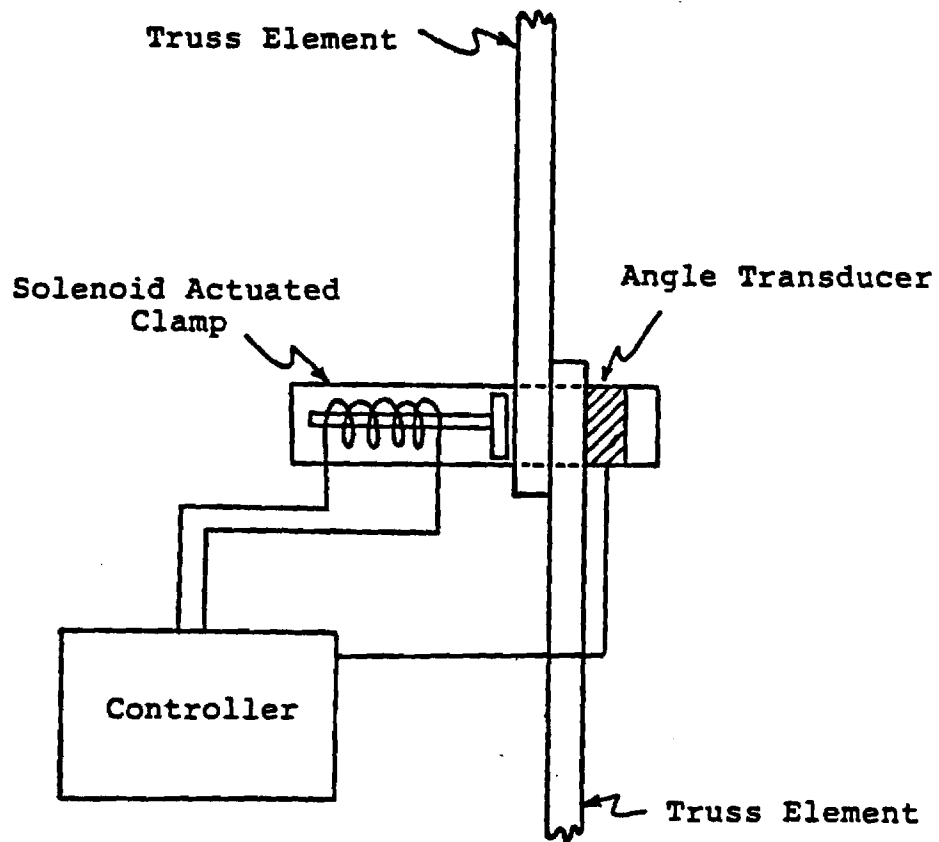
Figure 2: Active joint shown in a truss structure.
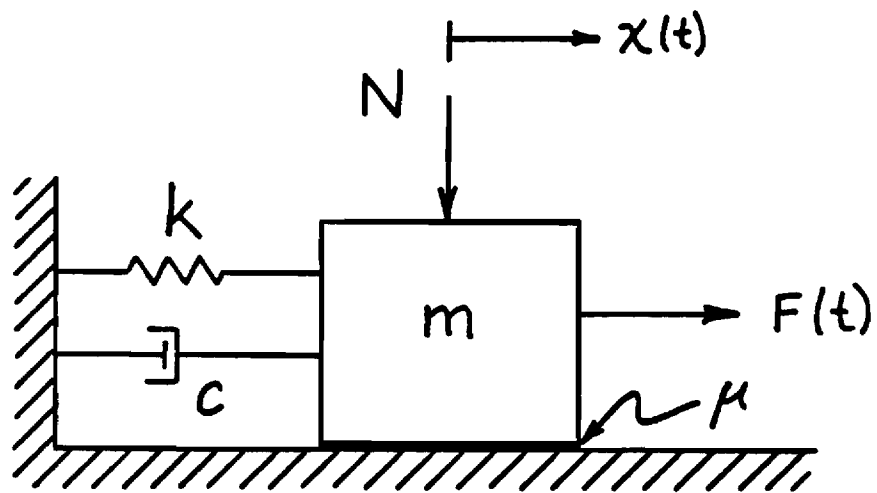
Figure 3: SDOF Dry-Friction Damped System.
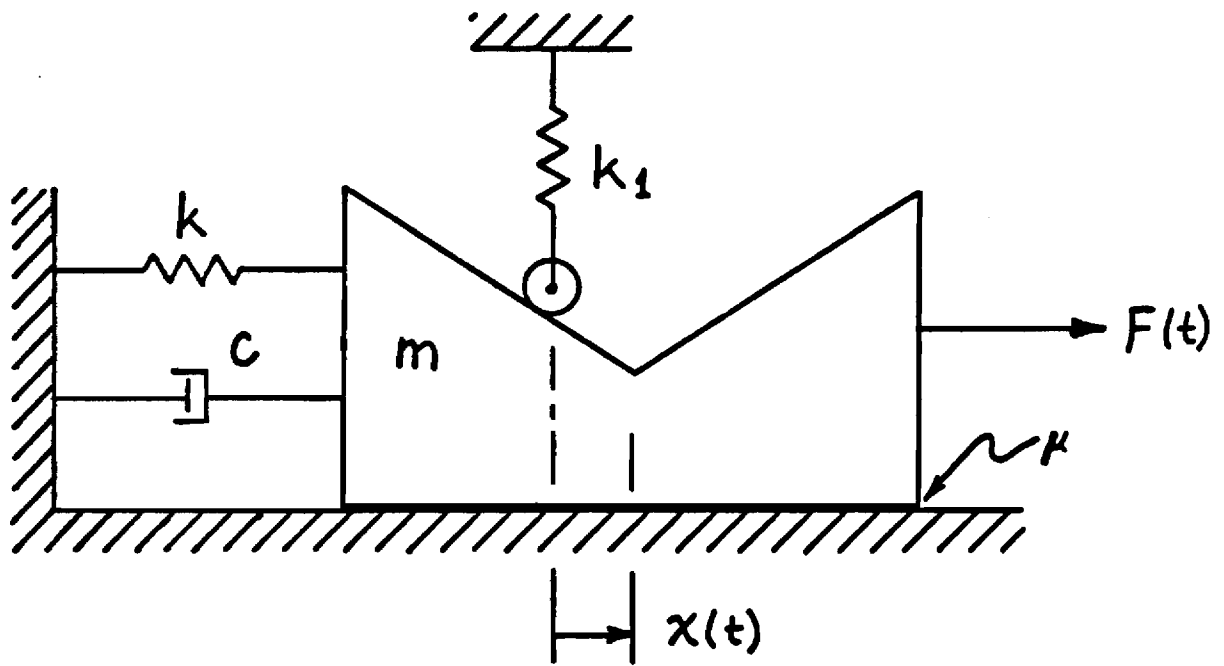
Figure 4: SDOF passive joint model.
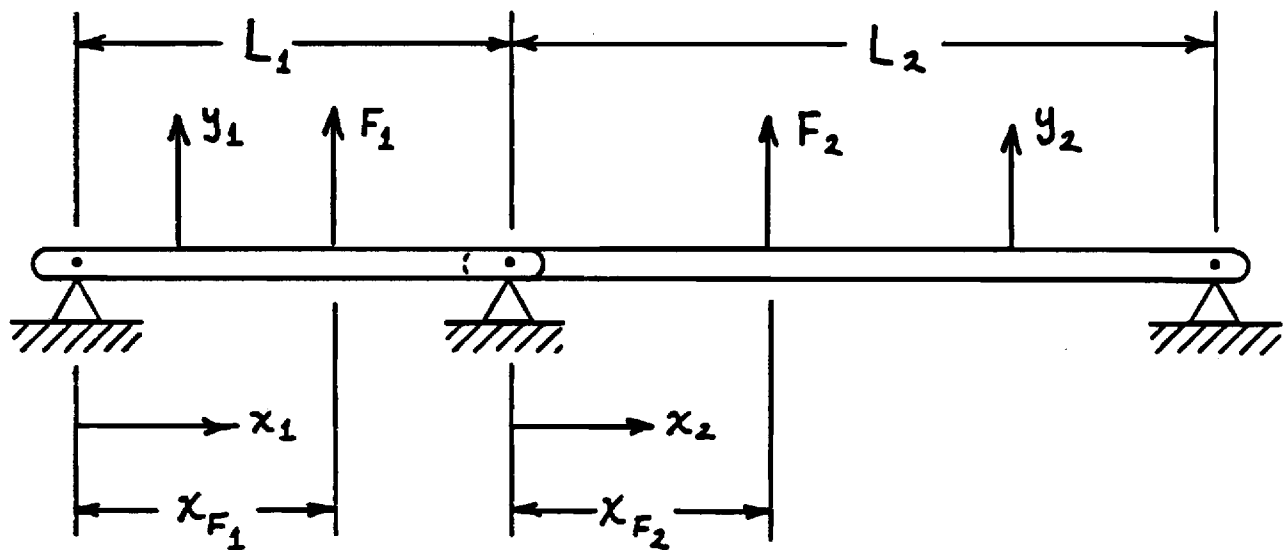
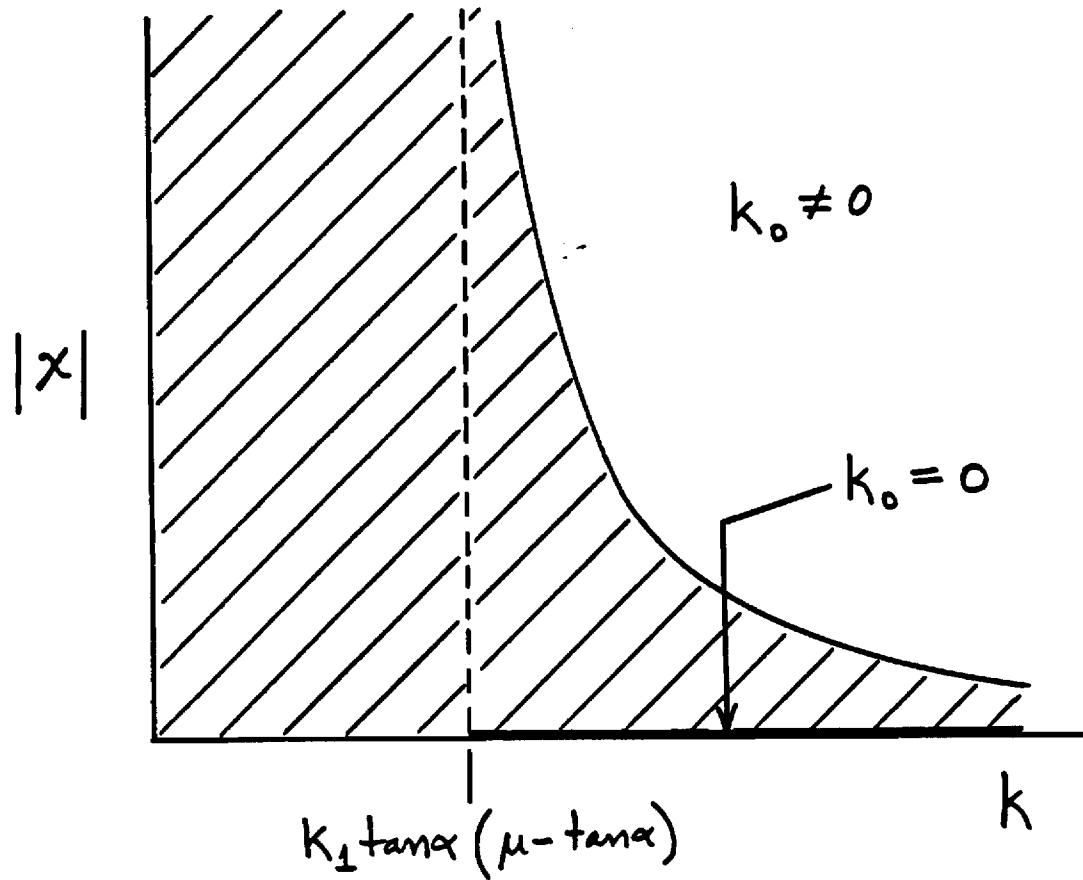Figure 5: Two-span flexible beam system connected through an active/passive revolute joint.

Figure 6: Sticking values of x as a function of the elastic spring constant k for the case $\mu > \tan\alpha$. The shaded region is the region in which sticking will occur. Note that for $k < k_1\tan\alpha(\mu-\tan\alpha)$, sticking occurs for all values of x regardless of the value of k_0.
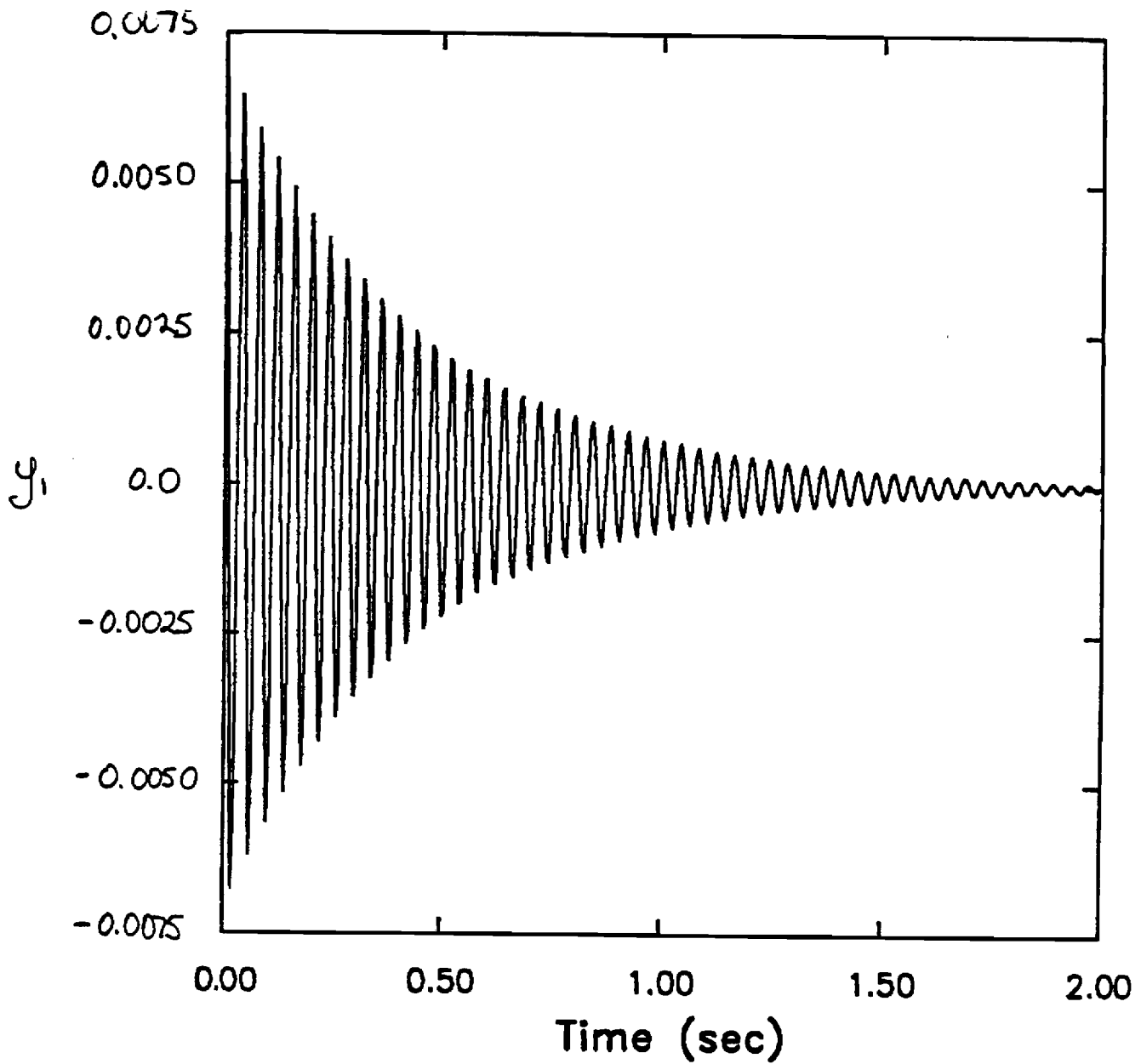
Figure 7:   Free response of y_1 for two-span beam system with passive joint ($k_0 = 0$, $k_1 = 10,000$, $\alpha = 10°$).
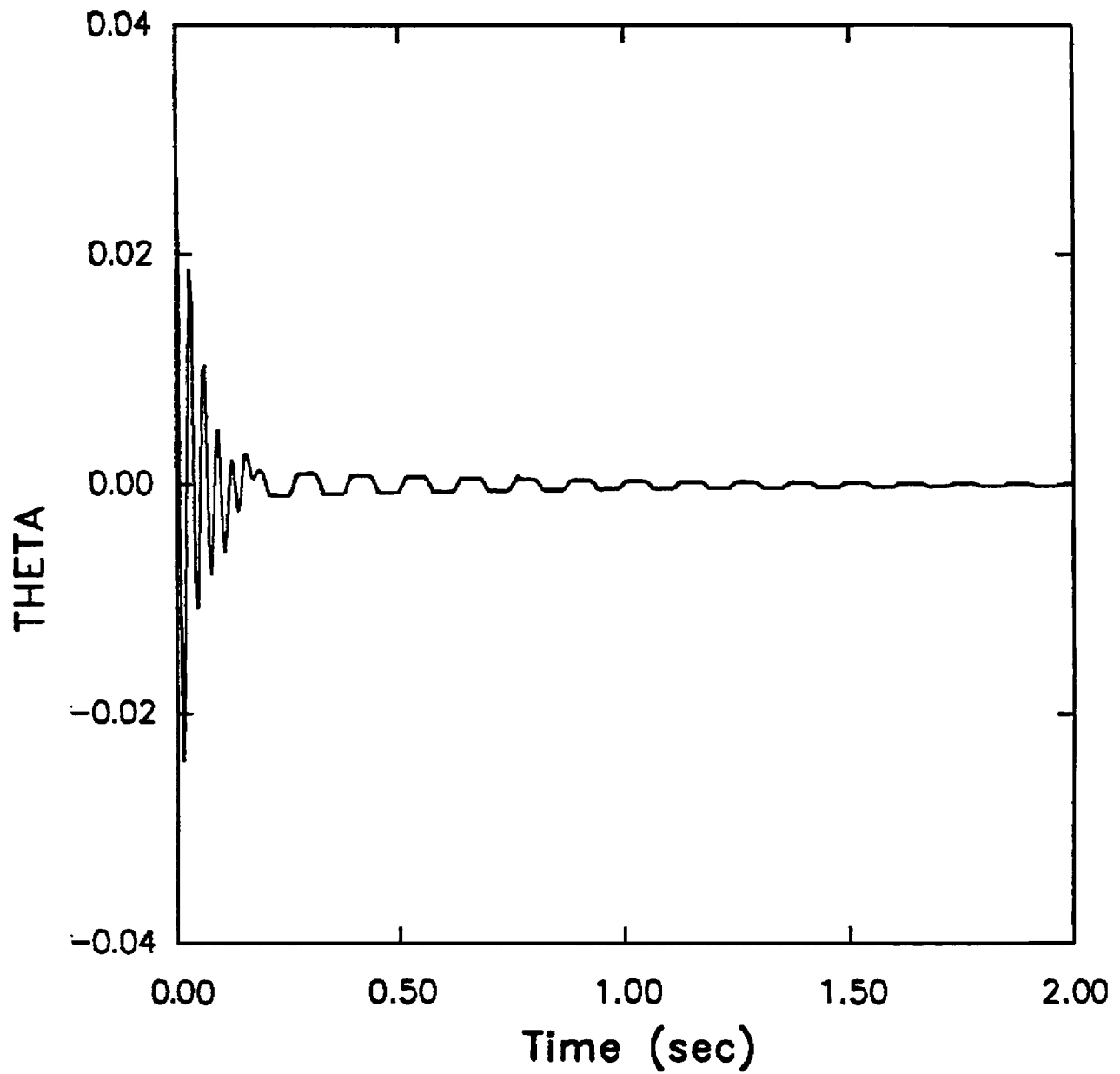
Figure 8:   Free response of θ for two-span beam system with passive joint   ($k_0 = 0$, $k_1 = 100{,}000$, $\alpha = 10^\circ$).
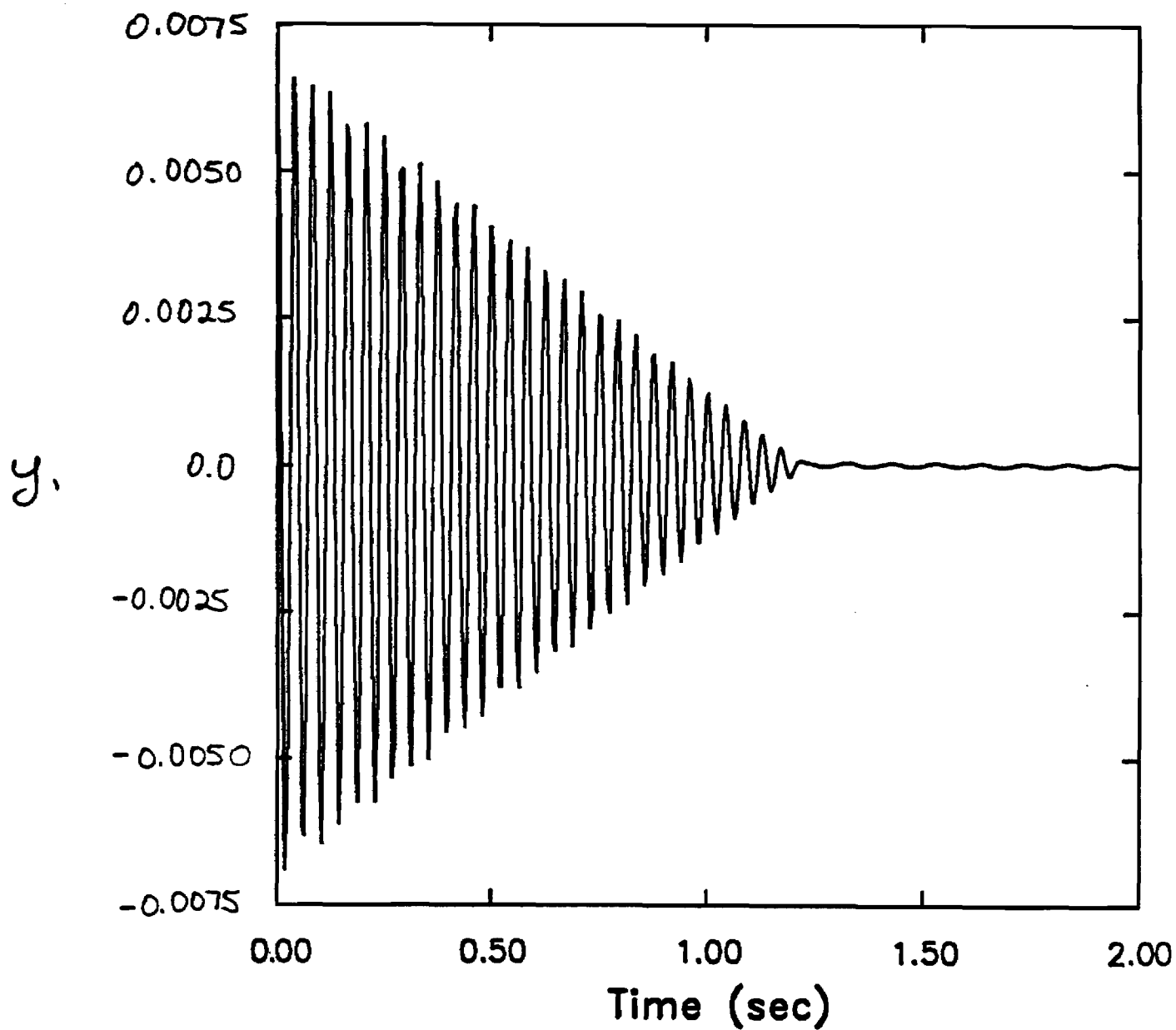
Figure 9: Free response of y_1 for two-span beam system with passive joint ($k_0 = 10$, $k_1 = 0$, $\alpha = 0^\circ$).
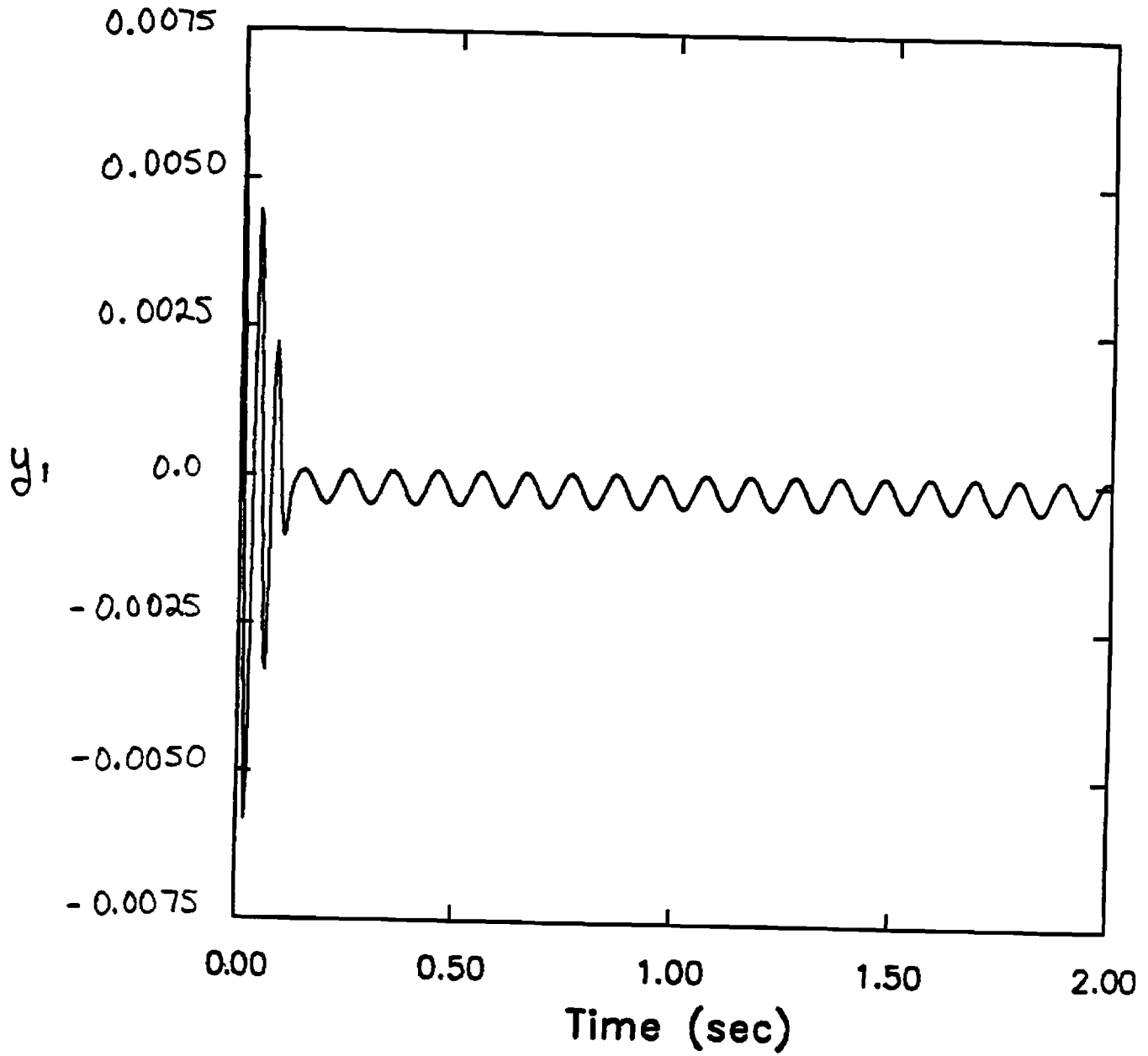
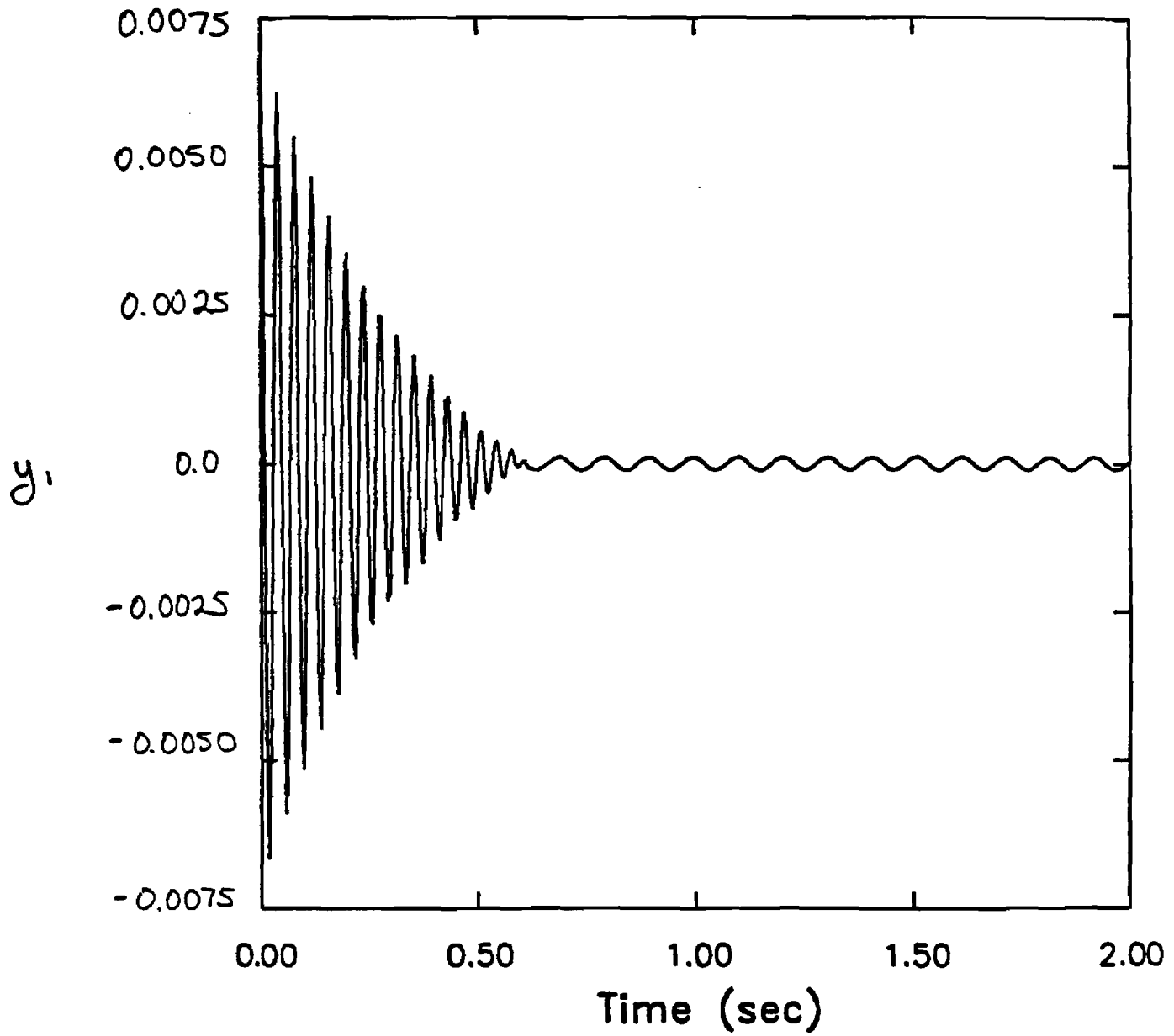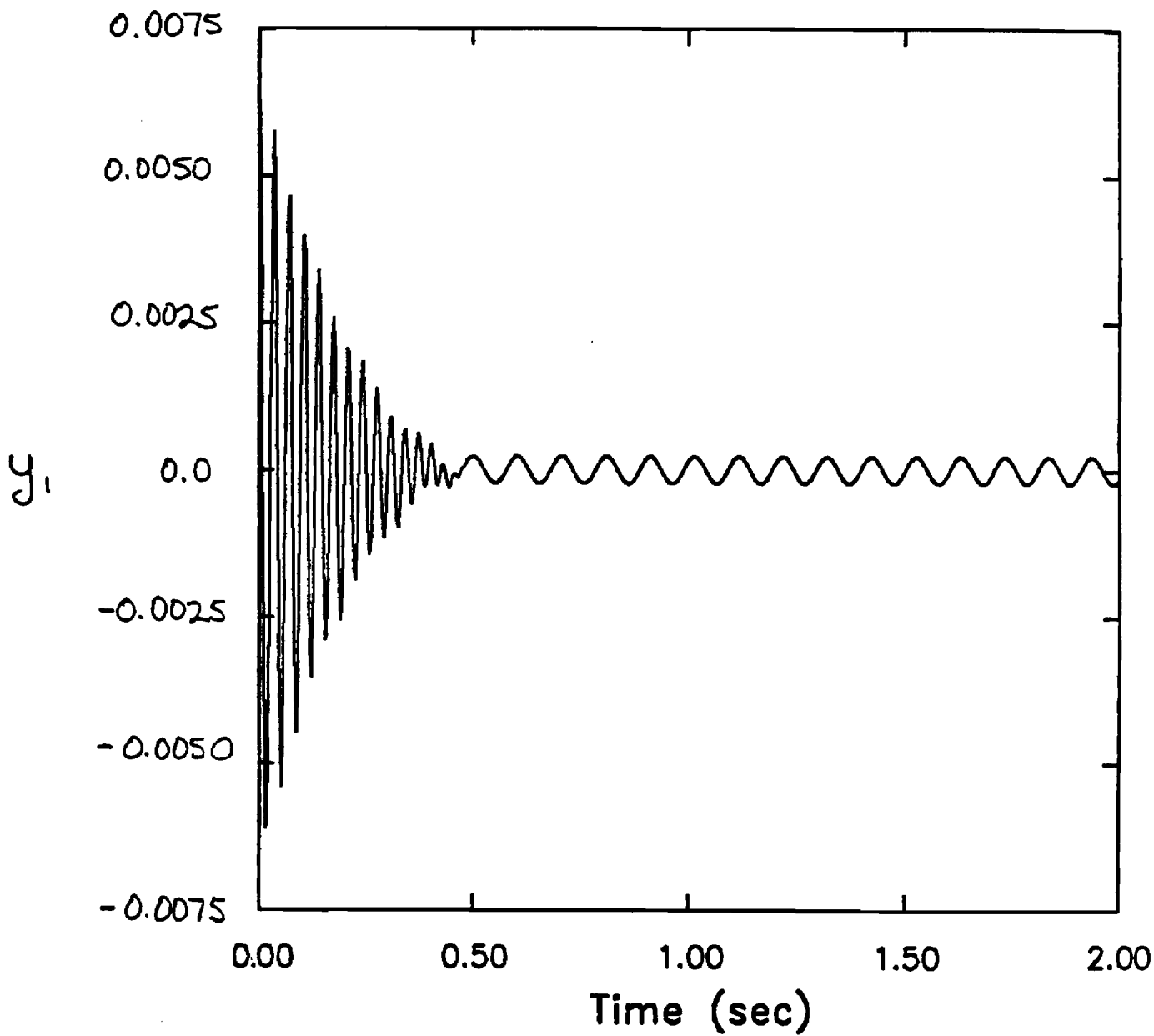Figure 10: Free response of y_1 for two-span beam system with passive joint ($k_0 = 100$, $k_1 = 0$, $\alpha = 0°$).

Figure 11:   Free response of y_1 for two-span beam system with passive joint ($k_0 = 10$, $k_1 = 10,000$, $\alpha = 10°$).

Figure 12:   Free response of y_1 for two-span beam system with passive joint (k_0 = 10, k_1 = 10,000, α = 20°).
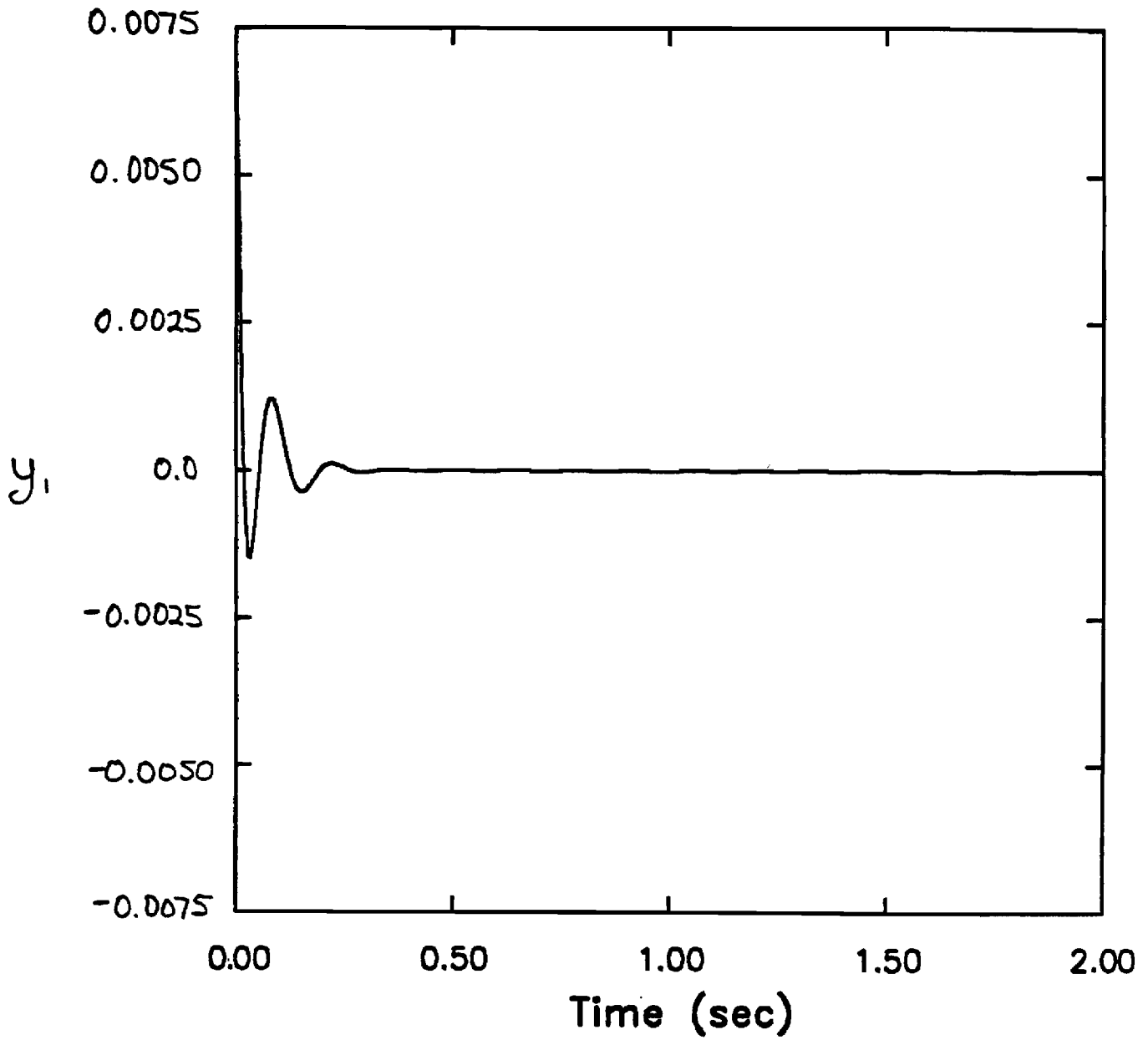
Figure 13: Free response of y_1 for two-span beam system with active joint ($K_0 = 0$, $K_1 = 0$, $K_2 = 399$).